Mineralization Halos and Diagenesis in Water-Laid Tuff of the Thomas Range, Utah

GEOLOGICAL SURVEY PROFESSIONAL PAPER 818-B

Mineralization Halos and Diagenesis in Water-Laid Tuff of the Thomas Range, Utah

By DAVID A. LINDSEY

BERYLLIUM-BEARING TUFFS IN WESTERN UTAH

GEOLOGICAL SURVEY PROFESSIONAL PAPER 818-B

A statistical study of the petrogenesis of water-laid tuff adjacent to the Spor Mountain beryllium and fluorspar district

UNITED STATES GOVERNMENT PRINTING OFFICE, WASHINGTON : 1975

UNITED STATES DEPARTMENT OF THE INTERIOR

GEOLOGICAL SURVEY

V. E. McKelvey, *Director*

Library of Congress Cataloging in Publication Data
Lindsey, David A.
Mineralization halos and diagenesis in water-laid tuff of the Thomas Range, Utah.
(Beryllium-bearing tuffs in western Utah)
(Geological Survey Professional Paper 818-B)
Bibliography: p.
Supt. of Docs. no.: I 19.16:818-B
1. Volcanic ash, tuff, etc.—Utah—Thomas Range. 2. Ore-deposits—Utah—Thomas Range. 3. Diagenesis—Utah—Thomas Range.
I. Title. II. Series. III. Series: United States Geological Survey Professional Paper 818-B.
QE461.L624 552'.2 75-619026

For sale by the Superintendent of Documents, U.S. Government Printing Office
Washington, D.C. 20402
Stock Number 024-001-02706-2

CONTENTS

	Page
Abstract	B1
Introduction	1
Geographic and geologic setting	3
Methods of study	3
Sampling plan	3
Laboratory procedure	3
Composition of the water-laid tuff	5
Lithology and petrography	5
Abundance of mineral and chemical components	7
Sources of variation	9
Geographic variation	11
Petrogenesis	B12
Problems in petrogenetic interpretation	12
A petrogenetic model	12
R-mode factor analysis	13
Factor analysis of water-laid tuff data	13
Interpretation of stratigraphic and geographic anomalies	16
Conclusions	17
Mineralization halos	17
Diagenesis	17
References cited	18

ILLUSTRATIONS

		Page
FIGURE 1.	Map showing location of the Thomas Range study area and mineral occurrences in the western Utah beryllium belt	B2
2.	Map showing geographic features, distribution of beryllium, fluorspar, and uranium deposits, and distribution of water-laid tuff in the southern part of the Thomas Range	4
3.	Photographs of water-laid tuff of the younger volcanic rocks	6
4.	Map and sections showing classification of water-laid tuff into vitric, zeolitic, and feldspathic facies	9
5–12.	Histograms showing frequency distribution and maps showing mean values at each collection station in water-laid tuff in the Thomas Range for the following:	
	5. Bulk density	23
	6. Powder density	24
	7. Porosity	25
	8. Clinoptilolite content	26
	9. Quartz content	27
	10. α-cristobalite content	28
	11. Potassium feldspar content	29
	12. Glass content	30
13.	Map showing occurrence of calcite in water-laid tuff in the Thomas Range	31
14.	Map showing occurrence of fluorite and halite in water-laid tuff of the Thomas Range	32
15–40.	Histograms showing frequency distribution and maps showing mean values at each collection station in water-laid tuff in the Thomas Range for the following:	
	15. Silica content	33
	16. Alumina content	34
	17. Total iron content (as Fe_2O_3)	35
	18. Magnesium oxide content	36
	19. Calcium oxide content	37
	20. Sodium oxide content	38
	21. Potassium oxide content	39
	22. Carbon dioxide content	40
	23. Water-soluble chlorine content	41
	24. Fluorine content	42
	25. Cesium content	43
	26. Lithium content	44
	27. Rubidium content	45
	28. Equivalent uranium content	46
	29. Barium content	47
	30. Beryllium content	48
	31. Chromium content	49

FIGURE 15–40. Histograms and maps — Continued.

Page

32. Gallium content ---------- B50
33. Lanthanum content ---------- 51
34. Manganese content ---------- 52
35. Niobium content ---------- 53
36. Strontium content ---------- 54
37. Titanium content ---------- 55
38. Vanadium content ---------- 56
39. Yttrium content ---------- 57
40. Zirconium content ---------- 58

41. Graph showing eigenvalues and cumulative proportion of total variance explained by the first 10 principal components ---------- 59

TABLES

Page

TABLE 1. Stratigraphic section in the southern part of the Thomas Range and Spor Mountain ---------- B3

2. Summary statistics for physical properties, mineral composition, and chemical composition of 160 samples of water-laid tuff from the Thomas Range ---------- 7

3. Estimates of total variance, variance components in a four-level nested sampling design, and variance ratios for physical properties, mineral composition, and chemical composition of water-laid tuff ---------- 10

4. Sum of squares of the deviations from the mean and percent reduction of the sum of squares by polynomial surfaces of degree 1 through 5 fitted to data on physical properties, mineral composition, and chemical composition of 160 samples of water-laid tuff ---------- 11

5. Table of correlation coefficients based on analyses of 160 samples of water-laid tuff ---------- 14

6. Communalities (in percent) for four-, five-, six-, and seven-factor Varimax solutions compared to the percent of nonerror variance ---------- 15

7. A six-factor petrogenetic model for the water-laid tuff as defined by the Varimax loadings ---------- 16

BERYLLIUM-BEARING TUFFS IN WESTERN UTAH

MINERALIZATION HALOS AND DIAGENESIS IN WATER-LAID TUFF OF THE THOMAS RANGE, UTAH

By DAVID A. LINDSEY

ABSTRACT

Pliocene water-laid tuffs are widespread in western Utah and provide the host rock for beryllium-fluorite mineralization at Spor Mountain. Systematic study of the mineral and chemical composition of the tuff in the southern part of the Thomas Range was undertaken to examine regional effects of mineralization at Spor Mountain and to differentiate these from the effects of other petrologic processes.

The water-laid tuff is zoned inward from the periphery of the Thomas Range; successive mineral zones are outlined by the vitric, zeolitic, and feldspathic facies. Study of thin sections indicates that the inward succession of facies reflects the alteration of glass to clinoptilolite and finally to potassium feldspar. The zonation of mineral facies and paragenesis is similar to that in other zeolitized tuffs where alkaline waters derived from leaching of glass are believed to have altered vitric tuff to zeolites and potassium feldspar.

R-mode factor analysis was used to test and further develop a petrogenetic model for the water-laid tuff. Important factors in tuff petrogenesis are beryllium-fluorite mineralization, three stages of diagenetic alteration of glass, concentration of calcite versus silica, and concentration of detrital heavy minerals. Mineralization effects occur mainly as a halo around the Spor Mountain beryllium-fluorspar district. Diagenetic effects are most intense in the tuff of the interior of the Thomas Range. The highest concentration of calcite occurs mainly in tuff beneath Topaz Mountain; heavy mineral elements are concentrated locally. The concentration of some elements, notably chlorine, is affected by additional factors.

Although the tuff in the southern part of the Thomas Range is mineralized only weakly or not at all, the beryllium-fluorite mineralization at Spor Mountain has left a strong imprint on the trace element content of the tuff. The elements F, Cs, Li, Be, Ga, Nb, Y, and to a lesser extent MgO and Rb were concentrated by mineralization and constitute a distinct geochemical signature which should be useful in searching for other beryllium-fluorspar mineral districts. Most of the mineralization-related elements form primary dispersion halos extending 1–2 miles (1.6–3.2 km) outward from Spor Mountain into unaltered tuff. Such large halos nearly triple the exploration target presented by a mineralized district like Spor Mountain.

Diagenesis has been of major importance in changing the chemical composition of tuff. Soda, K_2O, F, Rb, U, Mn, and Pb are depleted during zeolitization and MgO, Ba, Cr, and Sr are concentrated. Potassium feldspar diagenesis did not affect the chemical composition of the tuff. Possible release of F, U, and Mn during zeolitization suggests a potential diagenetic contribution of these elements to ore deposits, notably the sedimentary uranium deposits found nearby.

INTRODUCTION

Water-laid tuffs of Pliocene age are widespread in the western Utah beryllium belt which extends west from the Sheeprock Mountains into Nevada (Cohenour, 1963; Erickson, 1963) (fig. 1). The tuffs occur locally in the Honeycomb Hills (McAnulty and Levinson, 1964), throughout the Thomas Range and the southern part of the Dugway Range (Staatz and Carr, 1964, p. 86–102), in the northern part of the Drum Mountains (Shawe, 1964), and throughout the Keg Mountain area (Shawe, 1972). The tuffs provide the host rock for beryllium-fluorite mineralization at Spor Mountain (Staatz and Griffitts, 1961) and at the Honeycomb Hills (McAnulty and Levinson, 1964). They offer an opportunity to study the regional effects of beryllium-fluorite mineralization in the western Utah beryllium belt.

This is the second in a series of reports on beryllium-bearing tuffs in western Utah. In the first report, the hydrothermally altered host tuff at Spor Mountain was reexamined and compared with unmineralized tuff in the southern part of the Thomas Range (Lindsey and others, 1973). From that study it was concluded that hydrothermal alteration of the tuff was accomplished mainly by argillization (formation of montmorillonoid clay) and feldspathization of the volcanic constituents and by dedolomitization, silicification, and fluorite replacement of dolomite clasts in the tuff. Alteration was accompanied by introduction and concentration of beryllium in bertrandite, lithium in trioctahedral montmorillonoid clay, manganese oxides, and uranium. It was concluded that the alteration at Spor Mountain was produced by fluorine-rich hydrothermal solutions which derived metals at depth and transported them to the tuff as stable metal fluoride complex ions. (See also Staatz and Griffitts, 1961.) Declining temperature was probably responsible for fluorite and silica precipitation, and

hydrolysis of large amounts of carbonate ions released during alteration of the dolomite clasts probably caused potassium fixation and widespread feldspathization of the tuff. These conditions, together with declining fluorine concentration, were variously responsible for the breakdown of stable metal-fluoride complex ions and the precipitation of beryllium, uranium, and other minerals.

The present report examines in detail the more distant effects of the mineralization at Spor Mountain, as suggested by geochemical halos in the weakly mineralized and unmineralized water-laid tuff east of Spor Mountain in the southern part of the Thomas Range. The tuff here is well exposed and forms nearly continuous outcrops. It was sampled to study the regional distribution of physical properties, mineral components, and chemical components, including trace elements. From these data, effects of various petrologic processes, including those related to mineralization at Spor Mountain, were identified and mapped. This study is aimed at identifying true mineralization halos, and distinguishing them from other regional petrologic effects, thus establishing a basis for geochemical exploration for beryllium, fluorspar, and perhaps other ore deposits in tuffaceous rocks of the intermontane basins of the Western United States. A secondary objective is the clarification of some of the petrologic processes responsible for the diagenesis of tuff, with emphasis on assessing the role which these processes may play in migration and concentration of trace elements. Data used in preparing this report are available from the U.S. Dept. Commerce National Technical Information Service, Springfield, Va. 22161 (Lindsey and others, 1974).

I thank the employees of Brush Wellman Inc. for their hospitality during fieldwork. J. J. Connor, George Van Trump, Jr., and Josephine Boerngen, all employees of the U.S. Geological Survey, gave advice and assistance concerning statistical analysis and computer programming. Statistical analysis was performed on the Survey's IBM 360/65 computer in Washington, D.C. Many other employees of the U.S. Geological Survey assisted in the laboratory and made chemical analyses; they are acknowledged in table 2.

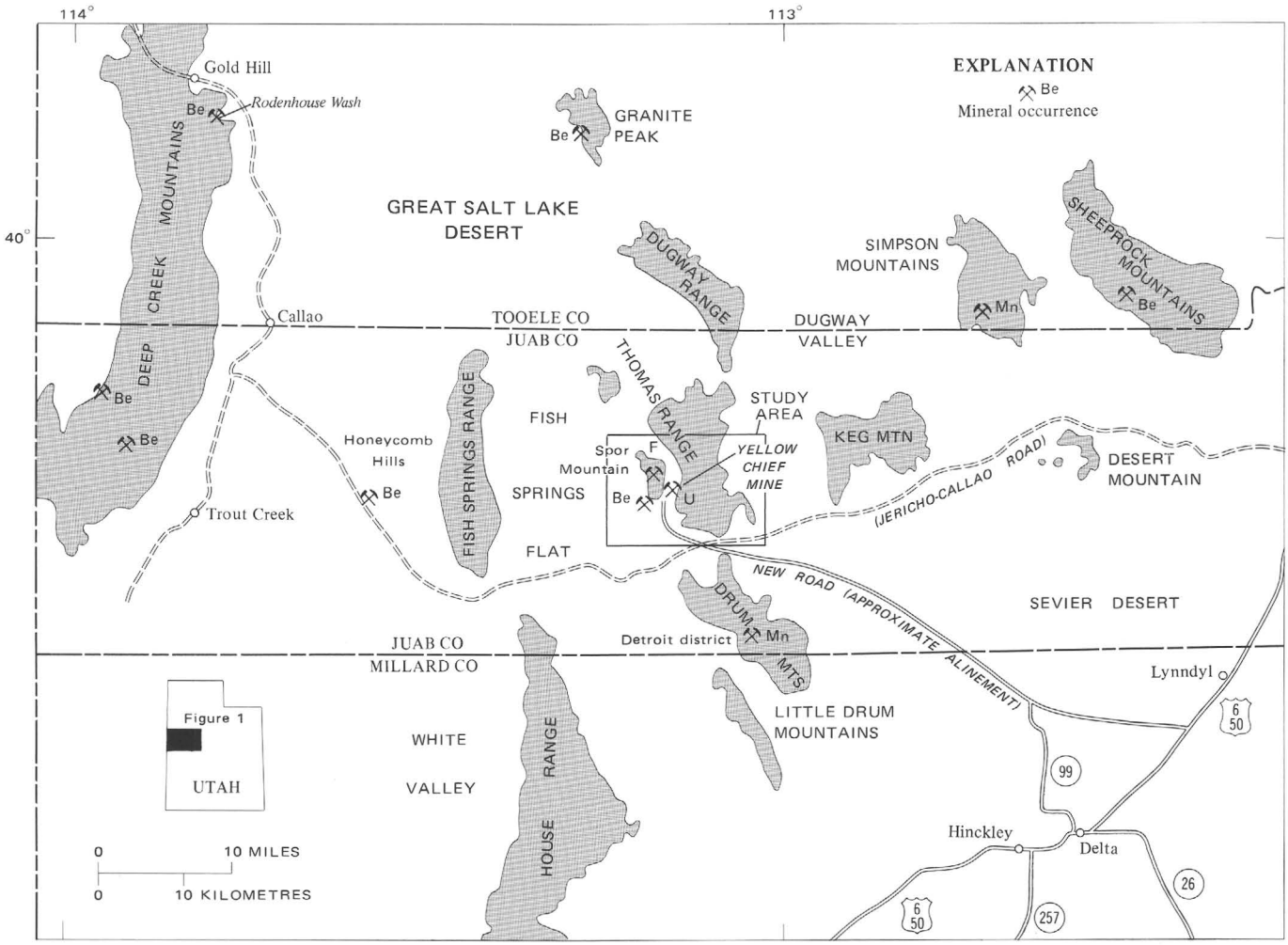

FIGURE 1. — Location of the Thomas Range study area and mineral occurrences in the western Utah beryllium belt.

GEOGRAPHIC AND GEOLOGIC SETTING

The study area covers the entire southern two-thirds of the Thomas Range (fig. 2) in the Basin and Range province in Juab County, Utah. The principal geographic features in the study area are Spor Mountain, an uplifted block of Paleozoic rocks just west of the southern part of the Thomas Range; The Dell, a narrow valley between Spor Mountain and the Thomas Range; Topaz Mountain, the highest point in the southern part of the Thomas Range; and Antelope Ridge, the southeasternmost promontory of the Thomas Range.

The stratigraphic section (table 1) in the study area consists of four main sequences: Upper Cambrian to Upper Devonian sedimentary rocks, an older volcanic group (Eocene), a middle volcanic group (Oligocene), and a younger volcanic group (Pliocene) (Staatz and Carr, 1964; Shawe, 1972). A 3,950-foot (1,200-m) section of Lower Ordovician to Upper Devonian sedimentary rocks consisting of mostly dolomite crops out on Spor Mountain; smaller exposures of Upper Cambrian dolomite and Lower Ordovician limestone occur south of Topaz Mountain. Rocks of the older and middle volcanic groups crop out mainly around the southern and eastern edges of the Thomas Range and in The Dell. The younger volcanic rocks make up most of the Thomas Range and also crop out in parts of The Dell and southwest of Spor Mountain. They overlie an erosion surface of considerable extent, resting on Paleozoic rocks south of Topaz Mountain and southwest of Spor Mountain and upon volcanic rocks of Eocene age along the east side of the Thomas Range and of Oligocene age in The Dell.

The distribution of water-laid tuff, termed vitric tuff by Staatz and Carr (1964, p. 86–102), is shown in figure 2. The tuff forms the basal unit in each of five overlapping sequences of tuff and topaz rhyolite which comprise most of the younger volcanic group. It approaches 300 feet (92 m) in thickness in a few places but is missing entirely elsewhere. The tuff is everywhere overlain by topaz rhyolite; at many localities the basal rhyolite consists of volcanic breccia and vitrophyre. The tuff is cut by faults in a few places, notably southwest of Spor Mountain and along the east side of The Dell.

Most of the beryllium deposits occur in water-laid tuff on the southwest side of Spor Mountain, and numerous pipelike deposits of fluorspar occur in the Paleozoic rocks on Spor Mountain (fig. 2) (Griffitts, 1964, p. 73–74; Thurston and others, 1954, p. 24–45). The water-laid tuff is mineralized only weakly or not at all in the Thomas Range, north and east of the Spor Mountain beryllium and fluorspar deposits. The present study deals with the water-laid tuff outside the area of intense beryllium-fluorite mineralization.

METHODS OF STUDY

SAMPLING PLAN

The physical properties, mineral composition, and chemical composition of the water-laid tuff in the southern part of the Thomas Range were studied systematically. All the tuff east of the limit of fluorspar and beryllium deposits was sampled at regular intervals (fig. 2). Tuff from four of the five sequences in the younger volcanic group is present here, and figure 2 shows the classification of sampling stations into tuff units 2, 3, 4, and 5 (ranging from oldest to youngest) which belong to the youngest four sequences of Staatz and Carr (1964, p. 86–102). Tuff unit 1, from the oldest sequence, is present north of the study area and was not sampled.

A stratified random sampling plan (Krumbein and Graybill, 1965, p. 156–157) was used as a basis to select samples from all available tuff outcrops in the southern part of the Thomas Range. Each sampling station was chosen randomly from 100 possible locations within each linear mile (1.6 km) of tuff outcrop. In practice, stations were moved laterally to the nearest good exposure of tuff so that samples could be obtained at every sampling station. Stations were located for each of the four tuff units in this manner. Some of the sampling stations are necessarily close to each other because they represent two different tuff units, as along the northeastern side of The Dell. Seven stations were added arbitrarily to fill gaps left by the random sampling plan. The stratigraphic thickness of the tuff at each station was then estimated from the geologic map (Staatz and Carr, 1964, pl. 1) and in the field. Random number tables were used to select four 1-foot (0.3 m) intervals for sampling from the entire thickness of tuff exposed at each station. The sampling program resulted in 160 samples being collected from 40 stations. The samples consisted of fresh chips and averaged about 2 lbs (0.9 kg) in weight.

TABLE 1. — *Stratigraphic section in the southern part of the Thomas Range and Spor Mountain*

[Adapted from Shawe (1972) and Staatz and Carr (1964); ages are from author's unpublished data; query (?) indicates thickness unknown]

Age	Rock Unit	Thickness (ft)	Thickness (m)
Quaternary	Alluvium and Lake Bonneville Group	0–500+	0–152+
	Unconformity		
Pliocene	Younger volcanic group:		
	Topaz rhyolite (breccia and vitrophyre at base). (sequence occurs five times)	0–1,000	0–305
	Water-laid tuff (sampled for this study).	0–300	0–92
	Unconformity		
Oligocene	Middle volcanic group:		
	Intrusive breccia.	?	?
	Rhyolitic welded ash-flow tuff.	500	152
	Quartz-latitic welded ash-flow tuff.	200	61
	Unconformity(?)		
Eocene	Older volcanic group: Latitic and andesitic flows; also some rhyolitic ash-flow tuff.	?	?
	Unconformity		
Late Devonian to Late Cambrian	Numerous formations—mainly dolomite and limestone with minor quartzite and shale.	3,950+	1,200+

LABORATORY PROCEDURE

Twenty samples were selected at random for splitting before any other laboratory procedures began. These

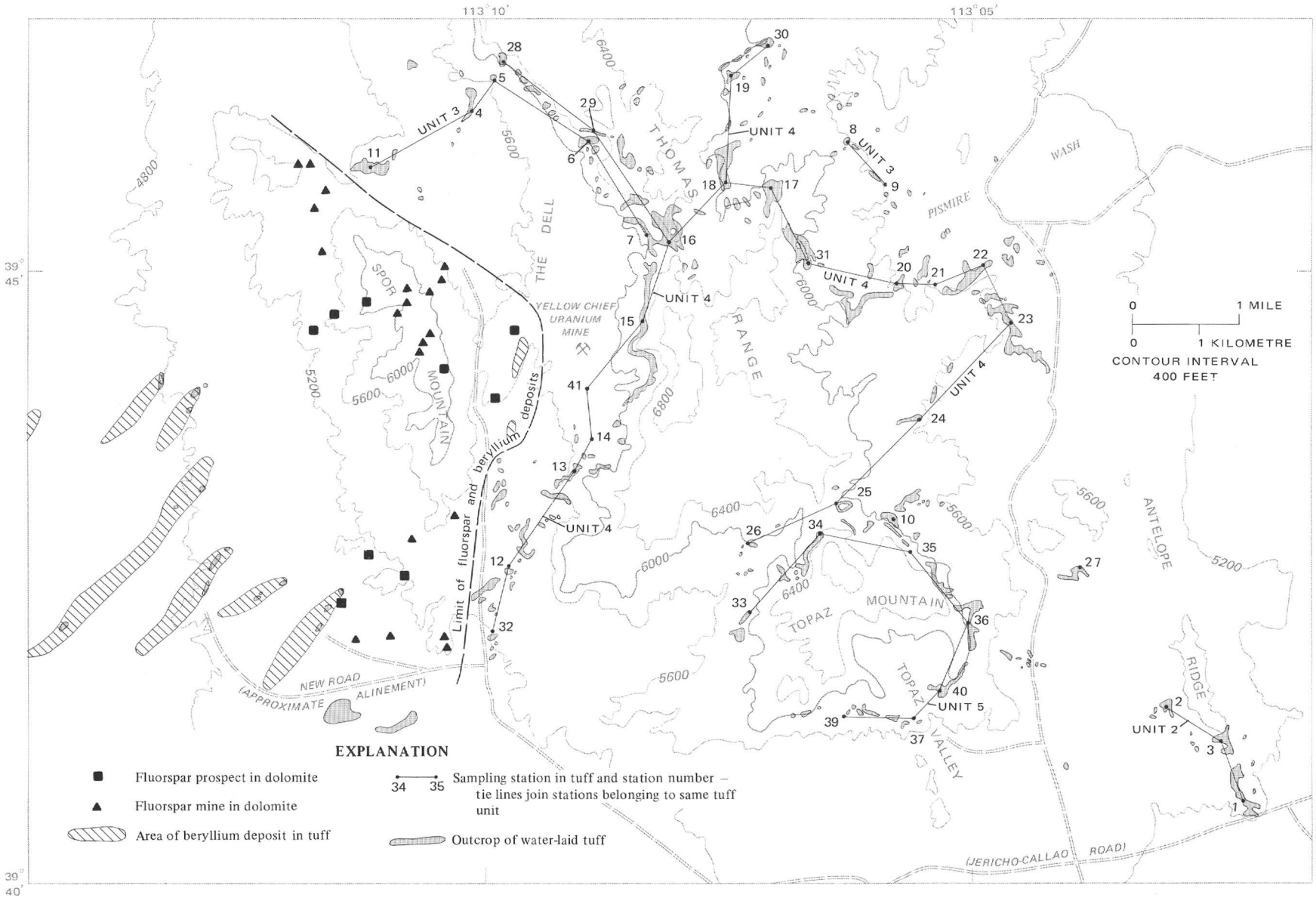

FIGURE 2. — Geographic features, distribution of beryllium, fluorspar, and uranium deposits, and distribution of water-laid tuff in the southern part of the Thomas Range. Base map from Staatz and Carr (1964, pl. 1).

splits and the original 160 samples were placed in random order prior to sample preparation. The purpose of these precautions is twofold. (1) Splitting of some samples allows independent estimation of various mineral and chemical components on the same sample, thus making possible calculation of laboratory errors. (2) Randomization of the sample population ensures that analytical drift and other laboratory effects did not produce undesirable manmade trends in the data; this is particularly important because I have plotted the data on maps. A specimen for thin sectioning was removed from each sample before splitting and randomization.

All 160 samples plus the 20 additional splits were ground to finer than 60 mesh; approximately 120 g was split from each sample and ground to finer than 100 mesh. Splits of approximately 3 g and 2 g each were then removed for X-ray diffraction and spectrographic determinations, respectively; the remaining 100-mesh split was reserved for other chemical determinations. Density was determined on surplus 60-mesh powder by air pycnometer (McIntyre and others, 1965). Bulk density was determined on specimens reserved for thin sectioning by coating them with beeswax and weighing the specimens in water.

Estimation of mineral quantities by X-ray diffraction was necessary owing to the fine-grained nature of the tuff. The method involves no new technique, but is an application of principles established by others (Klug and Alexander, 1954; Schultz, 1964; Tatlock, 1966). Two to 3 g of each sample was ground 15 minutes in a shatterbox and mounted by the backpack mounting technique of McCreery (Klug and Alexander, 1954, p. 300–302). Standards were prepared and X-rayed in the same manner, so that the diffraction intensity of each mineral could be converted into percent. Amorphous glass and poorly crystallized minerals detected by X-ray diffraction were estimated by difference, that is, by adding all other components and subtracting them from 100.

All chemical analyses were performed in the laboratories of the U.S. Geological Survey at Denver. Major components were determined by a variety of methods, most of them modifications of published work. X-ray fluorescence analysis for SiO_2, Al_2O_3, Fe_TO_3(total Fe as Fe_2O_3), and CaO was done according to a modification of the borate fusion method of Claisse (1956); atomic absorption analysis for MgO, Na_2O, K_2O, Li, and Rb using the operating parameters published by Perkin-Elmer (1964); atomic absorption analysis for Cs according to Mountjoy and Wahlberg (1968); and gasometric analysis for CO_2 according to Rader and Grimaldi (1961, p. A33–A37). Fluorine was determined by a newly developed electrode method (D. R. Norton, Johnnie Gardner, and Claude Huffman, Jr., unpub. data, 1973). Water-soluble chlorine was determined by colorimetric reference method C (Am. Soc. for Testing and Materials, 1966, p. D512). Equivalent uranium (eU) was determined by a radiometric counting method based on the assumption that all beta and gamma radiation comes from decay of uranium. Although eU includes effects from such isotopes as ^{232}Th and ^{40}K, previous comparison of eU and chemical uranium in the tuff indicates that much of the measured eU is due to uranium decay (Staatz and Carr, 1964, p. 115). Numerous other trace elements were determined by direct-reader spectrometric analysis (Havens and Myers, 1973).

COMPOSITION OF THE WATER-LAID TUFF

LITHOLOGY AND PETROGRAPHY

The tuff of the younger volcanic group was termed "vitric tuff" by Staatz and Carr (1964) because of its glassy character and was termed "water-laid tuff" by Shawe (1968) because of its characteristic stratified aspect (fig. 3*A*). Much of the tuff is probably water laid, inasmuch as it is well stratified and contains abundant clasts derived from older volcanic rocks. The clasts locally compose as much as one-half the tuff and reach 4 feet (1.2m) in maximum dimensions (figs. 3*B*, *C*). Limestone pebbles are present in the tuff along the margins of Topaz Mountain (fig. 3*C*) and dolomite pebbles and cobbles are abundant in the tuff southwest of Spor Mountain, where they are altered to calcite, silica minerals, fluorite, and clay minerals (Lindsey and others, 1973). The carbonate clasts were derived from Paleozoic rocks nearby, such as those south of Topaz Mountain and on Spor Mountain. Air-fall tuffs, which are massive and consist mainly of featherweight pumice lapilli, are well exposed at the south end of The Dell (fig. 3*D*).

The tuff typically contains pumice, volcanic rock fragments, obsidian, a few sedimentary rock fragments, and pyroclastic and detrital crystals in a matrix of glass shards, fine-grained clinoptilolite, or fine-grained potassium feldspar accompanied by quartz and cristobalite. The pyroclastic crystals — euhedral quartz, sanidine, and biotite — commonly do not constitute more than 20 percent of the tuff. Many of the euhedral grains have been broken during transport. Small quantities of detrital minerals are also present in the tuff; listed in approximate order of decreasing abundance, they are plagioclase, magnetite, hematite, hornblende, sphene, topaz, augite, allanite, and zircon. Other minerals, formed after deposition of tuff, are present locally; they are montmorillonoid clay, fine-grained fluorite, halite, and locally abundant sparry calcite.

Gross mineralogy, determined by X-ray diffraction, was used to differentiate the tuff into three facies: vitric, zeolitic, and feldspathic (fig. 4). The vitric facies retains a large proportion of unaltered glass pumice and shards

and represents the original mineralogy of the water-laid tuff. The zeolitic facies contains clinoptilolite, which is widely distributed in the tuff and constitutes as much as 90 percent of some samples. The feldspathic facies contains abundant potassium feldspar, quartz, and α-cristobalite of diagenetic origin. It differs from the hydrothermally altered feldspathic tuff at Spor Mountain (Lindsey and others, 1973) in that it is not associated with beryllium mineralization. Generally, the vitric facies occurs around the margins of the Thomas Range, whereas the zeolitic and feldspathic facies are present in the central part of the range. The zonal arrangement of facies is toward the center of the Thomas Range and toward the bottom of tuff unit 4 (sections *A–A′* and *B–B′*, fig. 4) but it is very irregular in tuff unit 5 (section *C–C′*). The facies boundaries clearly transect stratigraphic boundaries and indicate a regional zonation.

Microscopic examination of the tuff reveals that the zeolitic and feldspathic facies have probably formed by diagenetic alteration of vitric tuff. Pumice fragments are commonly etched and obsidian fragments have bleached rinds, both features suggesting extensive leaching of glass. Microflakes of birefringent montmorillonoid clay outline glass fragments and pumice vesicles and are present in the matrix of vitric tuff. Tabular and prismatic crystals of clinoptilolite, as much as 0.03 mm long, line cavities and replace glass fragments. Zeolitic tuff has a very fine grained matrix of clinoptilolite, commonly accompanied by small quantities of montmorillonoid clay. Potassium feldspar of diagenetic origin forms fibrous mosaics which commonly replace volcanic rock fragments and obsidian in preference to matrix. No feldspar overgrowths were observed on pyroclastic phenocrysts, in contrast to those associated with the hydrothermal potassium feldspar at Spor Mountain. Equidimensional masses of anhedral quartz are common in some samples and appear to be cavity fillings.

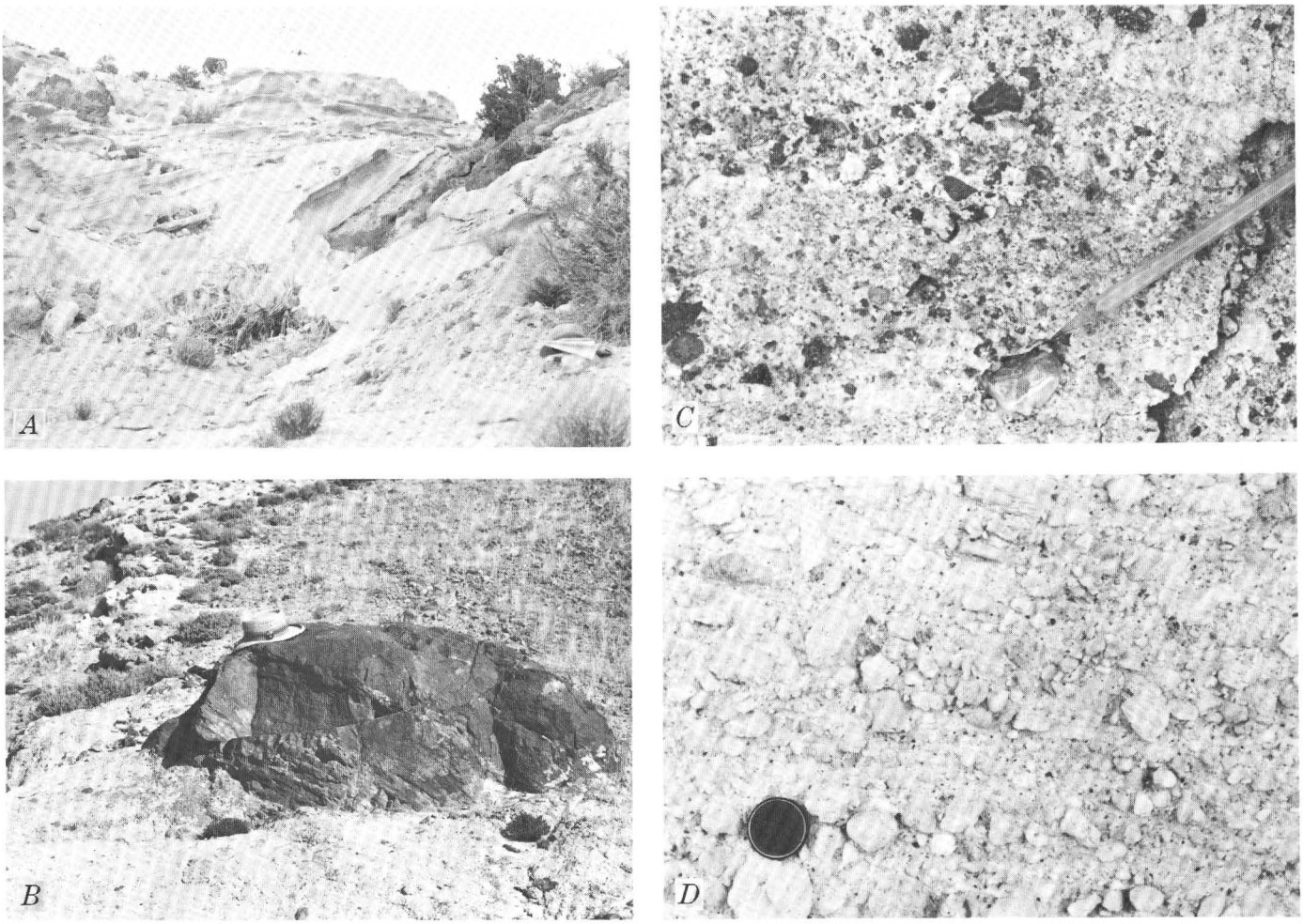

FIGURE 3. — Water-laid tuff of the younger volcanic rocks. *A*, Stratified tuff with steep initial dips in paleovalley on the east side of Topaz Mountain; dark rock to right is exhumed hill in older volcanic rocks. *B*, Large boulder of older volcanic rock in tuff at Antelope Ridge. *C*, Pebbles of older volcanic rock and limestone (at pencil point) in tuff at Topaz Valley. *D*, Pumice lapilli in air-fall tuff at the south end of The Dell; camera lens cap shows scale.

Very weak fluorite and beryllium mineralization of tuff is evident at a number of sampling stations around the edges of The Dell and along the south side of Topaz Mountain (fig. 4). Montmorillonoid clays and small fluorite nodules are only sparsely present at these stations; clay is present at stations 4, 5, and 37, and one fluorite nodule each was recovered from the base of the tuff at stations 11 and 37. Most of the tuff section at each of these stations did not show field or thin section evidence of mineralization. Clay alteration is more conspicuous, however, at station 41. The mineralization at station 14 was not recognized until laboratory analysis showed 2–3 percent fluorite and 160–300 ppm beryllium in tuff consisting mainly of quartz, clinoptilolite, and potassium feldspar.

ABUNDANCE OF MINERAL AND CHEMICAL COMPONENTS

Data on physical properties, mineral composition, and chemical composition of the tuff are summarized in table 2. Average silica content (68 percent), Al_2O_3 (11 percent), and alkalis (6 percent, with K_2O dominant) suggest a rhyolite composition for the tuff; although, as discussed later, the composition of the tuff has been changed considerably by diagenesis. Chemical analyses of vitric samples indicate a total alkali content of as much as 8–9 percent; the original tuff was therefore an alkali rhyolite similar in composition to the associated topaz rhyolite of Staatz and Carr (1964, table 15). The tuff also contains unusually large amounts of Cl (0.15 percent), F (0.16 percent), Li (56 ppm), U (38 ppm eU), Be (10 ppm), Ga (31 ppm), Nb (29 ppm), and Y (38 ppm).

The frequency distributions of each physical property, mineral component, and chemical component (hereafter referred to collectively as variables) are summarized by moment estimates and histograms (Freund, 1960, p. 3–105). Central tendency was estimated by the arithmetic and geometric means and by the median (50th percentile); variation was estimated by the standard deviation, geometric deviation, and the range between the 10th and 90th percentiles (table 2). Means and variation for censored frequency distributions, that is, where the concentration of a particular mineral or element is below the limit of detection for some samples, were estimated by the method of Cohen (Miesch, 1967a, p. B5–B8). Statistical parameters were not computed for variables for which more than 30 percent of the samples are below the limit of detection, although data for some are summarized later in histograms and maps.

Study of the skewness revealed that the frequency distributions for many variables depart significantly from the normal model. Normal distributions are symmetrical with a skewness near 0 and if the frequency distribution deviates significantly from the normal, various transformations of the data (Miesch, 1967a, p. B5) are necessary before further statistical analysis is done. Logarithmic transformations were helpful in normalizing the data for many variables; however, distributions which are nearly normal or are negatively skewed were not transformed. Thus distributions of density and porosity, some major

TABLE 2. — *Summary statistics for physical properties, mineral composition, and chemical composition of 160 samples of water-laid tuff from the Thomas Range*

[Bulk density determined by weighing wax-coated samples in water and powder density determined by air pycnometer; both by K. A. Buzard. Mineral composition determined by X-ray diffraction by W. R. Marsh. Silica, Al_2O_3, total Fe as Fe_2O_3 (designated as Fe O_3), and CaO determined by X-ray fluorescence using borate fusion by M. W. Solt and J. S. Wahlberg; MgO, Na_2O, K_2O, Li, and Rb determined by atomic absorption by V. M. Merritt; CO_2 determined gasometrically by I. C. Frost; water-soluble Cl determined by colorimetric ASTM Reference Method C by V. E. Shaw; F determined by electrode method by D. R. Norton and Johnnie Gardner; Cs determined by atomic absorption by Wayne Mountjoy; eU determined by beta-gamma scaler by E. J. Fennelly; all elements from B through Zr determined by direct reading spectrograph by R. G. Havens, N. M. Conklin, and L. M. Lee. Elements looked for but not found, with their detection limits in parts per million, are Ag(4), Au(20), Bi(20), Cd(100), Co(8), Ge(100), In(20), Pd(10), Re(70), Sb(300), Sc(10), Tl(50), W(500), and Zn(300)]

Variable	Number of samples below limit of detection	Lower limit of detection	Mean[1]	Standard[1] deviation	Percentiles 10th	50th	90th
Density (grams per cubic centimetre) and porosity (percent)							
Bulk density	0	1	1.65	.24	1.34	1.65	1.98
Powder density	0	.01	2.38	.08	2.26	2.38	2.50
Porosity	0	1	30.6	9.9	17.0	31.1	44.2
Mineral composition (weight percent)							
Montmorillonoid clay[2]	150	10	---	---	---	---	---
Mica[3]	108	1	---	---	---	---	1.6
Clinoptilolite	46	5	*18.3*	*3.89*	---	35.8	66.0
Quartz	1	1	*7.8*	*2.27*	3.7	8.2	18.1
α-cristobalite[4]	1	1	*5.0*	*2.28*	1.7	5.2	13.2
Potassium-feldspar[5]	4	1	*14.2*	*1.95*	6.9	13.4	37.1
Calcite	117	1	---	---	---	---	2.7
Fluorite	85	.5	---	---	---	---	1.3
Halite	154	.5	---	---	---	---	---
Glass[6]	106	30	---	---	---	---	80.9
Chemical composition (weight percent)							
SiO_2	0	1	67.9	4.9	62.8	68.1	73.9
Al_2O_3	0	1	11.4	1.1	10.2	11.4	12.8
Fe_TO_3	0	.1	1.13	.19	.95	1.15	1.39
MgO	0	.01	*.62*	*1.69*	.33	.62	1.13
CaO	0	.1	*2.08*	*1.67*	1.24	1.97	4.14
Na_2O	0	.01	2.11	.77	1.14	2.01	3.24
K_2O	0	.01	3.84	1.02	2.38	4.03	5.04
CO_2	51	.05	*.11*	*5.61*	---	.10	1.00
Cl	0	.01	*.15*	*2.54*	.05	.14	.45
F	0	.02	*.16*	*2.42*	.05	.16	.40
Chemical composition (parts per million)							
Cs	0	.5	*14.6*	*1.87*	8.2	13.4	39.8
Li	0	3	*56.5*	*1.81*	25.1	48.4	131.8
Rb	0	5	320	109	182	318	456
eU	0	10	38.1	11.0	20.8	39.6	53.8
B	136	30	---	---	---	---	30.0
Ba	0	10	*117*	*1.92*	48	118	235
Be	2	4	*9.9*	*1.96*	5.5	9.5	16.6
Cr	35	5	*6.2*	*1.52*	---	5.6	11.0
Cu	0	1	*4.2*	*1.34*	2.8	4.4	5.1
Ga	0	10	*30.8*	*1.13*	25.9	30.8	35.3
La	109	50	---	---	---	---	61.6
Mn	0	7	*434*	*1.81*	174	494	780
Mo	158	20	---	---	---	---	---
Nb	21	20	*28.6*	*1.47*	---	26.8	53.8
Ni	156	7	---	---	---	---	---
Pb	19	20	*26.6*	*1.32*	---	26.4	36.6
Sn	152	20	---	---	---	---	---
Sr	0	10	*234*	*2.06*	103	209	696
Ti	0	20	*557*	*1.45*	308	570	866
V	88	10	---	---	---	---	16.3
Y	1	20	*37.8*	*1.29*	27.3	36.6	55.7
Zr	0	20	*96*	*1.10*	84	98	110

[1]Italic indicates geometric mean and deviation.
[2]Dioctahedral montmorillonoid clay.
[3]Mainly pyroclastic biotite.
[4]Includes some opal.
[5]Pyroclastic sanidine plus secondary potassium feldspar. Plagioclase (<5 percent) was not detected by X-ray.
[6]Quantity determined by difference.

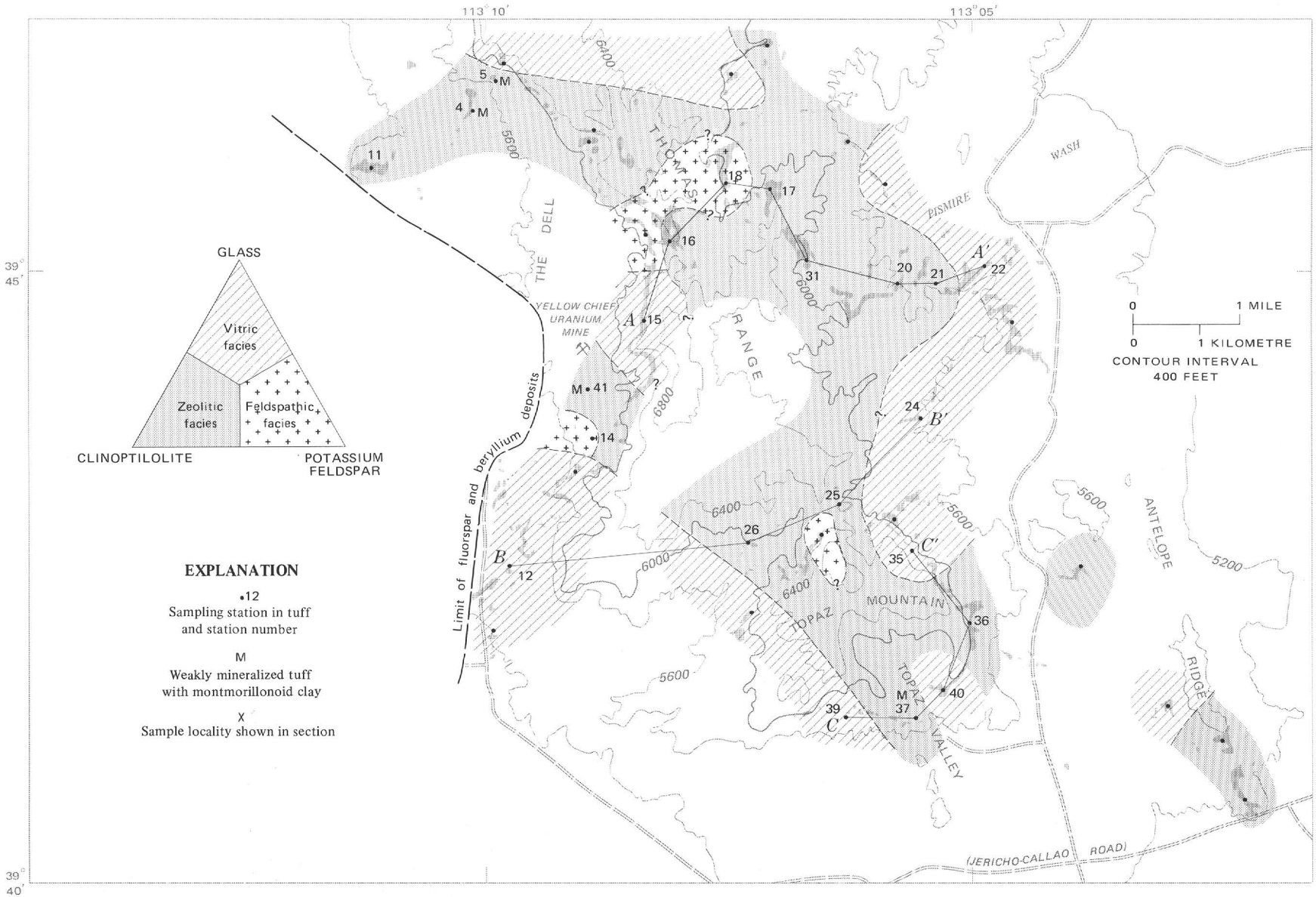
113°10′
113°05′
39° 45′
39° 40′
GLASS
Vitric facies
Zeolitic facies
Feldspathic facies
CLINOPTILOLITE
POTASSIUM FELDSPAR
EXPLANATION
•12
Sampling station in tuff and station number
M
Weakly mineralized tuff with montmorillonoid clay
X
Sample locality shown in section
Limit of fluorspar and beryllium deposits
THOMAS
THE DELL
YELLOW CHIEF URANIUM MINE
RANGE
PISMIRE
WASH
MOUNTAIN
TOPAZ
TOPAZ VALLEY
ANTELOPE
RIDGE
(JERICHO-CALLAO ROAD)
0 1 MILE
0 1 KILOMETRE
CONTOUR INTERVAL 400 FEET
6400
5600
6000
6800
5200
A
A′
B
B′
C
C′

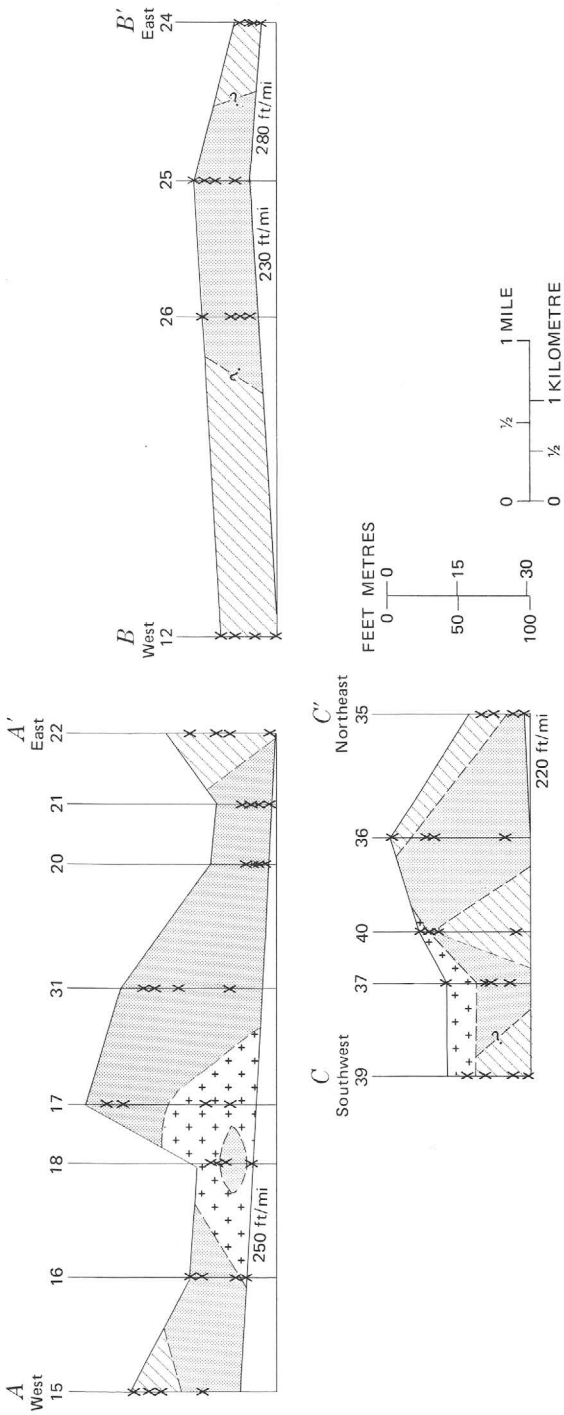

FIGURE 4.—Map and sections showing classification of water-laid tuff into vitric, zeolitic, and feldspathic facies.

oxides (SiO_2, Al_2O_3, Fe_TO_3, Na_2O, and K_2O), and the trace elements Rb and U (as eU) tend to be normally distributed or negatively skewed and were preserved in arithmetic form. Distributions of other variables, including minerals and most trace elements, were transformed to logarithms before further statistical analysis; such transformations are noted in the tables following table 2 by reference to the variable as "log clinoptilolite," etc. The geometric mean and deviations are given in table 2 as estimates of central tendency and variation for those variables which tend to exhibit lognormal frequency distributions. They are the antilogarithms of the arithmetic mean and standard deviations of the log concentrations.

Histograms, or bar diagrams, were constructed for most variables (figs. 5–40). The data were divided into classes of equal width for normally distributed data and into geometric classes for log normal data. The geometric class interval was usually selected so that six classes per order of magnitude were plotted, with the series 1, 1.5, 2, 3, 5, 7, 10, etc., serving as class midpoints. In a few cases (Ga and Zr) as many as 20 classes per order of magnitude were necessary to display the data adequately (figs. 32 and 40). Sturges' rule (Waugh, 1943, p. 45–46) was used as a guideline for the optimum number of classes in each histogram, but usually the optimum number of classes (for 160 samples the optimum number is eight classes) was exceeded in order to preserve information in the histogram.

SOURCES OF VARIATION

The total variance of each physical property, mineral, oxide, and trace element can be understood as the sum of numerous sources of natural and manmade variation. The observed value of each measurement is influenced by each of these sources of variation. The magnitude of these sources of variation can be determined by analysis of variance. In this study, the sampling design outlined earlier provides the basis for a four-level nested analysis of variance (Krumbein and Graybill, 1965, p. 215).

The statistical model of variation is:

$$x_{ijkm}=\mu+\alpha_i+\beta_{ij}+\gamma_{ijk}+\delta_{ijkm}$$

where x_{ijkm}=the mth measurement on the kth sample from the jth station of the ith tuff unit where $1\leq m\leq 2$, $1\leq k\leq 4$, $1\leq j\leq 22$, and $1\leq i\leq 4$. Thus each measurement may be viewed as the sum of a grand mean (μ) added to deviations introduced by a particular tuff unit (α_i), station (β_{ij}), sample (γ_{ijk}), and laboratory measurement (δ_{ijkm}). The latter term is identified with laboratory error, the preceding term (γ_{ijk}) may be called sampling error, and so on. A more extensive discussion of sampling models in geochemistry is given by Miesch (1967b).

Analysis of variance was used to partition the total variance of each variable into four components; these

components are assigned to variance among tuff units (s_α^2), among stations within tuff units (s_β^2), among samples within stations (s_γ^2), and among splits within samples (s_δ^2) (table 3). The analysis is based on the assumptions that α_i, β_{ij}, γ_{ijk}, and δ_{ijkm} are random variables with means of zero and variances of s_α^2, s_β^2, s_γ^2, and s_δ^2 and that the variance components are additive:

$$s_T^2 = s_\alpha^2 + s_\beta^2 + s_\gamma^2 + s_\delta^2$$

where S_T^2 is the total variance. Tuff unit variance (s_α^2) is a measure of large-scale stratigraphic variation; station variance (s_β^2) is a measure of geographic variation; sample variance (s_γ^2) is a measure of sampling errors; split variance (s_δ^2) is a measure of laboratory error and includes effects due to grinding, splitting, and analytical error.

The calculations used in analysis of variance are discussed, with examples, by Krumbein and Graybill (1965, p. 191–221). Calculations for the model described previously are complicated by an unbalanced design (Anderson and Bancroft, 1952, p. 327–330); that is, there are different numbers of stations per tuff unit (ranging from 3 to 22) and only 20 samples were split to determine laboratory variance. The seriousness of this problem was checked by repeated runs on variations of the model. In one run three levels comprising all tuff units, all stations, and all samples were used in the calculation of variance components; in a second run seven stations were randomly selected from each tuff unit, so that the number of stations per unit was nearly equal. In each of these two runs sample and laboratory variance were combined. A third run consisted of only two levels, those of stations and samples, so that tuff unit and station variance were combined at the upper level and sample and laboratory variance were combined at the lower level; a fourth run also used a two-level model, with tuff unit, station, and sample variance combined at the upper level and laboratory variance isolated at the lower level. The variance components in table 3 were derived from the first and fourth runs; the second and third runs produced estimates of variance components which were in substantial agreement with those listed in table 3, indicating that the unbalanced design did not seriously affect the variance component estimates. Data on total crystalline material were used to determine the variance components of glass in the analysis; glass has a highly censored frequency distribution and was computed as 100 minus total crystalline material when a glass hump was noted in the X-ray pattern.

The estimates of variance components in table 3 show that very little variation exists among tuff units. This conclusion is not surprising inasmuch as all the tuffs are part of the younger volcanic group and are related to the phase of topaz rhyolite volcanism in the Thomas Range (Staatz and Carr, 1964, p. 87–90). This means that the data for most variables may be analyzed for geographic trends without the complicating influence of stratigraphic position and, in fact, where station variance is much larger than tuff unit variance, even those variables with a sizable component among tuff units may be used in detecting geographic variation. Only CaO, CO_2, Nb, Pb, and Ti show a significant tendency toward concentration in individual tuff units; the maps showing regional abundance of these variables (figs. 19, 22, 35, and 37) confirm that CaO, Nb, Ti, and perhaps CO_2 may show high or low concentrations in unit 5 on Topaz Mountain. Unit 5 is known to contain limestone clasts, accounting for high CaO and CO_2. Low Nb and Ti in unit 5 may be due to a paucity of some heavy minerals.

Any search for regional trends in these data must be based on consideration of sampling and laboratory errors, as estimated by the s_γ^2 and s_δ^2 components (table 3). If the sum of these components becomes too large, geographic variation may be obscured by unwanted "noise" arising from laboratory and sampling errors. An example in table 3 is SiO_2, whose total variance is 24.1,

TABLE 3. — *Estimates of total variance, variance components in a four-level nested sampling design, and variance ratios for physical properties, mineral composition, and chemical composition of water-laid tuff*

[Asterisk (*) indicates significant differences (0.05 level) among tuff units and among stations. $V_m = \frac{s_\beta^2}{(s_\gamma^2 + s_\delta^2)/4}$ is the ratio of among-stations variance to the variance of the station means]

	Total variance	Components of variance as percent of total variance: Among tuff units (s_α^2)	Among stations (s_β^2)	Among samples (s_γ^2)	Among splits (s_δ^2)	Variance ratios V_m
	(g/cm³)²					
Bulk density	0.057	0	*55	----- [1]45	----	4.89
Powder density	.007	0	*27	56	17	1.48
	(percent)²					
Porosity	97.9	0	*51	----- [1]49	----	4.16
Log clinoptilolite	.348	11	*60	29	<1	8.28
Log quartz	.126	0	*79	18	3	15.05
Log α-cristobalite	.128	0	*65	21	14	7.43
Log potassium feldspar	.084	0	*59	25	16	5.76
Log glass	.096	1	*73	22	4	11.23
SiO_2	24.1	3	*25	19	53	1.39
Al_2O_3	1.113	1	*30	42	27	1.74
Fe O_3	.038	0	*54	39	7	4.70
Log MgO	.051	5	*50	42	3	4.44
Log CaO	.050	*17	*17	66	<1	1.03
Na_2O	.589	0	*63	32	5	6.81
K_2O	1.045	0	*43	56	1	3.02
Log CO_2	.561	*10	*31	53	6	2.10
Log Cl	.164	0	*33	52	15	1.97
Log F	.147	1	*61	30	8	6.42
	(ppm)²					
Log Cs	.074	0	*71	26	3	9.79
Log Li	.066	0	*55	43	2	4.89
Rb	11,920	0	*52	0	48	4.33
eU	121	0	*29	28	43	1.63
Log Ba	.080	3	*66	30	1	8.52
Log Be	.085	0	*87	9	4	26.77
Log Cr	.033	0	*38	49	13	2.45
Log Cu	.016	4	*10	0	86	.47
Log Ga	.003	10	*50	23	17	5.00
Log Mn	.066	0	*43	53	4	3.02
Log Nb	.028	*27	*54	7	12	11.37
Log Pb	.015	*7	*12	29	52	.59
Log Sr	.099	1	*56	35	8	5.21
Log Ti	.026	*16	*61	20	3	10.61
Log Y	.013	7	*66	19	8	9.78
Log Zr	.002	0	*24	60	16	1.26

[1]Variance component among samples plus component among splits.

of which 19 percent is due to differences among samples (sampling error) and 53 percent is due to laboratory error. Only 25 percent of the variance in the data is left to geographic effects (s_β^2), and the question arises as to whether this 25 percent can be used to define a trend in the presence of so much noise. In the case of Cu and Pb, the among-stations component accounts for only 10 and 12 percent of the variance, respectively. All the useful information regarding abundance of Cu and Pb is in table 2.

GEOGRAPHIC VARIATION

Regional patterns, or trends, are of special interest in the present study because they may represent the effects of important petrologic processes, such as the beryllium-fluorite mineralization at Spor Mountain, and diagenetic alteration. The geographic distribution of each variable is summarized on maps in figures 5–40. Only presence or absence is noted for the minerals calcite, fluorite, and halite (figs. 13 and 14). Distribution of all other variables is summarized by symbols for the arithmetic or geometric mean at each sampling station.

The potential for definition of geographic variation was estimated by computing V_m, the ratio of the among-stations variance to the variance of the station mean (table 3), as described by Connor, Feder, Erdman, and Tidball (1972). In general, V_m values below about 1.00 indicate that the error in any station mean based on four samples is so high that comparisons among stations may be unreliable, and further sampling at each station is necessary if stable maps are to be constructed. Values of V_m above 1.00 indicate greater potential for constructing stable maps. It is evident that maps of Cu and Pb and perhaps powder density, SiO_2, Al_2O_3, CaO, and Zr would not be expected to reliably show geographic variation because the error of the station mean is relatively high. Bulk density, porosity, clinoptilolite, quartz, α-cristobalite, potassium feldspar, glass, Fe_TO_3, MgO, Na_2O, F, Cs, Li, Rb, Ba, Be, Ga, Nb, Sr, Ti, and Y all show reasonably high ratios (4.0 or higher), suggesting a high potential for defining geographic variation.

The relative strength of the trends fitted to the data is presented in table 4. Random effects can also give rise to weak trends, and Howarth (1967) considered that reductions in the percent sum of squares smaller than 6.0, 12.0, and 16.2 for linear, quadratic, and cubic surfaces respectively can be taken as an upper limit for trends that may arise by accident. In the present study, data for powder density, α-cristobalite, SiO_2, Al_2O_3, Fe_TO_3, K_2O, Cl, Cr, Cu, and Zr showed weak trends which could be due to noise of various kinds. Either linear, quadratic, or cubic trends for the remaining variables account for sufficiently large percentage reductions of the sum of squares to suggest that the trends are real.

Another method of evaluating trend surfaces is by analysis of variance of the sums of squares (Krumbein and Graybill, 1965, p. 333–337). This method was applied and the percent reduction values marked by asterisks (*) in table 4 indicate those surfaces which result in a significant (0.05 level) reduction of the sum of squares. Both Howarth's (1967) limits and analysis of variance were used to select trend surfaces for mapping in figures 5–40. Only variables having surfaces which exceed Howarth's limits were considered for mapping; the highest degree surface which shows a significant reduction in the sum of squares was chosen as the best representation of the regional trend.

TABLE 4. — *Sum of squares of the deviations from the mean and percent reduction of sum of squares by polynomial surfaces of degree 1 through 5 fitted to data on physical properties, mineral composition, and chemical composition of 160 samples of water-laid tuff*

[Italic indicates percent reduction of sum of squares above Howarth's (1967) limits for random data (linear, quadratic, and cubic surfaces only). Asterisk (*) indicates significant reduction of the sum of squares (0.05 level). Leaders (– –) indicate no surface fitted to data because of significant among-tuff units variance component]

	Sum of squares	Cumulative percent reduction of sum of squares				
		Linear	Quadratic	Cubic	Quartic	Quintic
	(g/cm³)²					
Bulk density	8.920	1	*17	*23	26	29
Powder density	1.140	*5	7	*15	20	20
	(percent)²					
Porosity	15,380	1	*19	*24	25	28
Log clinoptilolite	55.34	*5	*18	*27	31	32
Log quartz	20.11	0	*16	*47	*54	57
Log α-cristobalite	20.37	0	3	*11	13	17
Log potassium feldspar	13.32	1	4	*17	*27	30
Log glass	15.26	3	*17	*23	28	32
SiO_2	3,834	*5	8	12	14	18
Al_2O_3	177.	1	*11	15	21	22
Fe_TO_3	5.999	*6	8	12	13	14
Log MgO	8.182	*12	16	20	22	*29
Log CaO	7.967	– – –	– – –	– – –	– – –	– – –
Na_2O	93.69	*8	*17	*25	*39	41
K_2O	166.1	0	2	*10	14	16
Log CO_2	59.33	– – –	– – –	– – –	– – –	– – –
Log Cl	26.02	1	3	*13	16	18
Log F	23.40	*13	15	*32	*37	39
	(ppm)²					
Log Cs	11.81	*14	*24	*40	*47	47
Log Li	10.51	*18	20	*35	*40	40
Rb	1.895×10^6	*8	12	*22	23	28
eU	19,300	*4	*9	*20	21	22
Log Ba	12.71	*19	22	*31	32	*38
Log Be	13.46	*20	*25	*39	40	*46
Log Cr	6.463	0	*8	11	12	*20
Log Cu	2.517	*4	7	9	10	16
Log Ga	.425	*19	*30	*37	*45	49
Log Mn	10.48	*5	*10	*17	*23	23
Log Nb	4.914	– – –	– – –	– – –	– – –	– – –
Log Pb	2.931	– – –	– – –	– – –	– – –	– – –
Log Sr	15.69	2	3	*18	23	26
Log Ti	4.123	– – –	– – –	– – –	– – –	– – –
Log Y	2.077	*6	*22	*32	35	*42
Log Zr	.285	0	1	5	10	15

Polynomial trend surfaces provide an objective method for studying the nature of geographic variation. Methods of least-squares surface fitting are discribed by Krumbein and Graybill (1965, p. 319–340). Trend surfaces of degrees 1 through 5 were fitted to data for all variables except those which show significant differences among tuff units. The model for the 5th degree polynomial is:

$$\hat{x}_{ij}=\beta_{00}+\beta_{10}U_i+\beta_{01}V_j+\beta_{20}U_i^2 +\beta_{11}U_iV_j+\beta_{02}V_j^2+\ \ldots\ +\beta_{05}V_j^5,$$

where $\hat{x}_{ij}$ is the predicted value of some variable observed in the sample collected at map coordinates (U_i, V_j). $\hat{x}_{ij}$ has the structure $x_{ij}=\hat{x}_{ij}+e_{ij}$, where x_{ij} is the observed

value and e_{ij} is the residual. β_{00}, β_{10}, . . ., β_{05} are the numerical coefficients chosen to minimize the variance of e_{ij}. For polynomials of lesser degree, the number of coefficients and terms is accordingly fewer. Thus it is possible to partition the variance into two parts: (1) that due to a regional trend as expressed by a polynomial equation and (2) that due to local variation (the residual). The proportion of variance explained by the trend should not exceed that due to the among-stations variance component listed in table 3.

PETROGENESIS

PROBLEMS IN PETROGENETIC INTERPRETATION

Assessment of mineral and chemical changes in terms of gains and losses is complicated by the expression of petrologic data in terms of percent or parts per million. One aspect of this problem is the interpretation of a proportionate increase in one or more constituents. For example, fluorine is thought to be introduced into the tuff by mineralization at Spor Mountain. Fluorine in the tuff ranges from 0.02 to more than 2 percent, a hundredfold increase. The concentration of fluorine is always expressed as a complex ratio,

$$\frac{\text{Weight F}}{\text{Weight all constituents}} \times 100,$$

and an increase in weight percent fluorine can be interpreted only as an increase in the ratio of that constituent to the sum of all other constituents. Either fluorine was actually added to the rock (as seems probable) or the other constituents were removed from the rock to leave a residue enriched in fluorine. In some cases it may be difficult to choose between addition or residual enrichment.

Another aspect of the gain-loss problem is the potential effect of bulk density and volume changes (Hemley and Jones, 1964). For example, the alteration of porous tuff may result in an equal volume of less porous rock with chemical gains required to account for filling of the pore spaces. Chemical gains or exchanges of a light element by a heavy element are also required if the powder density of a rock is increased by alteration. In both cases the volume has remained the same but the mass (bulk density) has increased. If compaction has accompanied alteration, however, the resulting volume decrease also must be taken into account (Cooper, 1957). Changes in bulk density and porosity have been mapped in the tuff of the Thomas Range (figs. 5 and 7), but it is not clear whether the changes are due to addition of mass by filling pore spaces or to decrease in pore space by compaction. The latter possibility is difficult to quantify from thin-section observation because of partial destruction of the original pyroclastic texture. No alternative exists except to interpret mineralogical and chemical changes as changes in ratio.

The effect of percentage and parts per million data also complicates the interpretation of correlation between minerals or elements. It is common to assume that two elements that are strongly correlated have the same origin and that two elements that are uncorrelated have independent origins. An important constraint on such interpretation arises from the effect of closure (Chayes, 1960). Data on mineral and chemical constituents form two groups of variables, each of which sum to 100 percent under ideal conditions. Laboratory error and omission of H_2O are responsible in the present case for deviations from a constant sum; nevertheless, each mineral and element is part of a closed array that should sum to 100 percent. For example, when one major constituent increases in a two-component closed array, the other must decrease, and a perfect negative correlation results. Effects of closure are more complex and difficult to predict as the number of constituents increases. At present there appears to be no solution to the problem of closure in percentage data (Miesch, 1969), although the problem has been sidestepped by examining correlations between simple ratios, such as element/oxygen or element/silicon (Miesch and others, 1966). In the present study an attempt has been made to recognize the obvious effects of closure in the covariation among major constituents (such as glass versus zeolite and SiO_2 versus CaO).

A PETROGENETIC MODEL

The petrogenesis of the water-laid tuff may be understood in terms of a model. The model must contain those processes, or factors, believed to be important in creating the observed variation in the mineral and chemical composition of the tuff. A general model may be stated as follows:

$$x_{ji} = \alpha_{j1} F_{1i} + \alpha_{j2} F_{2i} + \ldots + \alpha_{jp} F_{pi} + \alpha_j U_{ji},$$

where x_{ji} is the value of the ith sample for the jth variable and is a linear function of p common factors (F). Each factor (F) operates with an intensity of the coefficients α_{j1}, α_{j2}, . . ., α_{jp}, and U_{ji} is a unique factor accounting for the remaining variation in the data (Cooley and Lohnes, 1962, p. 160).

The identity of some of the factors can be easily anticipated from prior knowledge about the nature and proximity of processes known to have acted upon the tuff. The factors of mineralization, zeolitization, potassium feldspar diagenesis, and perhaps concentration of detrital components should be among the most intense. Variables that show geographic trends in the water-laid tuff reveal the obvious effects of these factors: large halos of F, Cs, Li, Be, Ga, and Nb (figs. 24, 25, 26, 30, 32, and 35) surround the Spor Mountain beryllium-fluorspar district and indicate the influence of mineralization; the distribution of glass, clinoptilolite, and potassium feldspar (figs. 4, 8, 11, and 12) indicates the influence of

zeolitization and feldspathization; and the concentration of calcite in tuff unit 5 suggests the influence of additional detrital and diagenetic factors.

R-MODE FACTOR ANALYSIS

Petrogenetic parameters (α's, F's) in the model may be defined by various methods. A common method and the one employed in this study is known as R-mode factor analysis; detailed discussions were presented by Harman (1960), Cooley and Lohnes (1962, p. 151–172), and Miesch, Chao, and Cuttitta (1966). The method involves four major steps:

1. An $m \times m$ correlation matrix (R-matrix) is computed, where m is the number of measured variables.
2. The characteristic equation associated with the R-matrix is solved for m roots (eigenvalues) and the number of large roots (p) is selected as the minimum number necessary to account for a major part of the total variance in the system.
3. A provisional coefficient matrix (the factor loadings) used to define the principal components is computed.
4. A final coefficient matrix defined by the Varimax criterion (Harman, 1960, p. 301) is derived from the factor-loadings matrix. The Varimax loadings are arbitrarily used as the α-coefficients in the model.

The data matrix, x_{ij}, is N by m in size where N is the number of samples and m is the number of variables. The degree of linear association between two variables j and k is measured by the correlation coefficient:

$$r_{jk}=\frac{s_{jk}}{\sqrt{s_j^2 s_k^2}},$$

where s_{jk}, the convariance, is computed by

$$s_{jk}=\frac{\sum_{i=1}^{N} x_{ij} x_{ik}}{N}-\bar{x}_j \bar{x}_k,$$

and $s_j{}^2$, the variance, is computed by

$$s_j{}^2=\frac{\sum_{i=1}^{N} x^2{}_{ij}}{N}-\bar{x}_j{}^2.$$

Linear covariation between the variables is expressed by the $m \times m$ matrix of correlation coefficients, or R-matrix. A correlation coefficient of $r=1.0$ indicates perfect linear interdependence, $r=0$ indicates no linear dependence, and $r=-1.0$ indicates perfect inverse linear dependence. Because the genetic significance of the correlation coefficients is subject to the restrictions of closure, the correlation coefficients between the petrologic variables in this study must be viewed as descriptive measures of covariation.

Factor analysis commonly begins with principal components extraction. Such analysis may be understood in terms of m-dimensional space, where m is the number of original variables. Each variable defines a dimension in the m-space and the position of each of N samples can be plotted in terms of the m coordinates. Presumably the N samples will tend to cluster as an elongate swarm of points in the m-space. The object of the principal component analysis is to find new uncorrelated variables which measure what the original variables have in common and which produce a maximum variance among samples. The first principal component is located along the major axis of the sample cluster so that the sample projections onto it are maximized. This axis is a new variable which describes the largest possible proportion of the variance. A second axis is located at right angles to the first so that the next largest proportion of variance is explained, and so on. As many as m axes are possible, but some number $p<m$ will commonly account for most of the variance. The variances of the principal components are equal to their eigenvalues. The principal components, following standardization to unit variance, are related to original variables by a new set of coefficients, the factor loadings.

If some number $p<m$ axes accounts for most of the variance (that is, the N points occur largely in p-dimensional space), it is often desirable to rotate the p axes so that they may be more readily interpreted. Rotation may be done in any manner that facilitates interpretation, but the most commonly used objective method of rotation utilizes the Varimax criterion (Harman, 1960, p. 301). The Varimax criterion requires that the variance of the squared factor loadings be maximized and this tends to simplify the resulting factors by yielding large positive or negative loadings for only a few variables on each factor. The rest of the loadings in each factor tend to be near zero. The resulting close association of a few variables with the Varimax factors will allow the factors to be more readily interpreted. The Varimax loadings specify the relationship of the original variables to the Varimax axes (factors); the axes may be used as a reference system to plot the original variables as vectors. If the sum of the first p eigenvalues of the R-matrix approaches m, the cosines of the angles between vectors in the p-space will approximate the original correlation coefficients.

Because only $p<m$ axes are retained in the model, less than 100 percent of the total variance will be explained. The proportion of variance explained for each variable in the factor solution is termed its "communality" (h^2). Geometrically, the square of the vector length of the original variable plotted in the p-space of the factor solution will be equal to h^2. The remaining, unexplained variance ($1-h^2$) is termed the unique component; it consists of unrecognized factors and laboratory error.

FACTOR ANALYSIS OF WATER-LAID TUFF DATA

Correlation coefficients were calculated between all variables for which more than 30 percent of the data

TABLE 5. — *Correlation coefficients based on analyses of 160 samples of water-laid tuff*

Variable	Powder density	Log clinoptilolite	Log quartz	Log α-cristobalite	Log potassium feldspar	Log glass	SiO_2	Al_2O_3	Fe_TO_3	Log MgO	Log CaO	Na_2O	K_2O	Log CO_2	Log Cl
Bulk density	0.14	0.37	0.25	0.38	0.47	−0.62	0.24	−0.30	−0.07	−0.04	−0.09	−0.23	0.01	−0.32	−0.01
Powder density		−.20	.25	.06	.42	−.01	.00	.11	.13	−.09	.12	.12	.38	.12	.00
Log clinoptilolite			.29	.05	.16	−.78	.00	−.31	−.01	.13	−.08	−.53	−.22	−.39	−.01
Log quartz				−.10	.44	−.33	.13	−.17	.06	−.05	−.09	−.25	.11	−.20	.08
Log α-cristobalite					.45	−.32	.23	−.08	.04	.01	−.12	.14	−.05	−.15	.01
Log potassium feldspar						−.47	.21	.04	.16	−.18	−.28	.04	.49	−.29	.16
Log glass							−.01	.31	−.07	−.18	.04	.49	.13	.36	−.03
SiO_2								.00	−.35	−.40	−.60	.01	.10	−.46	.04
Al_2O_3									.20	.04	−.18	.35	.22	−.03	.11
Fe_TO_3										.50	.09	.11	.12	.01	.07
Log MgO											.26	−.20	−.32	.06	.11
Log CaO												−.10	−.28	.71	−.11
Na_2O													.35	.09	.22
K_2O														−.05	.07
Log CO_2															−.16

Variable	Log F	Log Cs	Log Li	Rb	eU	Log Ba	Log Be	Log Cr	Log Cu	Log Ga	Log Mn	Log Nb	Log Pb	Log Sr	Log Ti	Log Y	Log Zr
Bulk density	0.02	−0.03	−0.06	0.01	−0.09	−0.03	0.24	−0.09	0.03	−0.16	−0.18	0.15	−0.20	0.12	−0.26	0.18	−0.03
Powder density	.15	−.06	.03	.16	.17	.12	.04	.07	.11	−.06	.11	−.15	−.13	−.08	.21	−.04	−.04
Log clinoptilolite	−.24	.03	−.05	−.18	−.46	.07	.06	.12	−.12	−.18	−.26	.00	−.18	.47	−.21	.08	−.14
Log quartz	−.03	−.02	.08	−.06	−.02	.25	.07	.26	−.07	−.10	−.13	−.13	−.28	.12	.07	.00	−.15
Log α-cristobalite	.02	.06	−.10	−.13	−.10	−.04	.15	−.14	.05	−.01	−.06	.20	.01	.12	−.21	.26	.01
Log potassium feldspar	.00	−.06	−.04	.20	.17	.16	.15	−.06	−.08	−.08	.03	−.01	−.19	−.02	.04	−.03	−.04
Log glass	.13	.03	.00	.12	.40	−.08	−.13	−.10	.07	.24	.26	−.05	.20	−.31	.16	−.12	.00
SiO_2	.00	−.15	−.26	−.02	.16	−.01	.05	−.29	−.03	.06	−.21	.14	.10	−.03	−.22	−.05	−.15
Al_2O_3	.12	.10	.06	.21	.25	−.03	.08	−.10	.00	.37	.32	.12	.23	−.13	.19	−.11	.22
Fe_TO_3	−.07	.19	.28	−.08	−.11	.19	.11	.33	.10	.13	.28	.01	−.08	.17	.32	.14	.34
Log MgO	.03	.33	.49	−.11	−.39	.00	.21	.36	.00	.17	−.01	.29	−.01	.15	−.01	.20	.22
Log CaO	.17	.10	.16	−.16	−.20	.18	−.07	.47	.29	−.19	.11	−.20	−.18	.06	.23	.08	.12
Na_2O	.25	.19	.06	.36	.42	−.24	.19	−.33	−.07	.27	.60	.03	.18	−.19	.10	.07	.00
K_2O	.05	−.21	−.01	.55	.63	.09	−.02	−.22	−.11	.00	.28	−.19	−.10	−.34	.25	−.25	.00
Log CO_2	−.01	−.10	.03	−.07	.06	.10	−.25	.23	.26	−.15	.19	−.20	.00	−.15	.26	.00	.18
Log Cl	.21	.28	.21	.14	.01	−.08	.10	−.03	−.07	.20	.12	.18	.01	−.08	−.12	.03	.07
Log F		.45	.49	.40	.27	−.23	.51	.01	.00	.40	.18	.33	.14	−.35	−.21	.19	−.06
Log Cs			.42	.25	−.09	−.30	.61	.00	−.13	.58	.19	.46	.14	.18	−.42	.42	−.18
Log Li				.28	.06	−.08	.56	.22	−.10	.44	.19	.41	.12	−.13	−.17	.34	.01
Rb					.49	−.34	.43	−.29	−.21	.33	.25	.26	.11	−.40	−.20	.09	−.18
eU						−.07	.04	−.28	−.14	.11	.26	−.04	.08	−.45	.13	−.14	−.04
Log Ba							−.41	.50	.28	−.42	−.03	−.58	−.27	.09	.63	−.38	.10
Log Be								−.11	−.18	.67	.11	.66	.17	.10	−.55	.54	−.18
Log Cr									.25	−.12	−.08	−.23	−.27	.06	.43	−.06	.11
Log Cu										−.09	−.02	−.11	−.07	.06	.21	−.04	.20
Log Ga											.18	.68	.44	.05	−.45	.40	−.06
Log Mn												−.01	.24	−.08	.16	.12	.12
Log Nb													.32	.05	−.71	.51	.06
Log Pb														−.07	−.20	.10	−.07
Log Sr															−.14	.12	−.03
Log Ti																−.53	.32
Log Y																	.02

were above the detection limit (table 5). In addition, the variable "glass" was also included because it proved helpful in interpreting relationships. Thus clay, mica, calcite, halite, fluorite, B, La, Mo, Ni, Sn, and V were not included in the analysis because more than 30 percent of the samples fell below the detection limit for those variables. Porosity was also dropped because it is derived directly from other variables. As before, a log transformation was made on those variables that tend to be log normally distributed prior to calculation of the *R*-matrix.

A principal-components analysis of the water-laid tuff data was carried out on the 33×33 *R*-matrix with unities in the diagonals. Selection of the *p* largest principal components to be preserved for rotation and interpretation proved to be somewhat subjective. The eigenvalues of the 10 largest principal components were plotted on a curve and examined for significant changes in magnitude, as indicated by breaks in the slope of the curve (fig. 41). Visible declines occur after the fourth and sixth eigenvalues, suggesting that either four or six principal components might be considered for rotation. Various experiments were then conducted by Varimax rotation of four, five, six, and seven axes; the communalities of the variables for each solution were compared with the percentage of nonerror variance calculated from table 3 (table 6). Study of the eigenvalues and the communalities for four through seven-factor solutions suggests that the six-factor solution is the most suitable choice. The four-factor solution explains only 52 percent of the total variance in the normalized data, whereas the six-factor solution explains 63 percent. Additionally, the communalities of some variables, notably bulk density, powder density, quartz, α-cristobalite, Al_2O_3, Fe_TO_3, CaO, CO_2, F, Mn, Sr, and Zr, are considerably increased in the six-factor solution. The communalities of powder density, quartz, Cl, F, Ba, Mn, Sr, Y, and Zr are still low, however, and this is due mainly to the tendency of these variables to load heavily on unique components. As can be seen by comparison of the communalities with the proportion of nonerror variance, the six-factor solution explains the maximum

amount of meaningful variance in the case of many variables. Copper, for example, has a communality of 32 percent and a nonerror variance component of only 14 percent; this fact indicates that the six-factor solution is "explaining" some error variance in copper.

Six principal components were rotated by the Varimax method and the loadings of each variable on the six Varimax factors were recorded (table 7); the Varimax loadings may be accepted as the α-coefficients of the petrogenetic model. Each factor ($F_1, F_2, \ldots, F_P$) can be interpreted from the association of variables which load most heavily on it. The factor interpretations are as follows:

Factor I (F_1): Mineralization. Fluorine, Y, Li, Ga, Cs, Nb, Be, and to a lesser extent MgO and Rb have high positive loadings. Titanium and Ba have high negative loadings.

Factor II (F_2): Initial diagenesis (zeolitization). Strontium, clinoptilolite, and to a lesser extent MgO have high positive loadings. Sodium oxide, Rb, K_2O, eU, and to a lesser extent F, powder density, glass, and Mn have high negative loadings.

Factor III (F_3): Concentration of calcite versus silica (both detrital and diagenetic). Calcium oxide, CO_2, Cr, and Cu have high positive loadings. Silica has a high negative loading.

Factor IV (F_4): Intermediate diagenesis (zeolitization and feldspathization). Clinoptilolite, potassium feldspar, quartz, and to a lesser extent Ba, Cr, and bulk density have high positive loadings. Glass, Pb, and to a lesser extent Na_2O have high negative loadings.

Factor V (F_5): Concentration of detrital heavy minerals. Zirconium, Al_2O_3, Fe_TO_3, and to a lesser extent Ti, MgO and Mn have high positive loadings.

Factor VI (F_6): advanced diagenesis (feldspathization). Potassium feldspar, α-cristobalite, and bulk density have high positive loadings.

It can thus be concluded that the petrogenetic model for the water-laid tuff is substantially as proposed earlier. Mineralization augments the concentration of F, Cs, Li, Be, Ga, Nb, Y, and to a lesser extent MgO and Rb relative to the concentration of Ba and Ti. The increase of some mineralization-related elements is orders of magnitude above background, indicating that these elements were actually added to the tuff rather than enriched by subtraction of other constituents. This is in agreement with the observed enrichment of the same elements in hydrothermally altered tuff associated with the beryllium ore at Spor Mountain (Lindsey and others, 1973).

Diagenetic effects appear as three distinct factors: (1) initial diagenesis (zeolitization) is represented by factor II, (2) intermediate diagenesis (zeolitization and feldspathization) is represented by factor IV, and (3) advanced diagenesis (feldspathization) is represented by factor VI. Factors II and IV mainly reflect the effects of closure induced by variations in the relative proportions of glass versus clinoptilolite and potassium feldspar. Nevertheless, they do describe the process whereby glass is altered first to clinoptilolite and finally to potassium feldspar; this diagenetic sequence has been observed in other tuffs and ascribed to ground water leaching of glass (Hay, 1963). The three-part division of diagenesis also suggests a sequence of chemical changes as the tuff undergoes diagenetic alteration. During the initial stage of diagenesis (factor II) the concentrations of Na_2O, K_2O, Rb, eU, and to a lesser extent F and Mn decline while Sr and to a lesser extent MgO increase. The concentration of Na_2O declines further and is accompanied by a decline in Pb during the intermediate stage of diagenesis. Barium and Cr show some increase. Advanced diagenesis is not accompanied by any substantial chemical change. It must be remembered that the changes in chemical concentrations are only relative to the sum of all constituents and do not necessarily indicate true addition or subtraction of elements to the tuff.

Factor III represents the concentration of calcite relative to that of silica and as such reflects closure almost entirely. The complementary concentrations of calcite and silica can be related to the presence of limestone clasts and calcite cement in some of the tuff. Thus factor III reflects both detrital and diagenetic processes.

TABLE 6. — *Communalities (in percent) for four-, five-, six-, and seven-factor Varimax solutions compared to the percent of nonerror variance*

	Number of rotated factors				Nonerror variance
	4	5	6	7	
Bulk density	52	55	70	70	?
Powder density	38	42	47	48	83
Log clinoptilolite	65	65	71	78	>99
Log quartz	42	45	55	56	97
Log α-cristobalite	19	24	67	68	86
Log potassium feldspar	80	81	84	84	84
Log glass	77	77	78	80	96
SiO_2	51	53	53	76	47
Al_2O_3	30	55	56	58	73
Fe_TO_3	50	73	73	75	93
Log MgO	60	63	65	65	97
Log CaO	58	78	85	86	>99
Na_2O	56	60	66	71	95
K_2O	76	76	76	79	99
Log CO_2	50	62	75	76	94
Log Cl	14	16	19	20	85
Log F	42	58	58	69	92
Log Cs	61	61	62	62	97
Log Li	60	63	69	71	98
Rb	56	64	66	70	52
eU	65	68	68	68	57
Log Ba	58	59	61	67	99
Log Be	79	80	80	80	96
Log Cr	60	62	66	74	87
Log Cu	16	16	32	53	14
Log Ga	69	72	74	78	83
Log Mn	40	45	47	61	96
Log Nb	74	75	76	80	88
Log Pb	33	39	39	39	48
Log Sr	34	45	46	52	92
Log Ti	81	85	86	86	97
Log Y	47	48	59	60	92
Log Zr	15	34	41	43	84

Factor V is interpreted as concentration of detrital heavy minerals. Examination of the heavy mineral suite in the water-laid tuff indicates that magnetite, hematite, sphene, topaz, and zircon are among those minerals present. Concentrations of some of these minerals would account for high loadings of Fe_TO_3, Al_2O_3, Mn, Ti, and Zr on factor V.

The six-factor model does not account for a large component of variance for a few variables. Chlorine is very poorly explained by the model; powder density, quartz, F, Ba, Mn, Sr, Y, and Zr also contain large unique components. Further explanation of each of these variables would require addition of unique factors to the model. The identity of the factor for concentration of Cl can be inferred from the following evidence. The chlorine is water-soluble, inasmuch as it was extracted for analysis by adding pure water to the sample; X-ray diffraction confirms the presence of halite in samples with large concentrations of Cl. Another point which may be pertinent is that all of the samples were collected from surface exposures. It seems likely that the distribution of Cl is determined by winds that bring salt off playas to the west and deposit it on outcrops of tuff in the Thomas Range. Rainwater dissolves the salt and percolates down into the porous tuff, precipitating Cl as halite within pore spaces. Identification of the unique factors that control concentration of other variables probably requires additional information and therefore will not be pursued.

INTERPRETATION OF STRATIGRAPHIC AND GEOGRAPHIC ANOMALIES

The factors that outline a petrogenetic model for formation of the water-laid tuff can be related back to the stratigraphic and geographic concentrations seen in figures 5–40. Each factor, if it is the equivalent to one or only a few processes, should have a characteristic pattern of concentration. Variables that tend to split their loadings on several factors should exhibit more complex patterns resulting from superposition of factor effects. Variables that are related to unique factors will have patterns determined by the regional effects of the unique factor. In practice, of course, the three categories will form a continuum, with some variables tending to load on a single factor, others on several, and still others on a unique factor.

The mineralization factor would be expected to produce a halo around ore deposits; halos of varying intensity for F, Cs, Li, Be, Ga, Nb, and Y are seen in figures 24, 25, 26, 30, 32, 35, and 39, respectively. Fluorine and yttrium (figs. 24 and 39), however, vary from the mineralization halo, and this fact can be related to their tendency load on factors II and VI, respectively (table 7). Barium (fig. 29), whose distribution is negatively affected by mineralization, shows a reverse halo. Titanium (fig. 37) does not show a pronounced geographic trend, presumably because it reflects the concentration of detrital heavy minerals (factor V).

TABLE 7. — *A six-factor petrogenetic model for the water-laid tuff as defined by the Varimax loadings*

[Coefficients less than −0.50 or greater then 0.50 are shown in italic]

Variable	Factor I	II	III	IV	V	VI
Log Ti	*−0.65*	−0.21	0.26	0.18	0.47	−0.23
Log Ba	−.54	.05	.17	.42	.29	−.12
Log Cl	.27	−.10	−.19	.09	.22	−.07
Log F	*.59*	−.41	.19	.03	−.10	−.04
Log Y	*.63*	.17	.14	−.10	−.02	.34
Log Li	*.69*	−.09	.20	.21	.20	−.25
Log Ga	*.74*	−.09	−.22	−.28	.19	−.11
Log Cs	*.77*	.06	.03	−.02	.11	−.07
Log Nb	*.77*	.13	−.20	−.24	−.01	.18
Log Be	*.86*	−.08	−.10	.09	.00	.15
Log Sr	.02	*.61*	−.08	.07	.16	.18
Log clinoptilolite	.04	*.59*	−.24	*.50*	−.15	.07
Log MgO	.40	.43	.27	.13	.42	−.16
Powder density	−.04	−.47	.18	.35	.13	.26
Na_2O	.14	*−.59*	−.04	−.41	.30	.13
Rb	.43	*−.65*	−.15	.05	−.10	−.08
K_2O	−.15	*−.76*	−.25	.23	.18	.04
eU	−.02	*−.80*	−.15	−.09	−.03	−.06
Log CaO	.02	.07	*.91*	.06	−.01	−.06
Log CO_2	−.14	−.17	*.79*	−.23	.00	−.05
Log Cr	−.07	.24	.49	.44	.26	−.28
Log Cu	−.21	.07	.42	−.08	.15	.23
SiO_2	−.11	−.08	*−.61*	−.05	−.24	.26
Log glass	−.07	−.44	.15	*−.62*	.06	−.39
Log Pb	.25	−.02	−.20	*−.51*	.05	−.07
Log potassium feldspar	−.02	−.31	−.31	*.57*	.18	*.52*
Log quartz	.00	−.01	−.14	*.72*	−.03	−.04
Log Mn	.15	−.40	.12	−.20	.46	.01
Log Zr	−.15	.09	.18	−.15	*.54*	.14
Al_2O_3	.07	−.29	−.23	−.28	*.56*	−.14
Fe_TO_3	.13	.09	.14	.20	*.80*	.01
Log α-cristobalite	.07	.08	−.07	−.03	.08	*.80*
Bulk density	.10	.09	−.08	.43	−.23	*.65*

The geographic effects of the factors for diagenesis (II, IV, and VI) are best represented by the geographic distribution of clinoptilolite (fig. 8) and potassium feldspar (fig. 11), which together display a pattern of concentration very nearly complementary to that of glass (fig. 12). Glass shows a northwest-trending low across the study area. Elements that tend to associate most with glass on factors II and IV are the alkalis (Na_2O, K_2O, and Rb), eU, and Pb (figs. 20, 21, 27, and 28). Sodium oxide, Rb, and eU trends best follow that of glass; K_2O and Pb have no strong regional trend. Strontium does not show a trend similar to that of clinoptilolite because it is also related to a unique factor. The end product of diagenesis, indicated by factors IV and VI, is a dense tuff composed of potassium feldspar, quartz, and α-cristobalite. The high bulk density (fig. 5) and abundant potassium feldspar (fig. 11) and quartz (fig. 9) in the region northeast of The Dell indicate that this is the locus of most intense diagenesis.

The distribution of calcite versus silica (factor III) is affected mainly by the presence of abundant limestone clasts in tuff unit 5 on Topaz Mountain (figs. 13, 19, 22). Alumina, Fe_TO_3, and Zr (figs. 16, 17, 40), which group together on the factor for concentration of detrital heavy minerals (factor V), tend not to form strong geographic trends but rather to be sporadically dispersed in local (1–2 miles or 1.6–3.2 km) concentrations.

CONCLUSIONS

MINERALIZATION HALOS

Study of the mineral and chemical components of the water-laid tuff has shown that the beryllium-fluorite mineralization at Spor Mountain has left a distinct geochemical signature in the tuff. This is identified by the association of F, Cs, Li, Be, Ga, Nb, and Y. Most of these elements tend to form primary dispersion halos around the Spor Mountain district.

The association of elements appears to be a sensitive indicator of the elements concentrated in hydrothermally altered tuff near the beryllium deposits. Comparison of mineralized versus unmineralized tuff showed that Cs, Li, Rb, Tl, eU, B, Be, Ga, La, Mn, Nb, Sc, Sn, Y, and Zn are at least twice as abundant in mineralized tuff (Lindsey and others, 1973, p. A9). All of the elements concentrated by the mineralization factor were also concentrated in hydrothermally altered tuff associated with deposits at Spor Mountain. Identification of this mineralization factor in other tuffaceous rocks should indicate the proximity of beryllium and fluorspar deposits. This approach could have considerable application in the Basin and Range province, where basin fillings of tuffaceous sediments are widespread.

The mineralization-related halos increase the target size which might be contemplated in searching for another Spor Mountain district. The Spor Mountain district presents a target of approximately 20 square miles (52 km^2); if the halos for beryllium and cesium were extended completely around the district, they would triple the original target to about 60 square miles (156 km^2). The use of this method as a guide to mineralization may be illustrated in the case of the small halo in the northeastern edge of the study area; that halo may indicate another mineralized area located to the northeast, beneath the alluvium of Dugway Valley.

Study of the petrogenetic model outlined by factor analysis (table 7) indicates that individual pathfinder elements for beryllium-fluorite mineralization must be selected with caution. It is tempting, for example, to use fluorine in tuff as a pathfinder for beryllium deposits because of the supposed mode of transport of beryllium as a fluoride complex ion. The model derived by factor analysis shows, however, that fluorine concentration was enhanced not only by mineralization but also by retention in glass which has survived zeolitization and perhaps by other, unidentified factors. This overprinting of fluorine concentration patterns by various processes has produced a complex regional picture of the distribution of fluorine in the water-laid tuff. Although the effect of mineralization is clearly discernible in the regional variation of fluorine (fig. 24), failure to consider the effect of other factors would lead to an erroneous prediction of the location of the Spor Mountain district. A more empirical choice for a pathfinder element is lithium, which exhibits a wider halo than beryllium or cesium but is closely associated with the mineralization factor. The distribution of lithium, however, is also affected by other factors (table 7). In addition, lithium occurs without beryllium in altered tuffaceous sediments at other localities in the Basin and Range province (Ames and others, 1958; Norton, 1965). Therefore it seems unwise to extend the application of lithium as a pathfinder beyond the Spor Mountain area. On the other hand, Be, Li, and F halos in schist have been found to be useful as indicators of molybdenum-beryllium mineralization in other geologic environments (Vlasov, 1966, p. 133–136).

The mechanisms responsible for the dispersion halos in tuff around Spor Mountain remain speculative, but some insight may be gained from the following observations. The trend surfaces of the halos demonstrate an approximate logarithmic decline in concentration of Cs, Li, and Be away from Spor Mountain, as seen by the even spacing of the logarithmic contour intervals (figs. 25, 26, and 30). The dispersion of mineralization elements was independent of host rock mineralogy and porosity, as shown by the petrogenetic model (table 7). This independence is also illustrated by comparison of the halos for Cs, Li, and Be (figs. 25, 26, and 30) with the distribution of mineral facies (fig. 4) and porosity (fig. 7) in the tuff. It is also pertinent that formation of zeolite and potassium feldspar, particularly the latter, are partially associated with increasing bulk density, and therefore decreasing porosity (table 7). If dispersion of mineralization elements occurred by fluid movement, their distribution should be associated with maximum porosity (the vitric facies). Because this is not the case, dispersion by static diffusion seems more likely. Diffusion of elements along a concentration gradient in interconnected water-filled pores in the tuff is envisioned. The logarithmic decline of the halos away from Spor Mountain is also in harmony with the static diffusion hypothesis. Although the scale of diffusion is much larger, the process is quite similar to that proposed for the Pb, Zn, and Cu dispersion halos noted in the wallrocks of veins in the Tintic district (Morris and Lovering, 1952, Pt. 2). Alternatively, it is possible that dispersion occurred prior to zeolitization and potassium feldspar diagenesis by fluid movement through vitric tuff having a uniform porosity.

DIAGENESIS

Three stages of diagenesis have been identified by factor analysis: zeolitization, both zeolitization and feldspathization, and feldspathization. Progressive alteration of vitric pumice-rich tuff to clinoptilolite and potassium feldspar is also suggested by the successive occurrence of these facies inward toward the center of the Thomas Range (fig. 4) and by thin-section study of mineral paragenesis. The mineral facies boundaries cut

across tuff units, as shown in the sections in figure 4, and by the low among-tuff-units variance components for various minerals (table 3). These relationships are similar to some of those observed in the Oligocene and Miocene John Day Formation (Hay, 1963), the Miocene and Pliocene Esmeralda Formation (Moiola, 1970), and the Pliocene Ricardo Formation (Sheppard and Gude, 1965), except that the distribution of the Thomas Range facies is inward instead of downward from the outcrop. In the examples cited it was concluded that groundwater leaching of vitric tuff yielded solutions having progressively greater alkali/hydrogen ion ratios which altered glass to clinoptilolite first and finally to potassium feldspar. A similar origin for the Thomas Range clinoptilolite and potassium feldspar facies is likely and accounts for the decline in concentration of alkalis noted during diagenesis of vitric tuff.

The petrogenetic model outlined by factor analysis reveals that diagenesis has played an important role in changing the chemical composition of the vitric tuff. Alteration of vitric to zeolitic tuff was accompanied by weight percent loss of Na_2O, K_2O, Rb, eU, Mn, and Pb, and by gain of MgO, Ba, Cr, and Sr. Fluorine concentration also declined during zeolitization, but this process was somewhat overshadowed by addition of fluorine during mineralization. The proportion of SiO_2 apparently was not affected by diagenesis. Although data are not available on water content of the samples used in this study, earlier work showed that the vitric tuff is hydrated (4–5 percent water) and that the zeolitic tuff may contain as much as 7–8 percent water (Lindsey and others, 1973, table 2). These conclusions are in general agreement with work on paired samples of glass and devitrified tuff, which showed that F, Cl, and U are lost during devitrification (Noble and others, 1967; Rosholt and others, 1971). Loss of Na_2O and K_2O has been noted in previous studies of the alteration of vitric tuff to clinoptilolite-rich tuff (Hay, 1963; Shepard and Gude, 1965; Hoover, 1968). Some of these studies reported that H_2O, CaO, and MgO are gained during zeolitization. I have found no evidence of any major oxide gains except perhaps MgO and H_2O. The observed increase in the trace elements Ba and Sr is probably due to the concentration of these elements in clinoptilolite (Hawkins, 1967a; 1967b). Further alteration to potassium feldspar was apparently isochemical. All of the chemical changes noted during diagenesis refer to relative changes in weight percent and do not necessarily indicate true addition or subtraction of constituents. In view of the proposed mechanism of alkali leaching, it seems probable that the alkalis actually were removed from the tuff.

The possibility of removal of U, Mn, and F from glass during zeolitization provides a nonhydrothermal source for these elements and raises the possibility of a diagenetic origin for nearby ore depostis that contain these constituents. The Spor Mountain beryllium deposits are of hydrothermal origin (Lindsey and others, 1973) and clear separation of mineralization and diagenetic factors in the petrogenetic model for water-laid tuff probably rules out a diagenetic source for uranium and fluorine in the beryllium deposits. Uranium leached from the vitric tuff may have been concentrated in sedimentary deposits, however, such as the nearby Yellow Chief uranium deposit described by Bowyer (1963). Evidence for large-scale leaching of uranium from tuff also supports the more general hypothesis of a volcanic origin for uranium in sedimentary deposits as proposed by Waters and Granger (1953).

REFERENCES CITED

American Society for Testing and Materials, 1966, Industrial water; atmospheric analysis, pt. 23 *of* 1966 book of ASTM standards: Philadelphia, 882 p.

Ames, L. L., Jr., Sand, L. B., and Goldich, S. S., 1958, A contribution on the Hector, California, bentonite deposits: Econ. Geology, v. 53, no. 1, p. 22–37.

Anderson, R. L., and Bancroft, T. A., 1952, Statistical theory in research: New York, McGraw-Hill Book Co., 399 p.

Bowyer, Ben, 1963, Yellow Chief uranium mine, Juab County, Utah *in* Beryllium and uranium mineralization in western Juab County, Utah: Utah Geol. Soc. Guidebook to the Geology of Utah, no. 17, p. 15–22.

Chayes, Felix, 1960, On correlation between variables of a constant sum: Jour. Geophys. Research, v. 65, no. 12, p. 4185–4193.

Claisse, Fernand, 1956, Accurate X-ray fluorescence analysis without internal standard: Quebec Dept. Mines, Lab. Br. Prelim. Rept. 327, 16 p.

Cohenour, R. E., 1963, The beryllium belt of western Utah, *in* Beryllium and uranium mineralization in western Juab county, Utah: Utah Geol. Soc. Guidebook to the Geology of Utah, no. 17, p. 4–7.

Cooley, W. W., and Lohnes, P. R., 1962, Multivariate procedures for the behavioral sciences: New York, John Wiley and Sons, 211 p.

Cooper, J. R., 1957, Metamorphism and volume losses in carbonate rocks near Johnson Camp, Cochise County, Arizona: Geol. Soc. America Bull., v. 68, no. 5, p. 577–610.

Connor, J. J., Feder, G. L., Erdman, J. A., and Tidball, R. R., 1972, Environmental geochemistry in Missouri — a multidisciplinary study: Internat. Geol. Cong., 24th, Symposium, no. 1, Montreal, Canada, p. 7–14.

Erickson, M. P., 1963, Volcanic geology of western Juab County, Utah, *in* Beryllium and uranium mineralization in western Juab County, Utah: Utah Geol. Soc. Guidebook to the Geology of Utah, no. 17, p. 23–35.

Freund, J. E., 1960, Modern elementary statistics [2d ed.]: Englewood Cliffs, N. J., Prentice-Hall, 413 p.

Griffitts, W. R., 1964, Beryllium, *in* Mineral and water resources of Utah: Utah Geol. and Mineralog. Survey Bull. 73, p. 71–75.

Harman, H. H., 1960, Modern factor analysis [2d ed., revised]: Chicago, Univ. Chicago Press, 471 p.

Havens, R. G., and Myers, A. T., 1973, Direct-reader spectrometric analyses, *in* Vine, J. D., and Tourtelot, E. B., Geochemistry of lower Eocene sandstones in the Rocky Mountain Region: U.S. Geol. Survey Prof. Paper 789, p. 13.

Hawkins, D. B., 1967a, Zeolite studies — [Pt.] 1, Synthesis of some alkaline earth zeolites: Materials Research Bull., v. 2, no. 10, p. 951–958.

———1967b, Zeolite studies — [Pt.] 2, Ion-exchange properties of some synthetic zeolites: Materials Research Bull., v. 2, no. 11, p. 1021–1028.

Hay, R. L., 1963, Stratigraphy and zeolitic diagenesis of the John Day Formation of Oregon: California Univ. Pubs. Geol. Sci., v. 42, no. 5, p. 199–262.

Hemley, J. J., and Jones, W. R., 1964, Chemical aspects of hydrothermal alteration with emphasis on hydrogen metasomatism: Econ. Geology, v. 59, no. 4, p. 538–569.

Hoover, D. L., 1968, Genesis of zeolites, Nevada Test Site, *in* Eckel, E. B., ed., Nevada Test Site: Geol. Soc. America Mem. 110, p. 275–284.

Howarth, R. J., 1967, Trend-surface fitting to random data — An experimental test: Am. Jour. Sci., v. 265, no. 7, p. 619–625.

Klug, H. P., and Alexander, L. E., 1954, X-ray diffraction procedures — for polycrystalline and amorphous materials: New York, John Wiley and Sons, 716 p.

Krumbein, W. C., and Graybill, F. A., 1965, An introduction to statistical models in geology: New York, McGraw-Hill Book Co. 475 p.

Lindsey, D. A., Ganow, Harold, and Mountjoy, Wayne, 1973, Hydrothermal alteration associated with beryllium deposits at Spor Mountain, Utah: U.S. Geol. Survey Prof. Paper 818-A, 20 p.

Lindsey, D. A., Wahlberg, J. S., Merritt, V. M., and Lee, L. M., 1974, Mineralogical and chemical data for water-laid tuff in the Thomas Range, Juab County, Utah: U.S. Geol. Survey Rept. U.S.G.S.-GD-74-013; available only from U.S. Dept. Commerce Natl. Tech. Inf. Service, Springfield, Va., 22161, as Rept. PB-231 921, 35 p.

McAnulty, W. N., and Levinson, A. A., 1964, Rare alkali and beryllium mineralization in volcanic tuffs, Honey Comb Hills, Juab County, Utah: Econ. Geology, v. 59, no. 5, p. 768–774.

McIntyre, D. B., Welday, E. E., and Baird, A. K., 1965, Geologic application of the air pycnometer — A study of the precision of measurement: Geol. Soc. America Bull., v. 76, no. 9, p. 1055–1060.

Miesch, A. T., 1967a, Methods of computation for estimating geochemical abundance: U.S. Geol. Survey Prof. Paper 574-B, 15 p.

———1967b, Theory of error in geochemical data: U.S. Geol. Survey Prof. Paper 574-A, 17 p.

———1969, The constant sum problem in geochemistry, *in* Merriam, D. F., ed., Computer applications in the earth sciences — Conf., Kansas Univ., 1969, Proc: New York, Plenum Press, p. 161–176.

Miesch, A. T., Chao, E. C. T., and Cuttitta, Frank, 1966, Multivariate analysis of geochemical data on tektites: Jour. Geology, v. 74, no. 5, pt. 2, p. 673–691.

Moiola, R. J., 1970, Authigenic zeolites and K-feldspar in the Esmeralda Formation, Nevada: Am. Mineralogist, v. 55, no. 9/10, p. 1681–1691.

Morris, H. T., and Lovering, T. S., 1952, Supergene and hydrothermal dispersion of heavy metals in wall rocks near ore bodies, Tintic district, Utah: Econ. Geology, v. 47, no. 7, p. 685-716.

Mountjoy, Wayne, and Wahlberg, J. S., 1968, Determination of micro amounts of cesium in geologic materials, *in* Geological Survey research 1968: U.S. Geol. Survey Prof. Paper 600-B, p. B119–B122.

Noble, D. C., Smith, V. C., and Peck, L. C., 1967, Loss of halogens from crystallized and glassy silicic volcanic rocks: Geochim. et Cosmochim. Acta, v. 31, no. 2, p. 215–223.

Norton, J. J., 1965, Lithium-bearing bentonite deposit, Yavapai County, Arizona, *in* Geological Survey research 1965: U.S. Geol. Survey Prof. Paper 525-D, p. D163-D166.

Perkin-Elmer, 1964, Analytical methods for atomic absorption spectrophotometry: Norwalk, Conn. [loose-leaf].

Rader, L. F., and Grimaldi, F. S., 1961, Chemical analyses for selected minor elements in Pierre shale: U.S. Geol. Survey Prof. Paper 391-A, 45 p.

Rosholt, J. N., Prijana, and Noble, D. C., 1971, Mobility of uranium and thorium in glassy and crystallized silicic volcanic rocks: Econ. Geology, v. 66, no. 7, p. 1061–1069.

Schultz, L. G., 1964, Quantitative interpretation of mineralogical composition from X-ray and chemical data for the Pierre Shale: U.S. Geol. Survey Prof. Paper 391-C, 31 p.

Shawe, D. R., 1964, A late Tertiary low-angle fault in western Juab County, Utah, *in* Geological Survey research 1964: U.S. Geol. Survey Prof. Paper 501-B, p. B13–B15.

———1968, Geology of the Spor Mountain beryllium district, Utah, *in* Ridge, J. D., ed., Ore deposits of the United States, 1933–1967 (Graton-Sales Volume): Am. Inst. Mining, Metall. and Petroleum Engineers, v. 2, pt. 8, chap. 55, p. 1148–1161.

———1972, Reconnaissance geology and mineral potential of Thomas, Keg, and Desert calderas, central Juab county, Utah, *in* Geological Survey research 1972: U. S. Geol. Survey Prof. Paper 800-B, p. B67–B77.

Sheppard, R. A., and Gude, A. J., 3d, 1965, Zeolitic authigenesis of tuffs in the Ricardo Formation, Kern county, southern California, *in* Geological Survey research 1965: U.S. Geol. Survey Prof. Paper 525-D, p. D44–D47.

Staatz, M. H., and Carr, W. J., 1964, Geology and mineral deposits of the Thomas and Dugway Ranges, Juab and Tooele Counties, Utah: U.S. Geol. Survey Prof. Paper 415, 188 p.

Staatz, M. H., and Griffitts, W. R., 1961, Beryllium-bearing tuff in the Thomas Range, Juab County, Utah: Econ. Geology, v. 56, no. 5, p. 941–950.

Tatlock, D. B., 1966, Rapid modal analysis of some felsic rocks from calibrated X-ray diffraction patterns: U.S. Geol. Survey Bull. 1209, 41 p.

Thurston, W. R., Staatz, M. H., Cox, D. C., and others, 1954, Fluorspar deposits of Utah: U. S. Geol. Survey Bull. 1005, 53 p.

Vlasov, K. A., ed., 1966, Geochemistry and mineralogy of rare elements and genetic types of their deposits, v. 3, Genetic types of rare-earth deposits [Translation from Russian by Z. Lerman, edited by R. Amoils, *of* Geokhimiya, mineralogiya i geneticheskie tipy mestorozhdenii redkikh elementov. Tom III. Geneticheskie tipy mestorozhdenii redkikh elementov — Izdatel'stvo "Nauka", Moskow]: Israel Prog. for Scientific Translations, Jerusalem, 1968, 916 p.

Waters, A. C., and Granger, H. C., 1953, Volcanic debris in uraniferous sandstones, and its possible bearing on the origin and precipitation of uranium [Colorado Plateau]: U.S. Geol. Survey Circ. 224, 26 p.

Waugh, A. E., 1952, Elements of statistical methods [3d ed.]: New York, McGraw-Hill Book Co., 532 p.

FIGURES 5–41

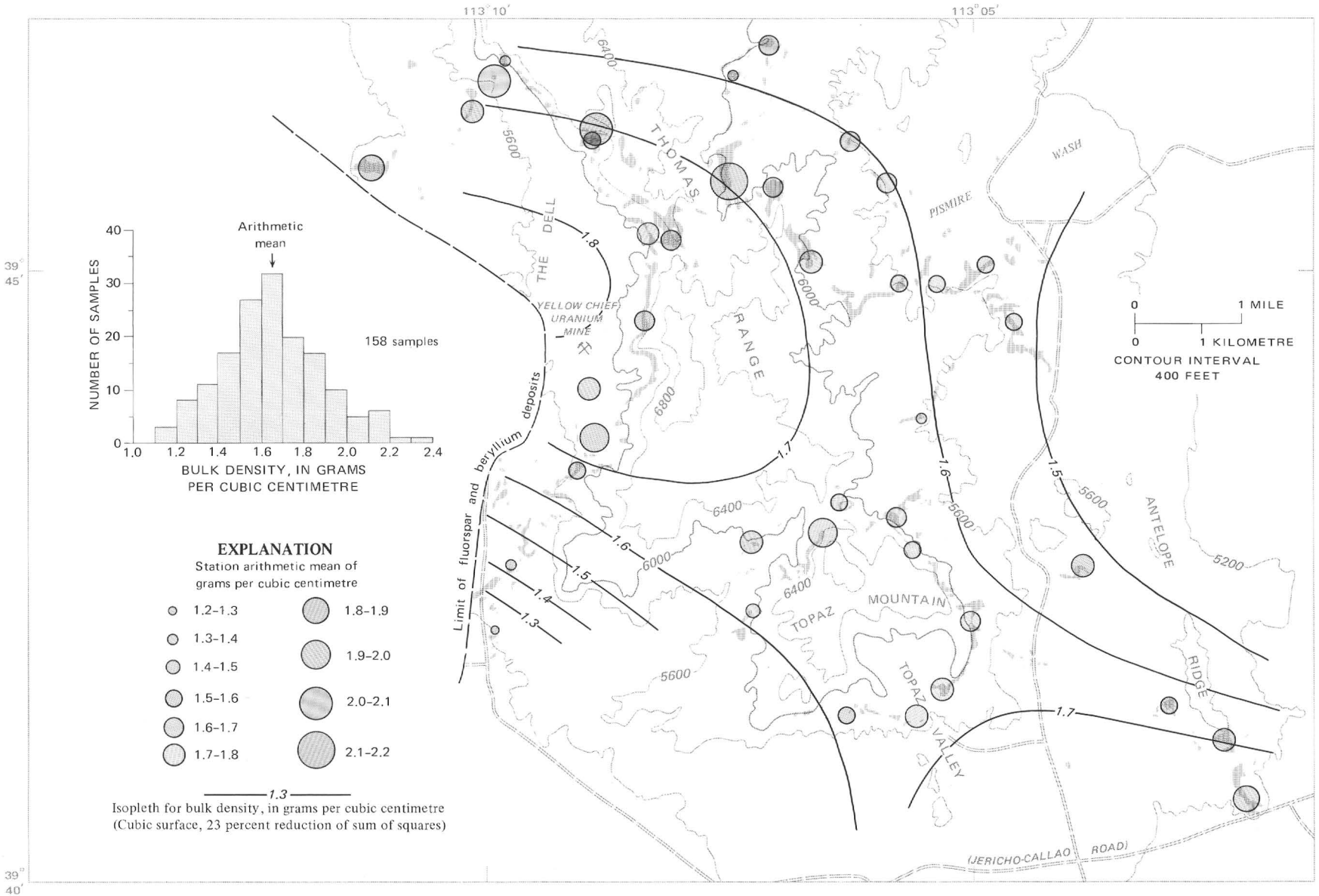

FIGURE 5. — Bulk density of water-laid tuff in the Thomas Range.

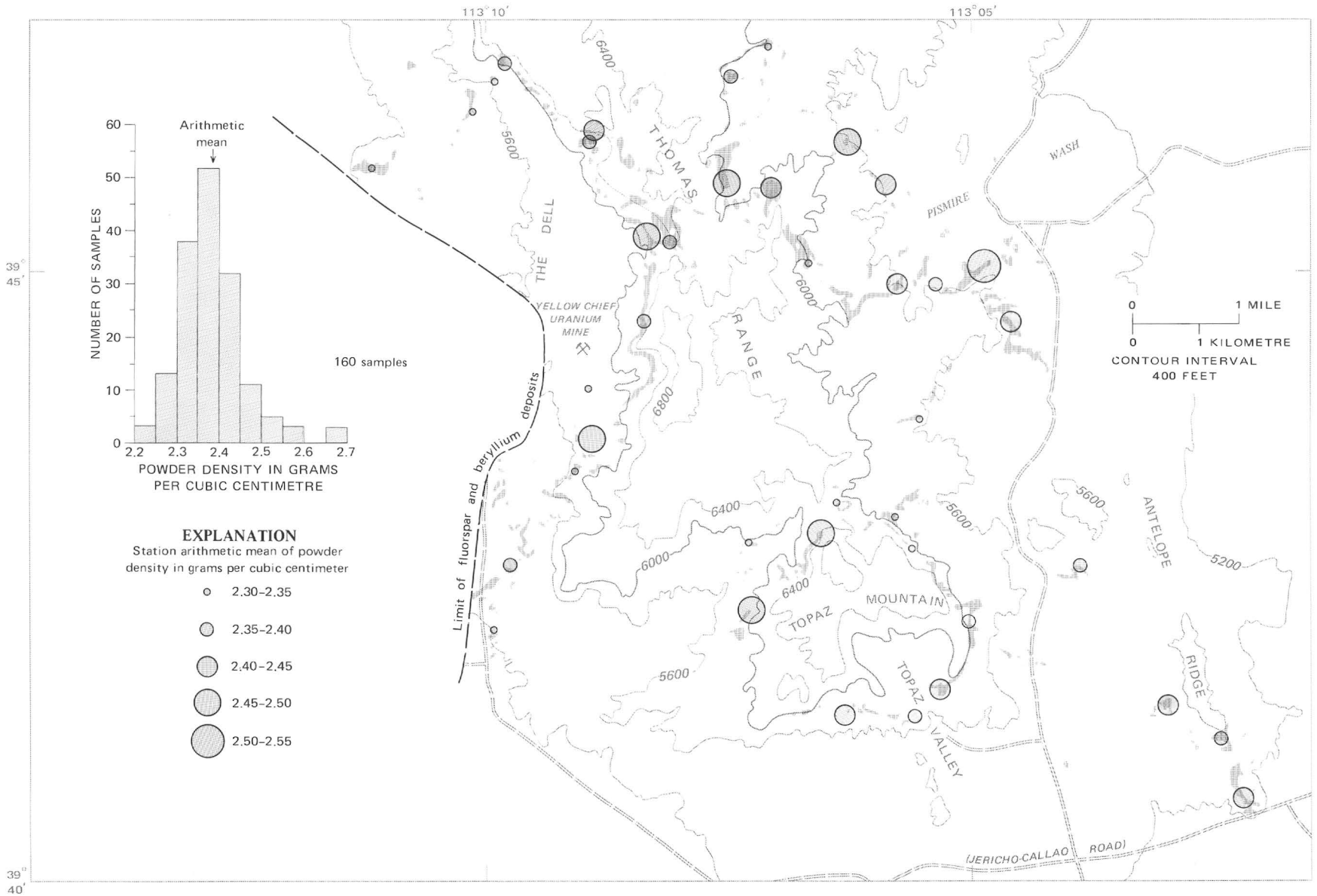

FIGURE 6. — Powder density of water-laid tuff in the Thomas Range.

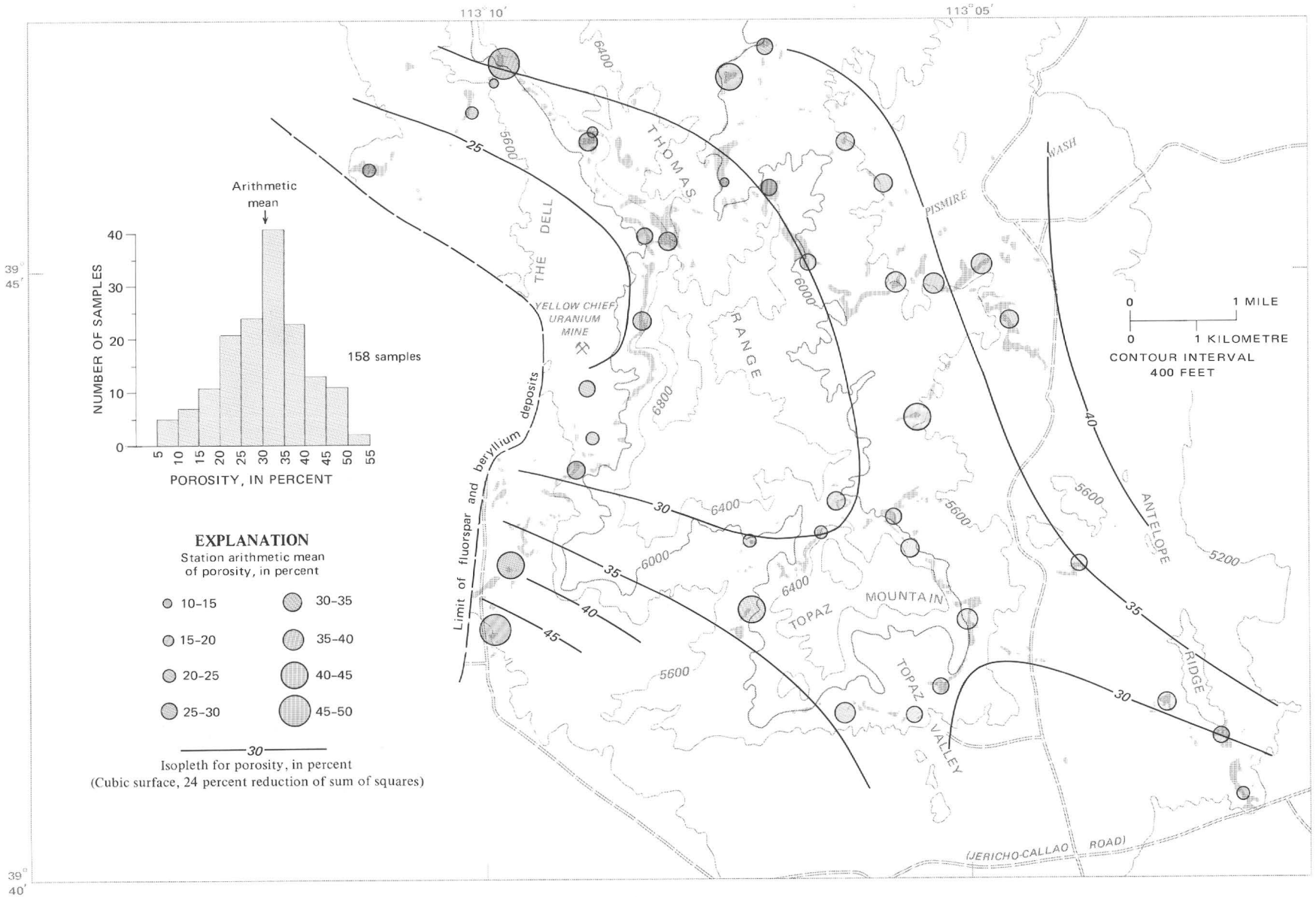

FIGURE 7. — Porosity of water-laid tuff in the Thomas Range.

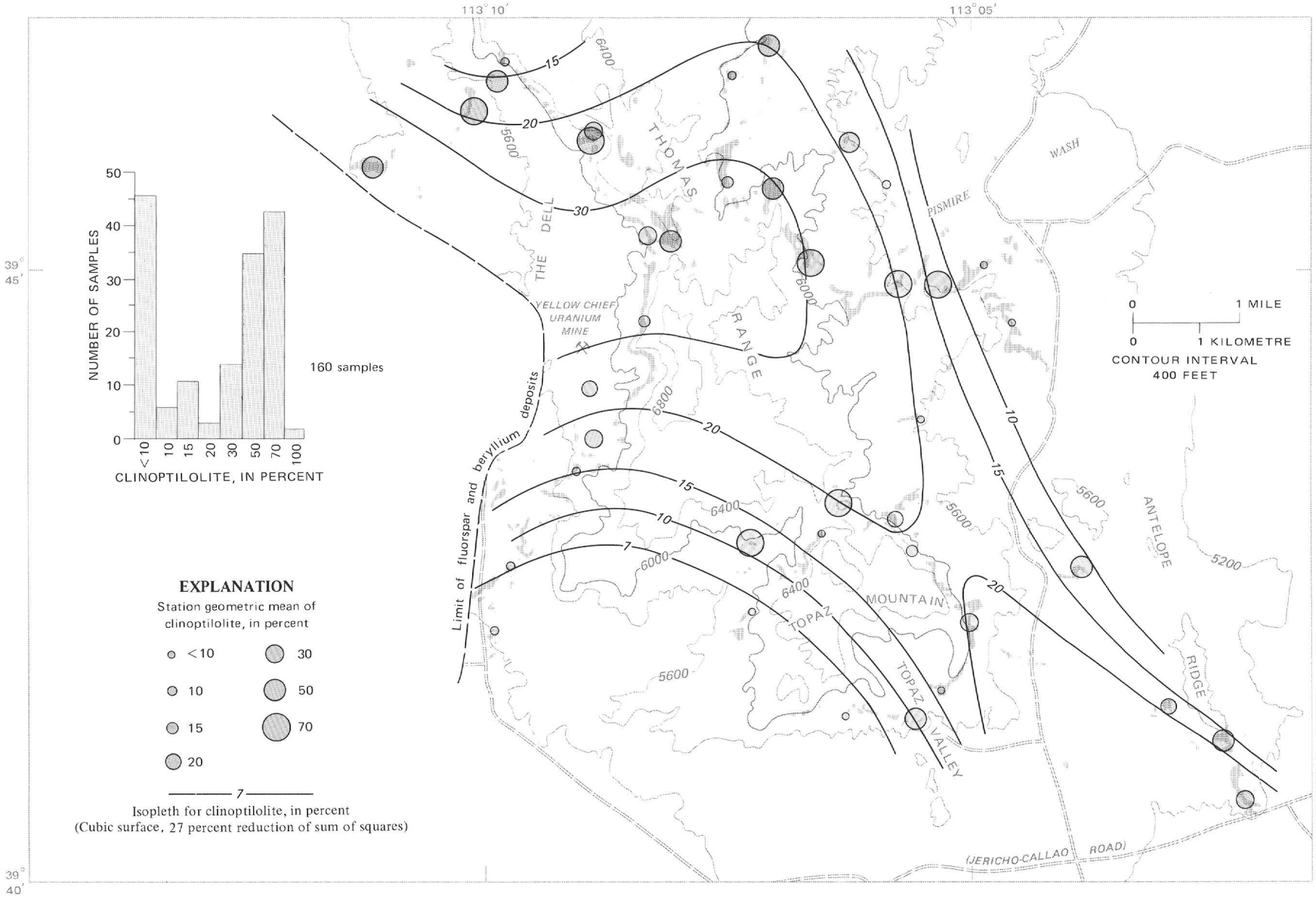

FIGURE 8. — Clinoptilolite content of water-laid tuff in the Thomas Range.

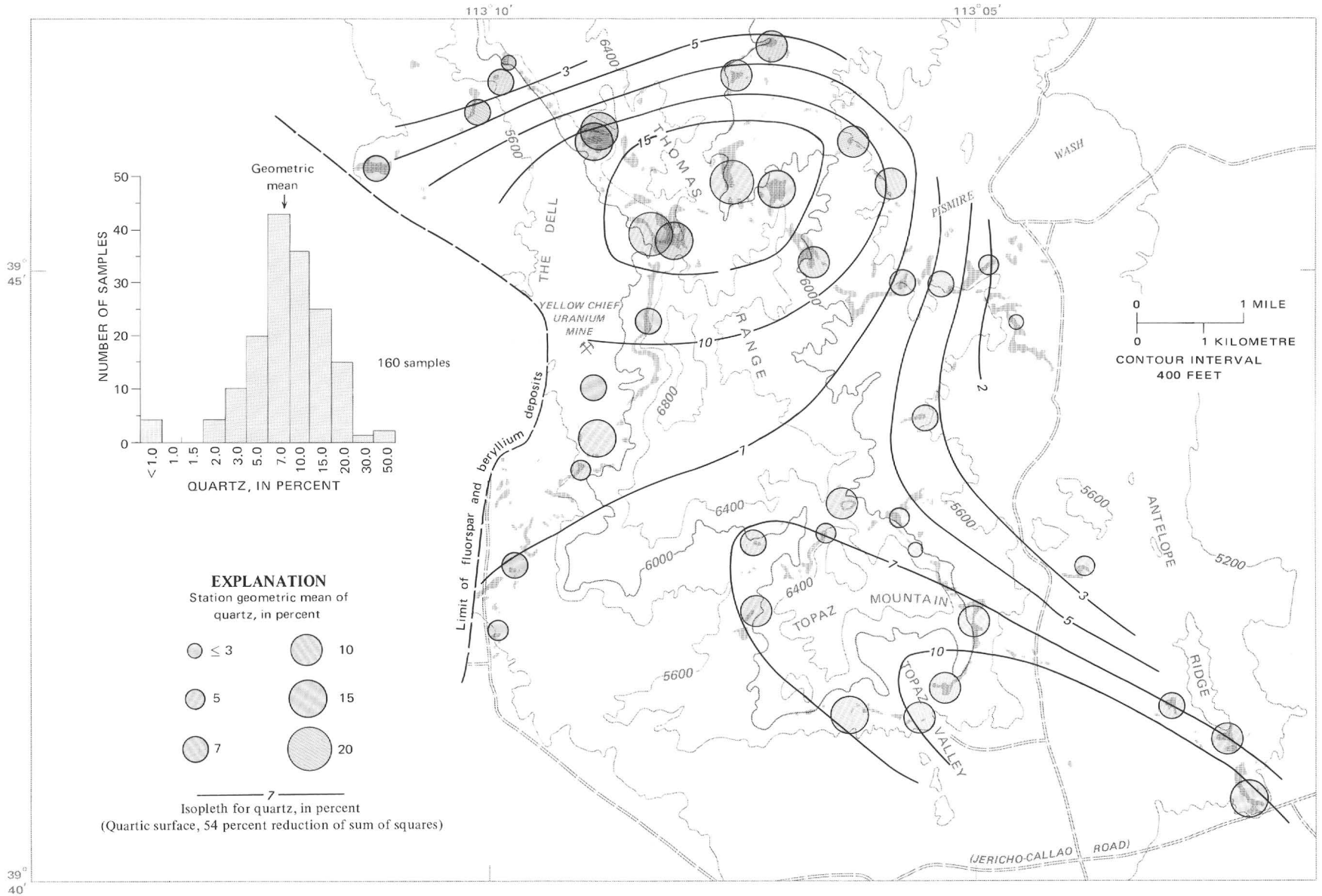

FIGURE 9. — Quartz content of water-laid tuff in the Thomas Range.

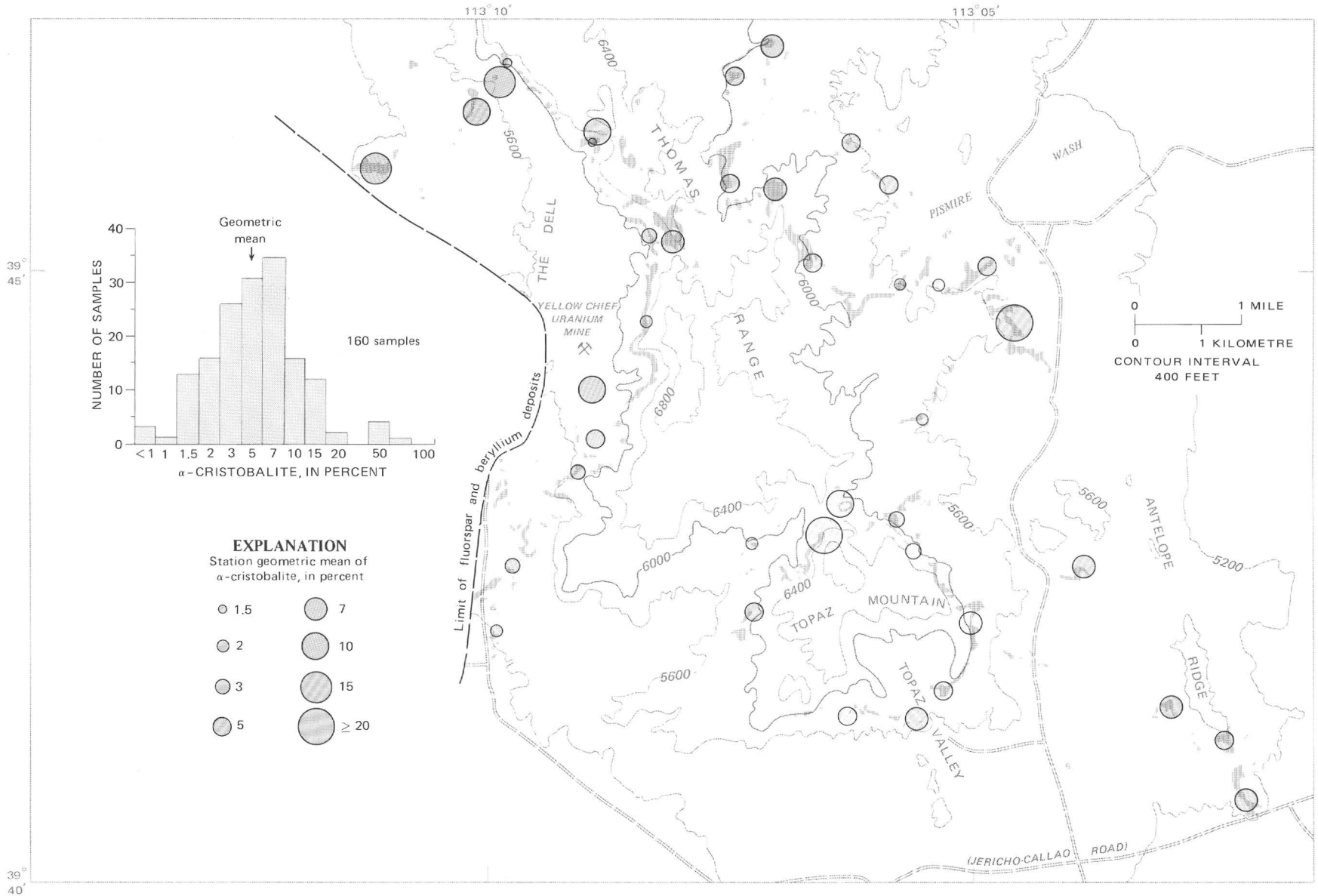

FIGURE 10. — α-cristobalite content of water-laid tuff in the Thomas Range.

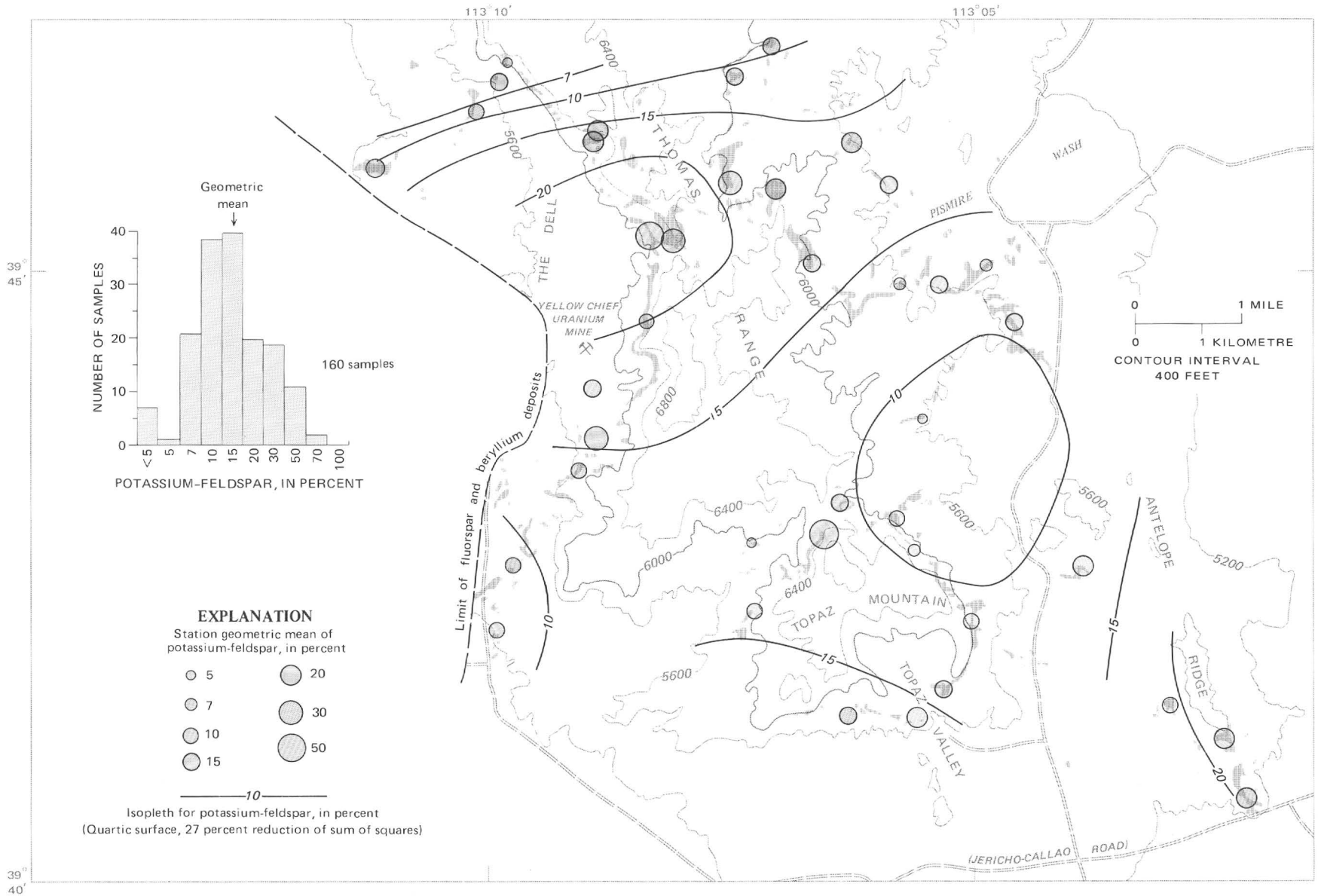

FIGURE 11. — Potassium feldspar content of water-laid tuff in the Thomas Range.

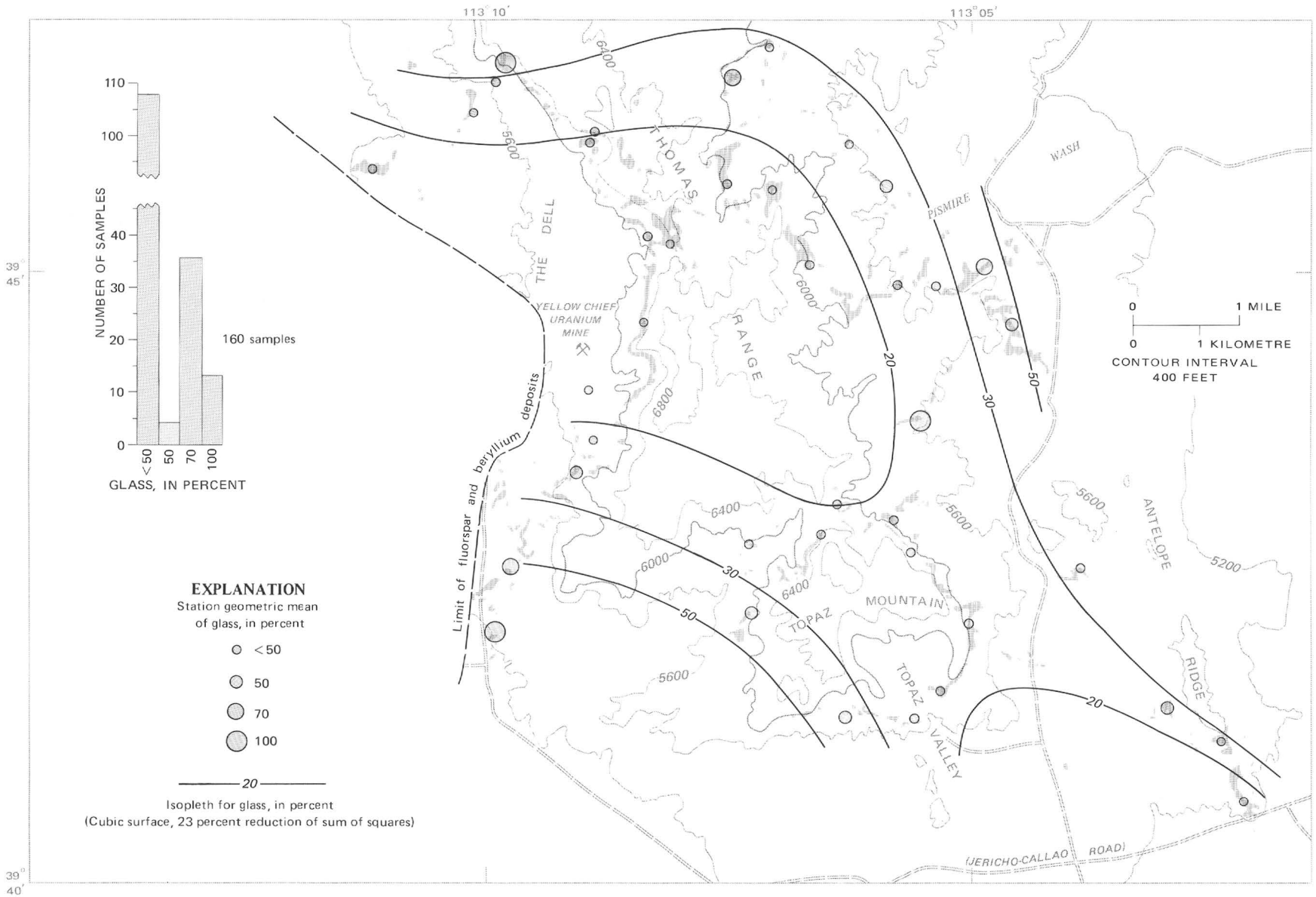

FIGURE 12. — Glass content of water-laid tuff in the Thomas Range.

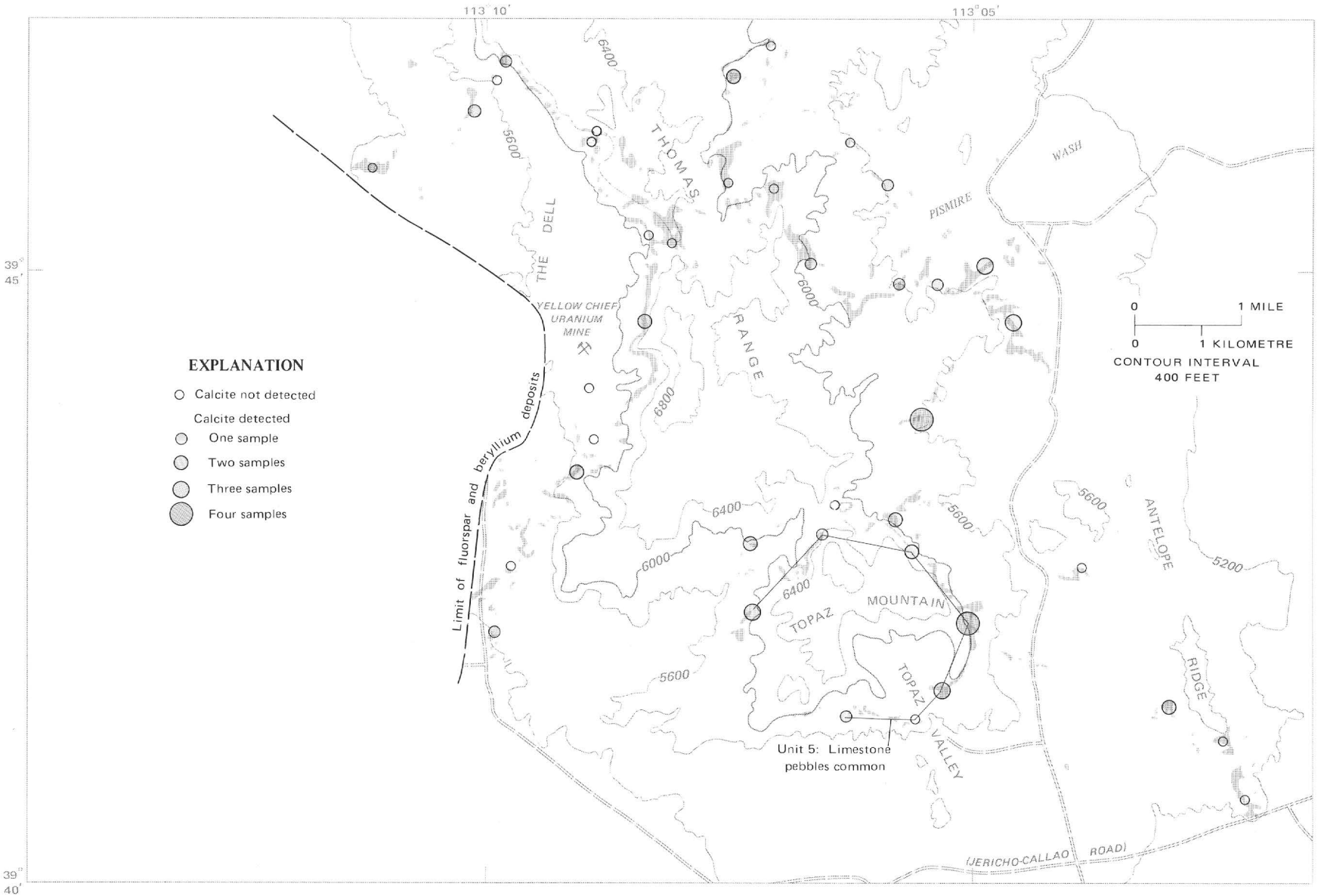

FIGURE 13. — Occurrence of calcite in water-laid tuff in the Thomas Range.

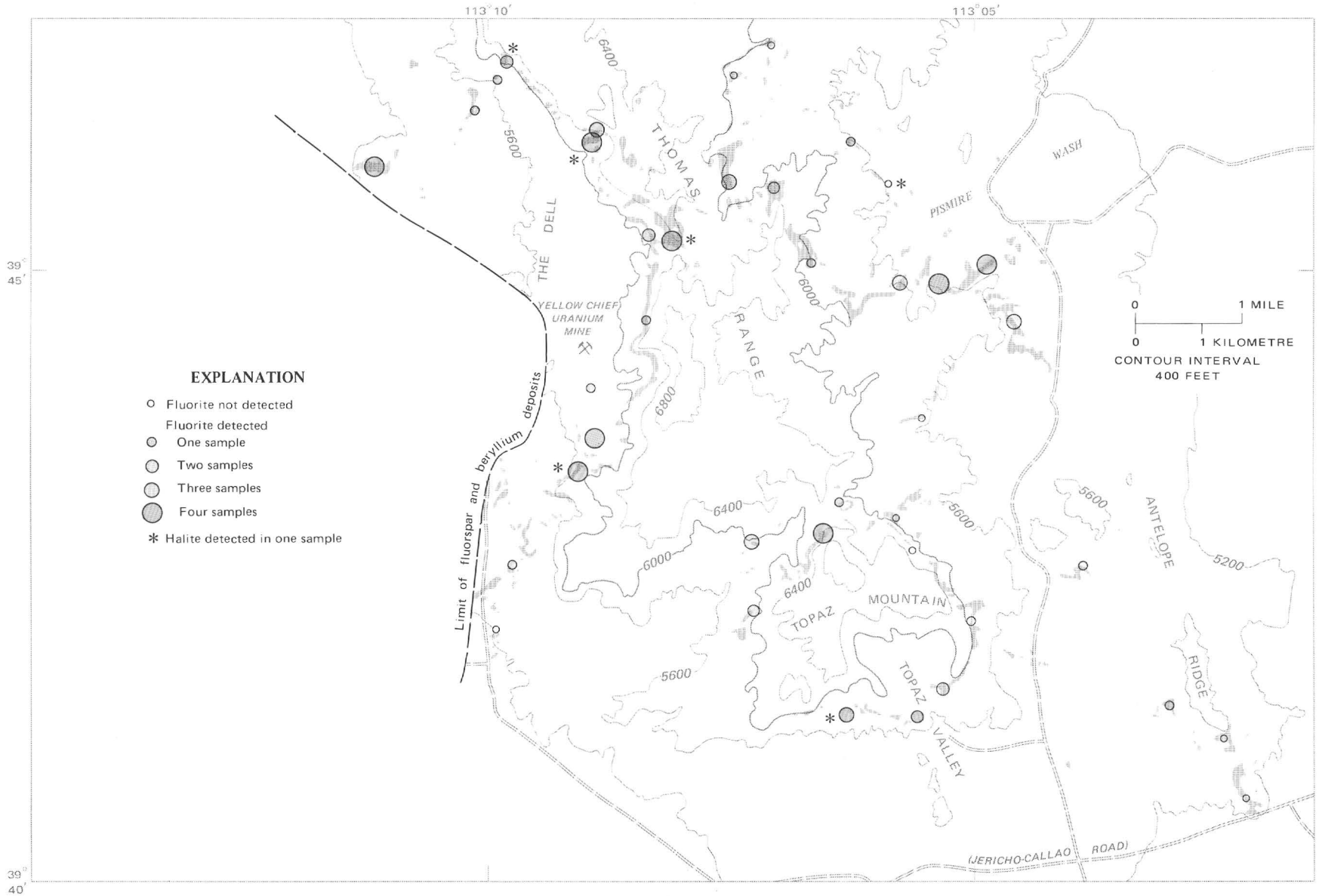

FIGURE 14. — Occurrence of fluorite and halite in water-laid tuff of the Thomas Range.

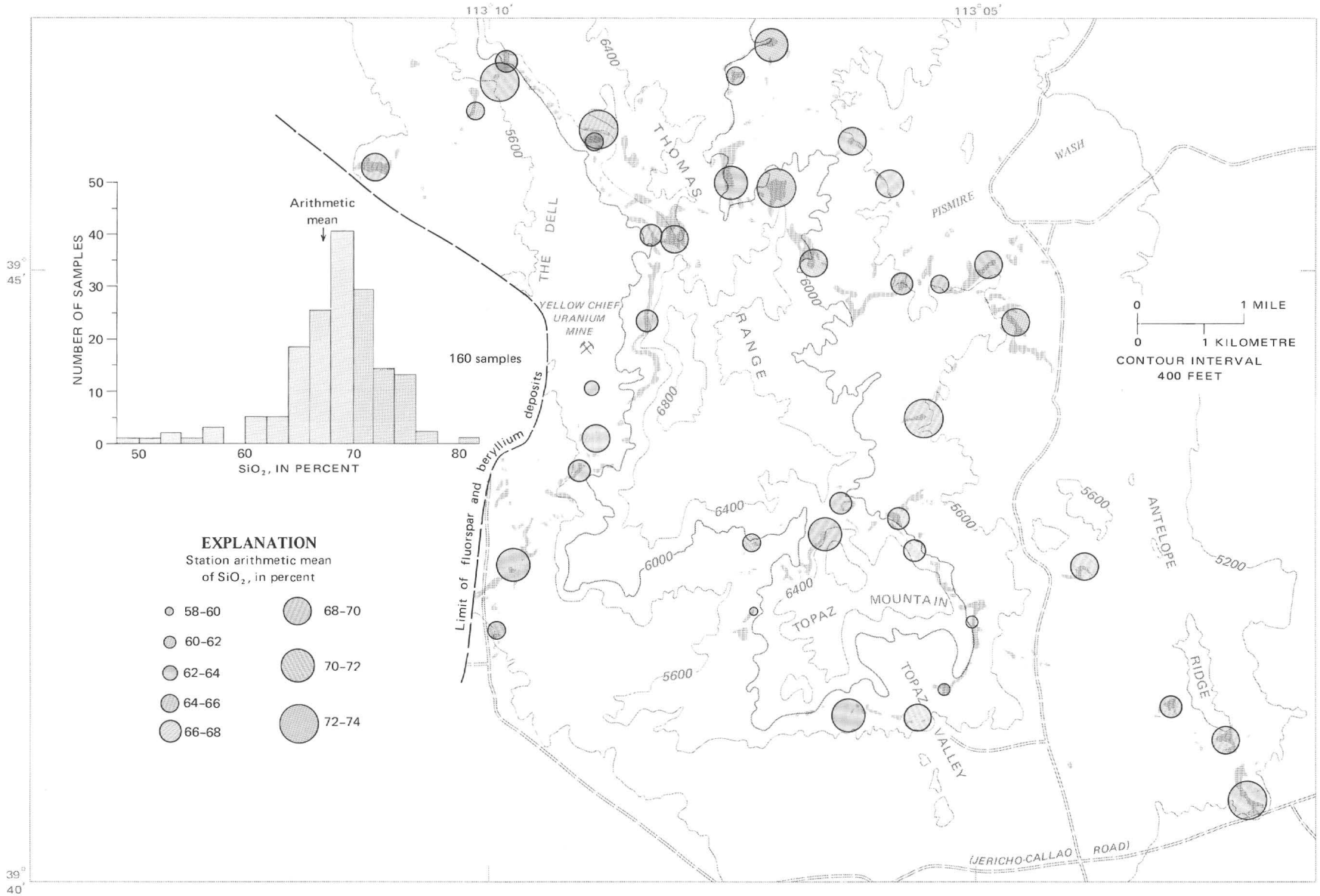

FIGURE 15. — Silica content of water-laid tuff in the Thomas Range.

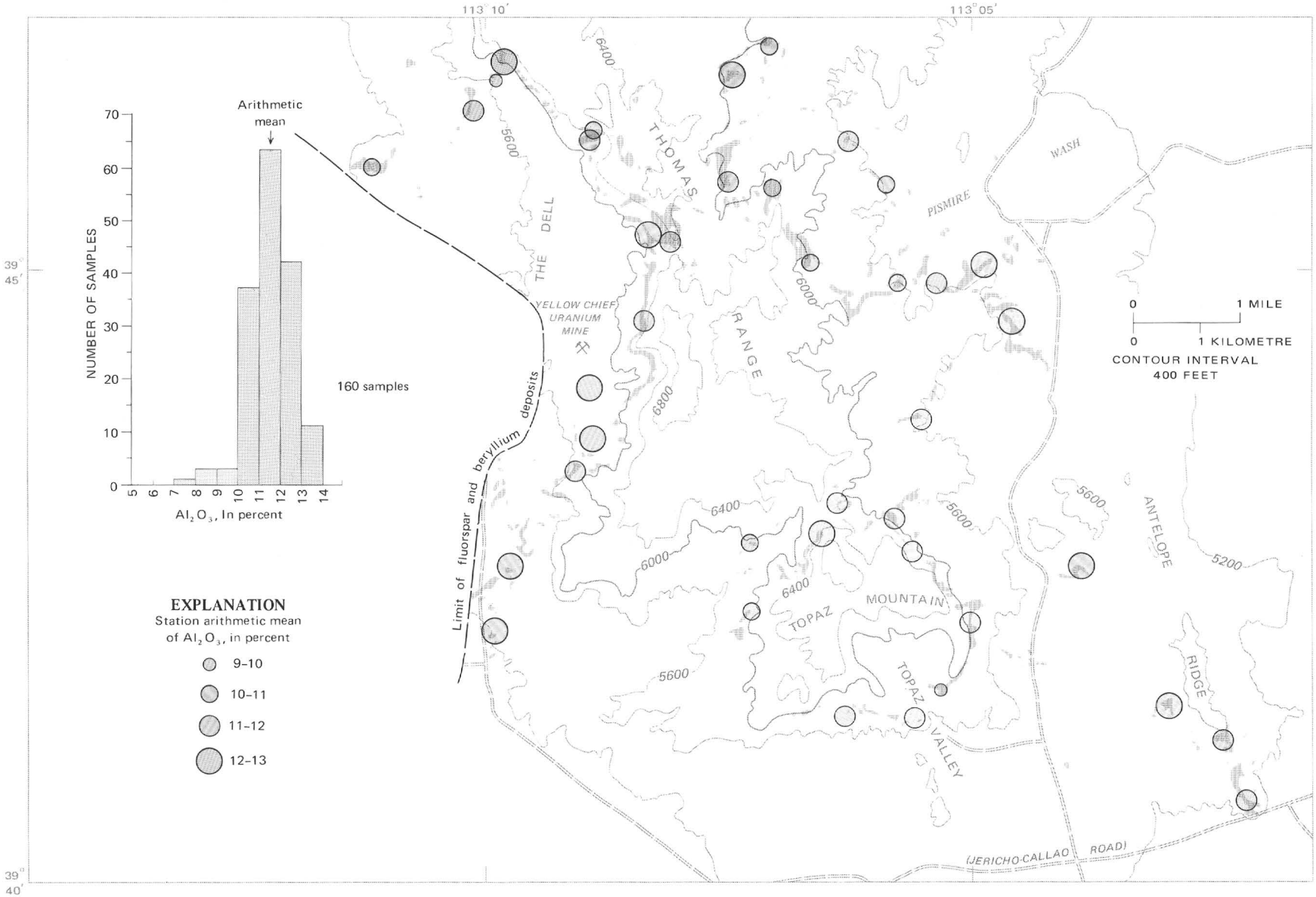

FIGURE 16. — Alumina content of water-laid tuff in the Thomas Range.

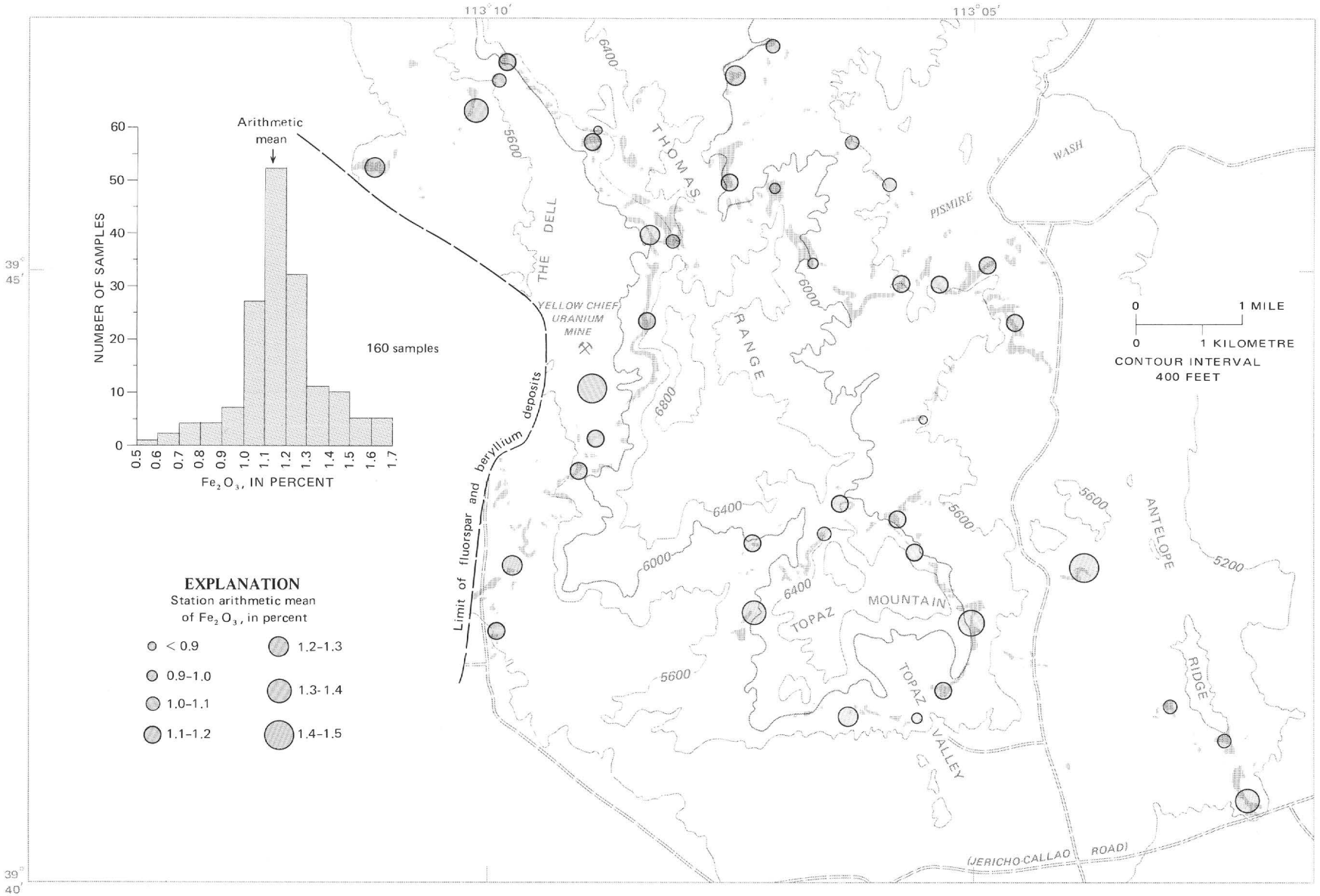

FIGURE 17. — Total iron content (as Fe_2O_3) of water-laid tuff in the Thomas Range.

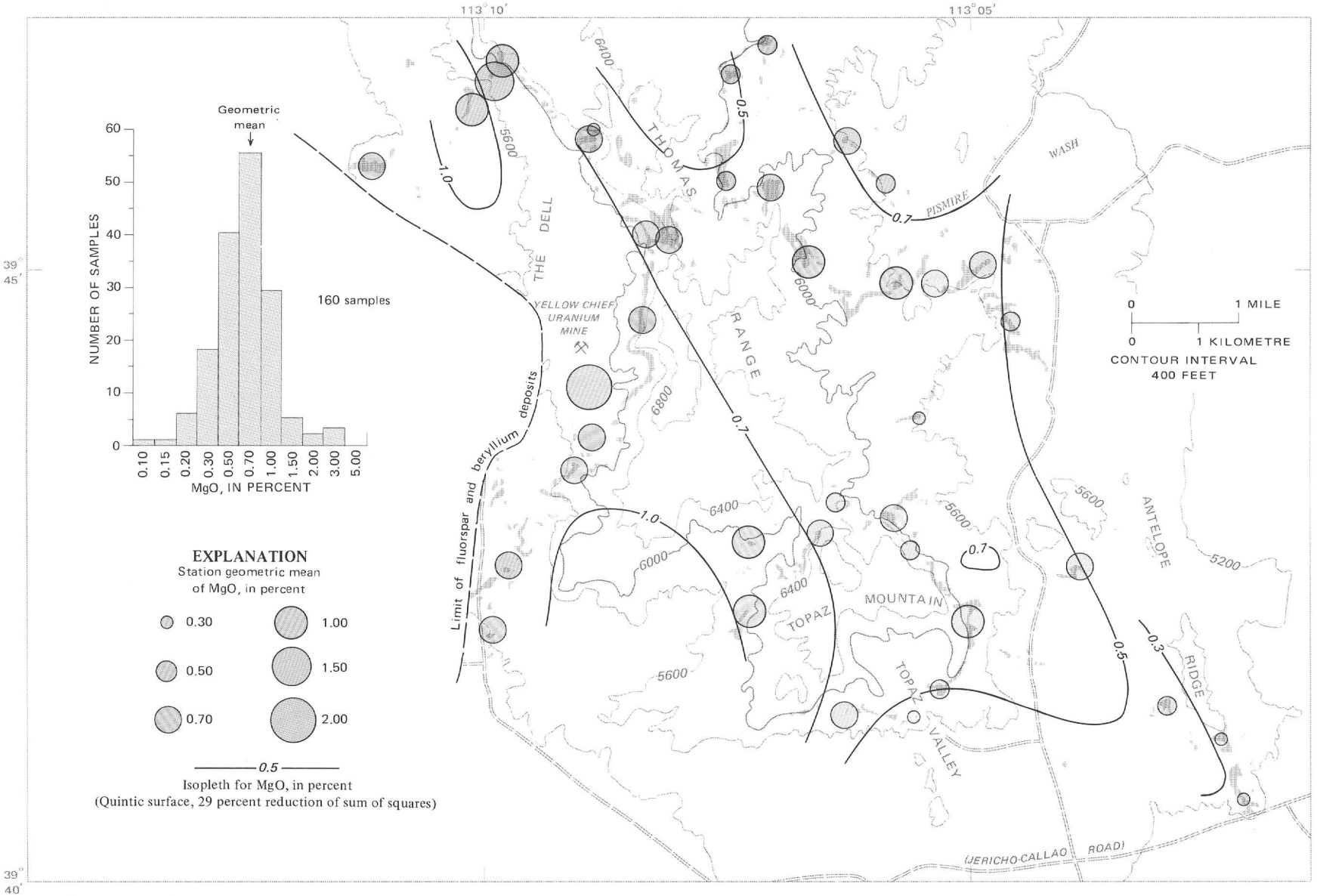

FIGURE 18. — Magnesium oxide content of water-laid tuff in the Thomas Range.

FIGURE 19. — Calcium oxide content of water-laid tuff in the Thomas Range.

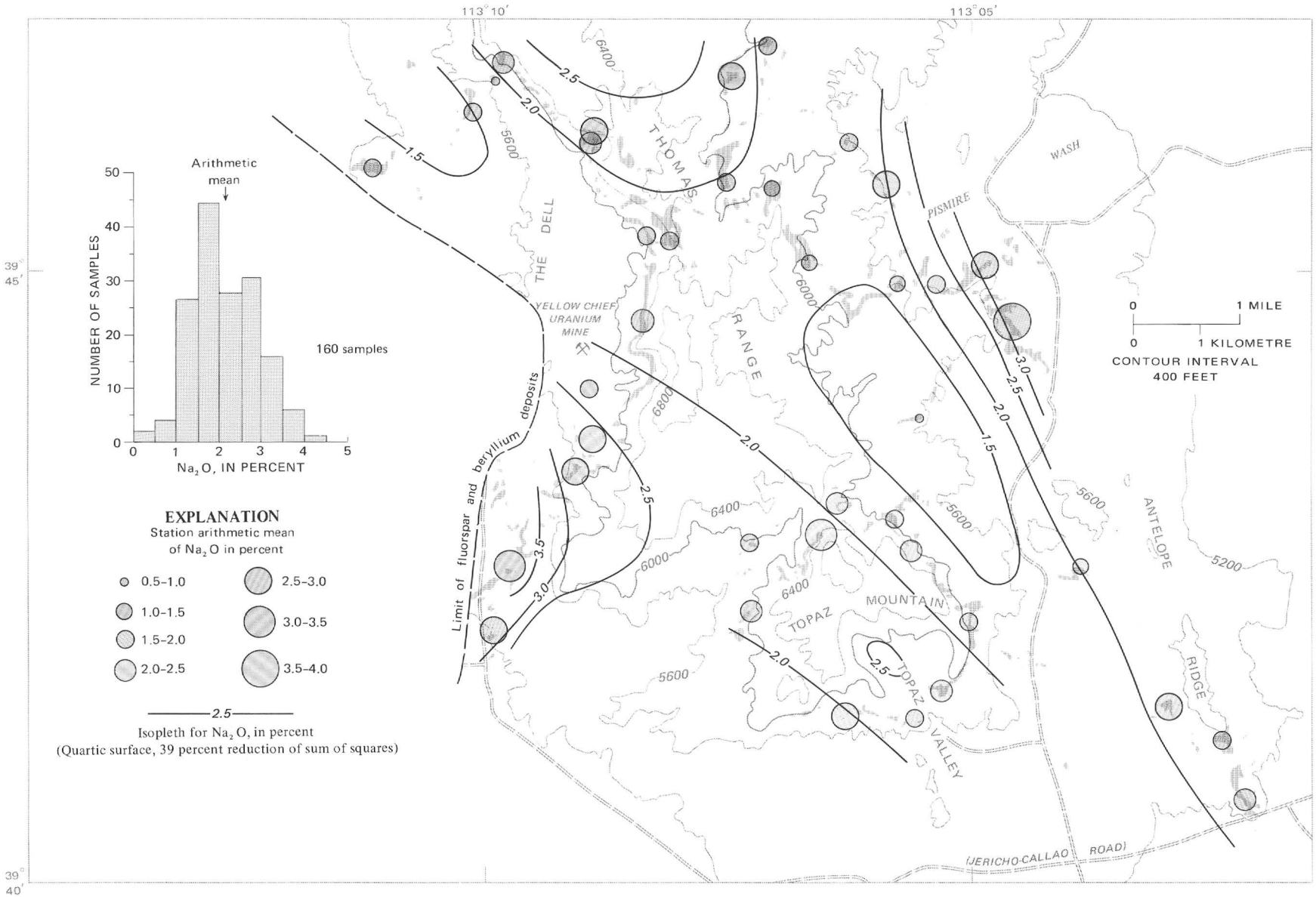

FIGURE 20. — Sodium oxide content of water-laid tuff in the Thomas Range.

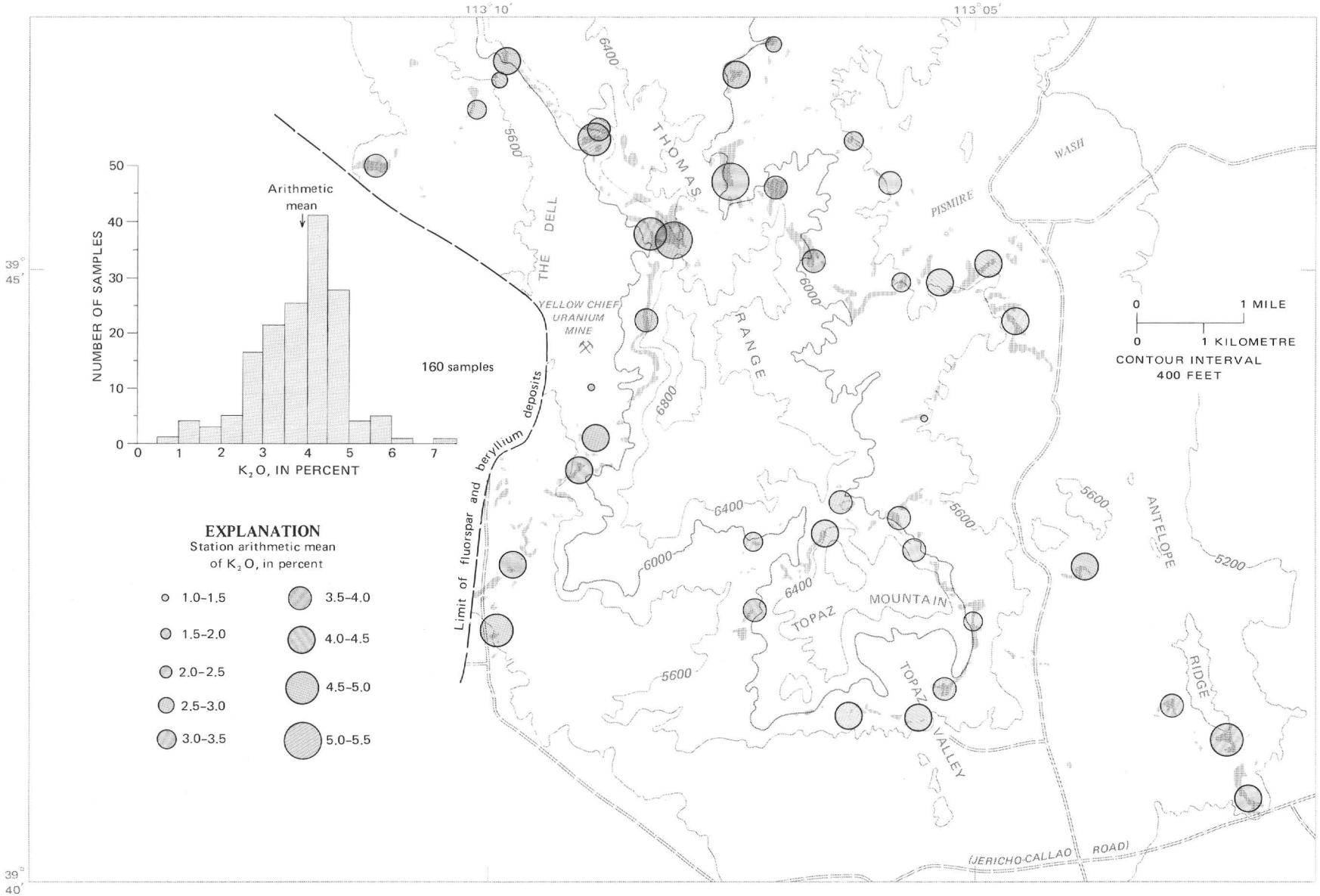

FIGURE 21. — Potassium oxide content of water-laid tuff in the Thomas Range.

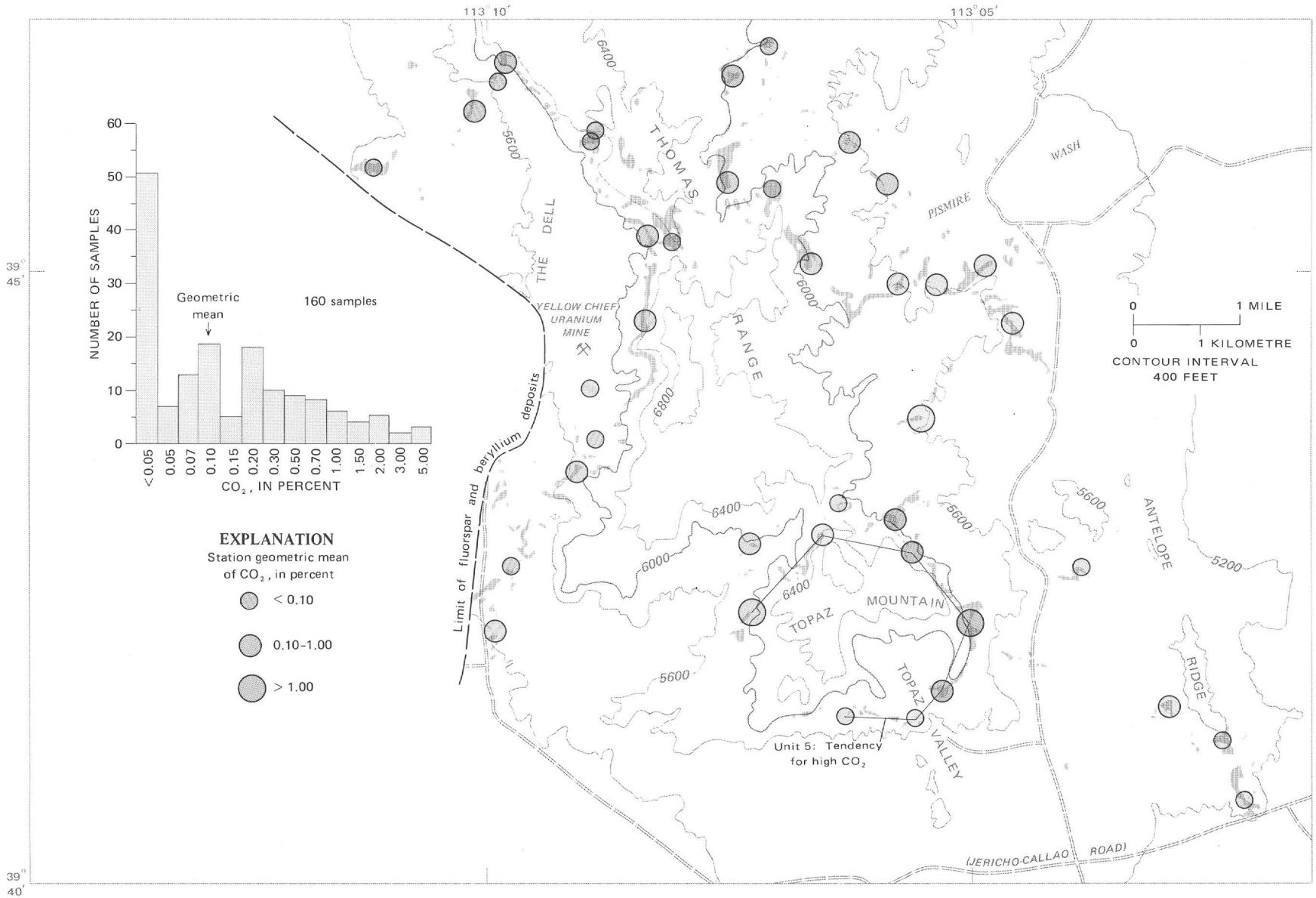

FIGURE 22. — Carbon dioxide content of water-laid tuff in the Thomas Range.

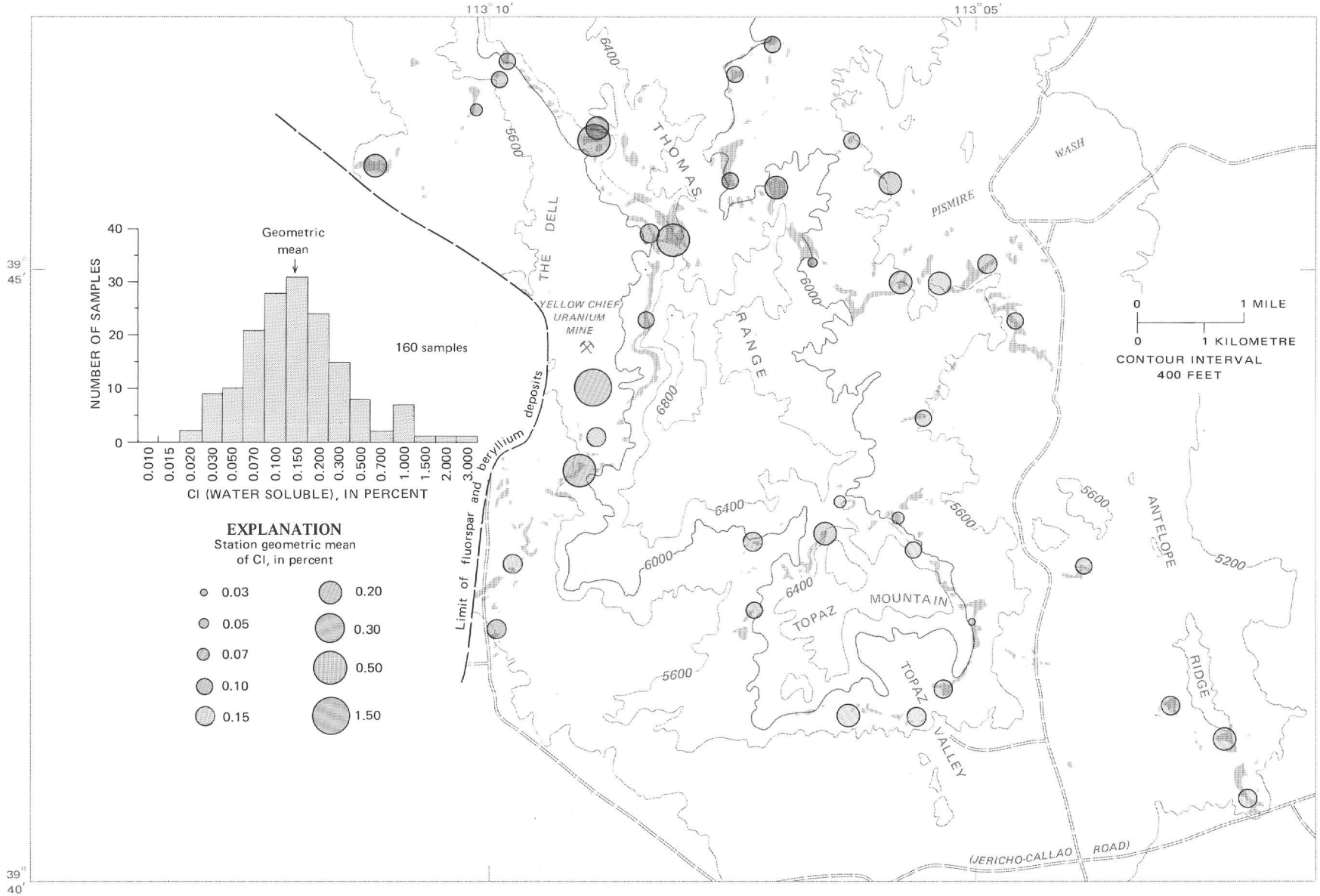

FIGURE 23. — Water-soluble chlorine content of water-laid tuff in the Thomas Range.

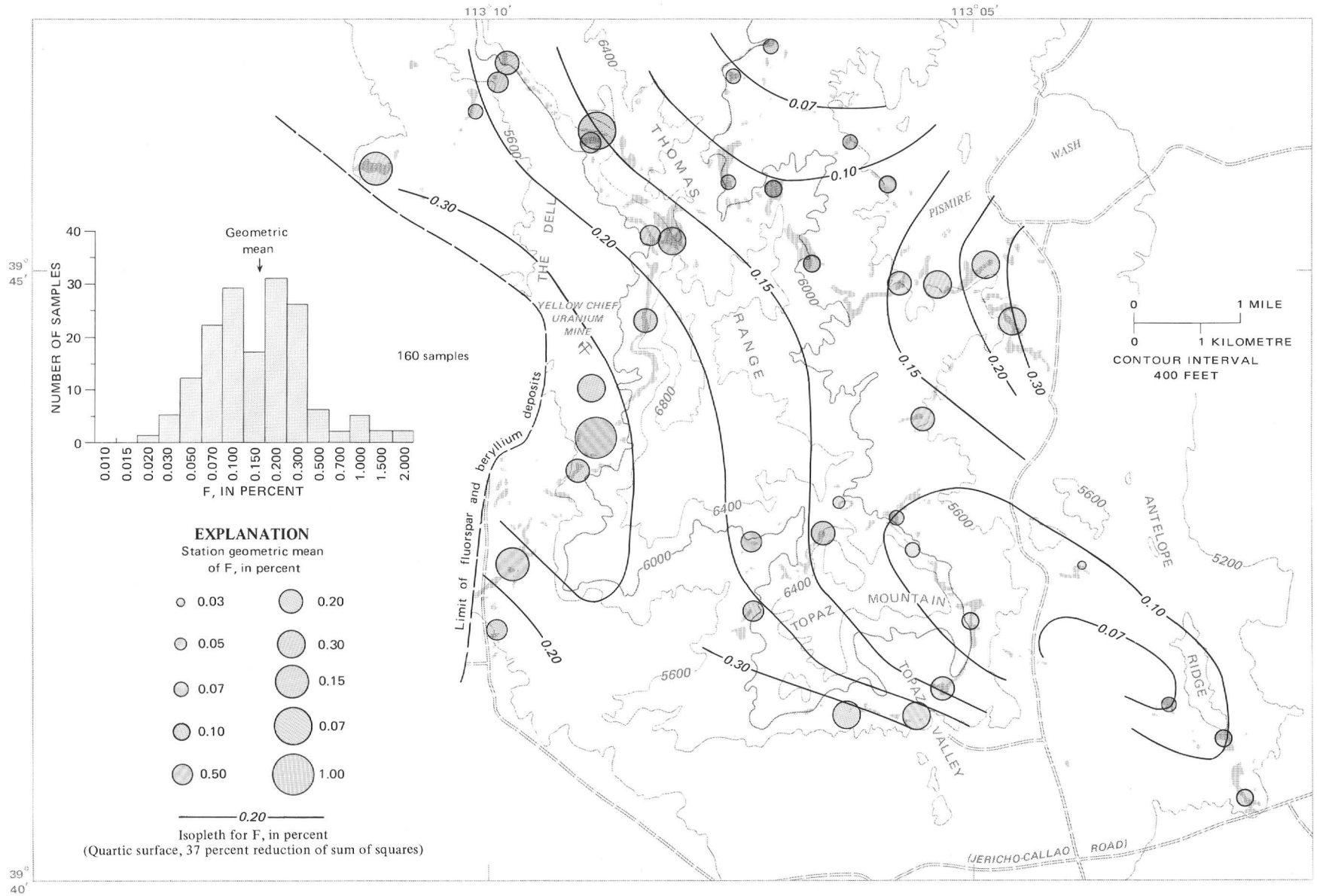

FIGURE 24. — Fluorine content of water-laid tuff in the Thomas Range.

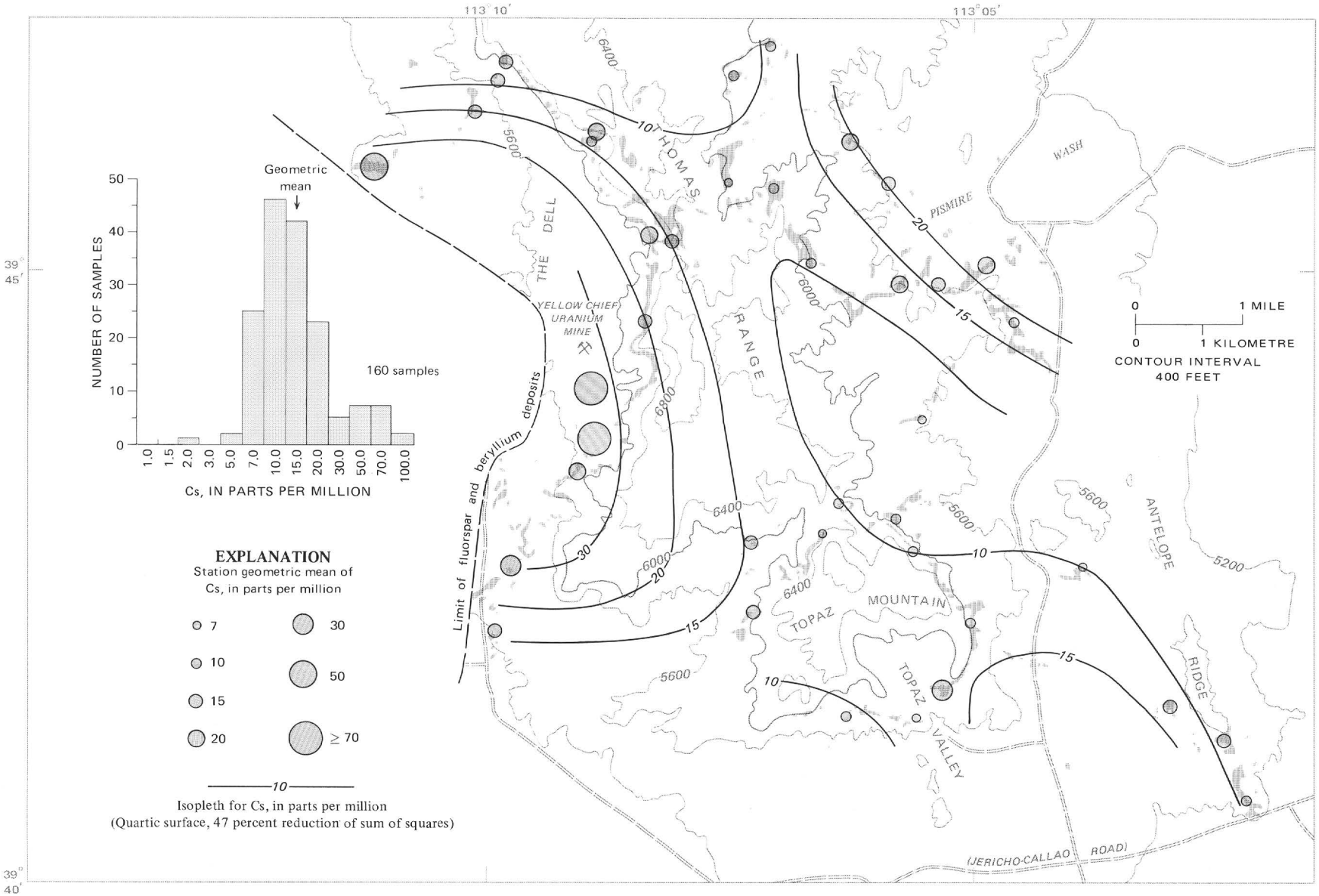

FIGURE 25. — Cesium content of water-laid tuff in the Thomas Range.

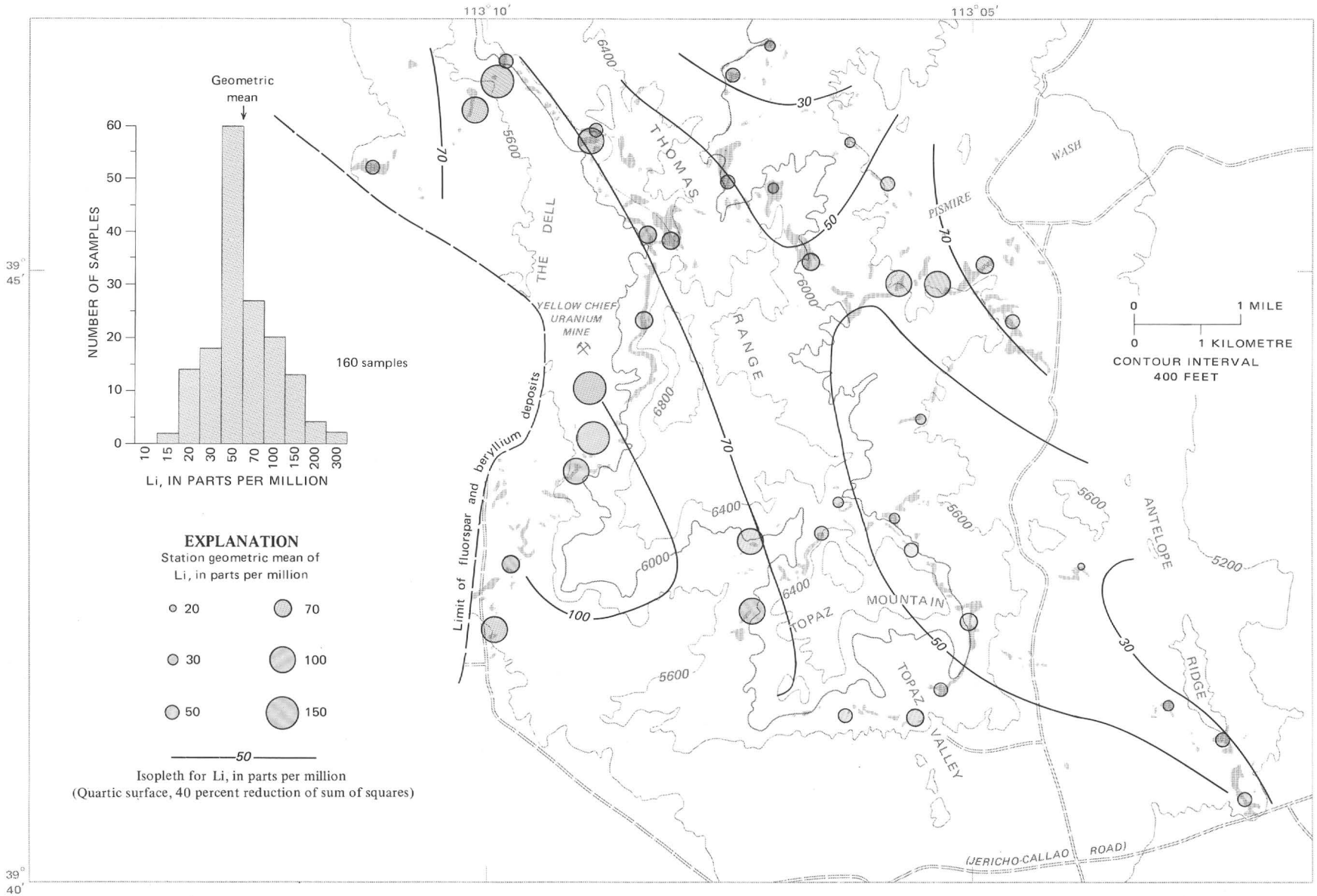

FIGURE 26. — Lithium content of water-laid tuff in the Thomas Range.

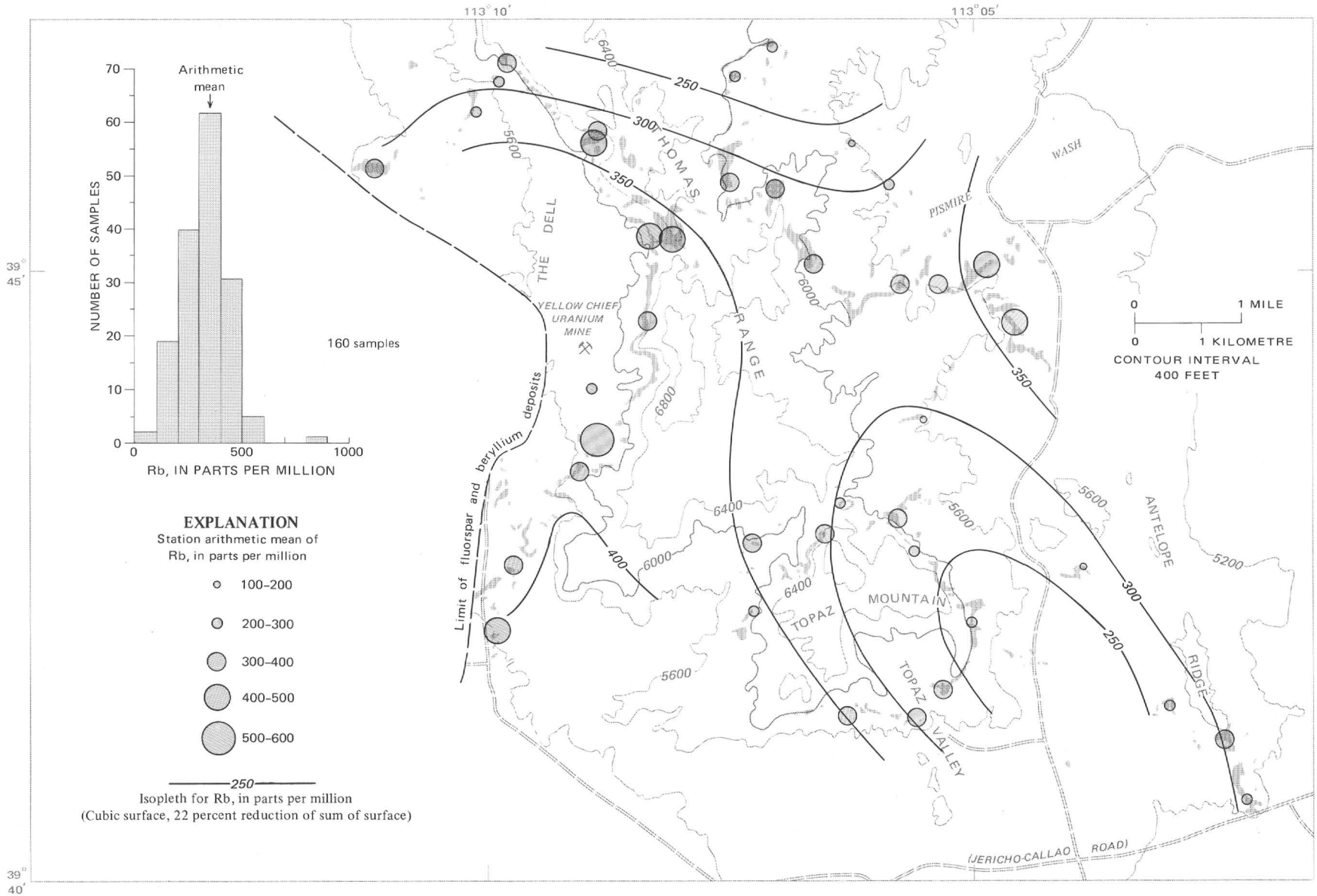

FIGURE 27. — Rubidium content of water-laid tuff in the Thomas Range.

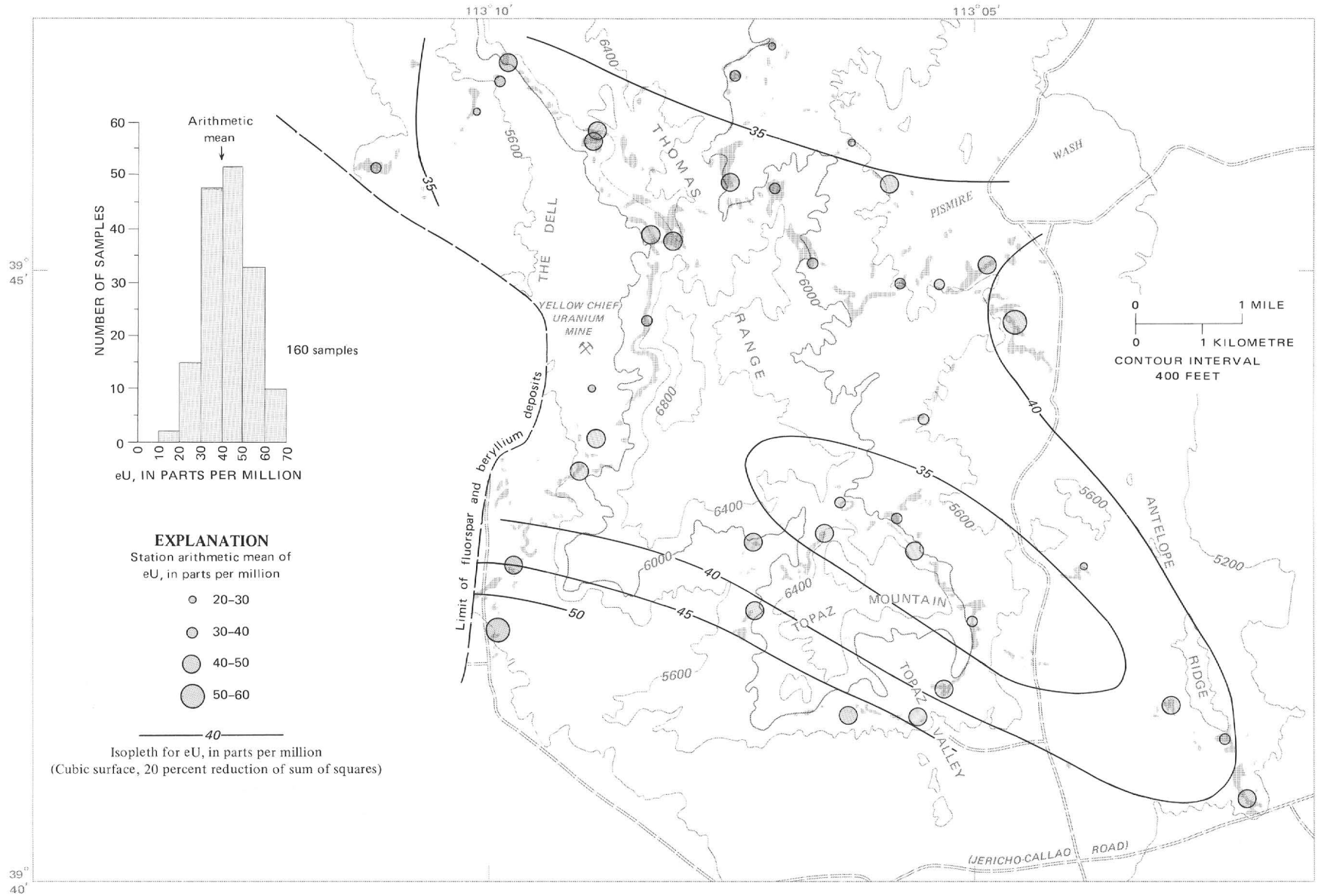

FIGURE 28. — Equivalent uranium content of water-laid tuff in the Thomas Range.

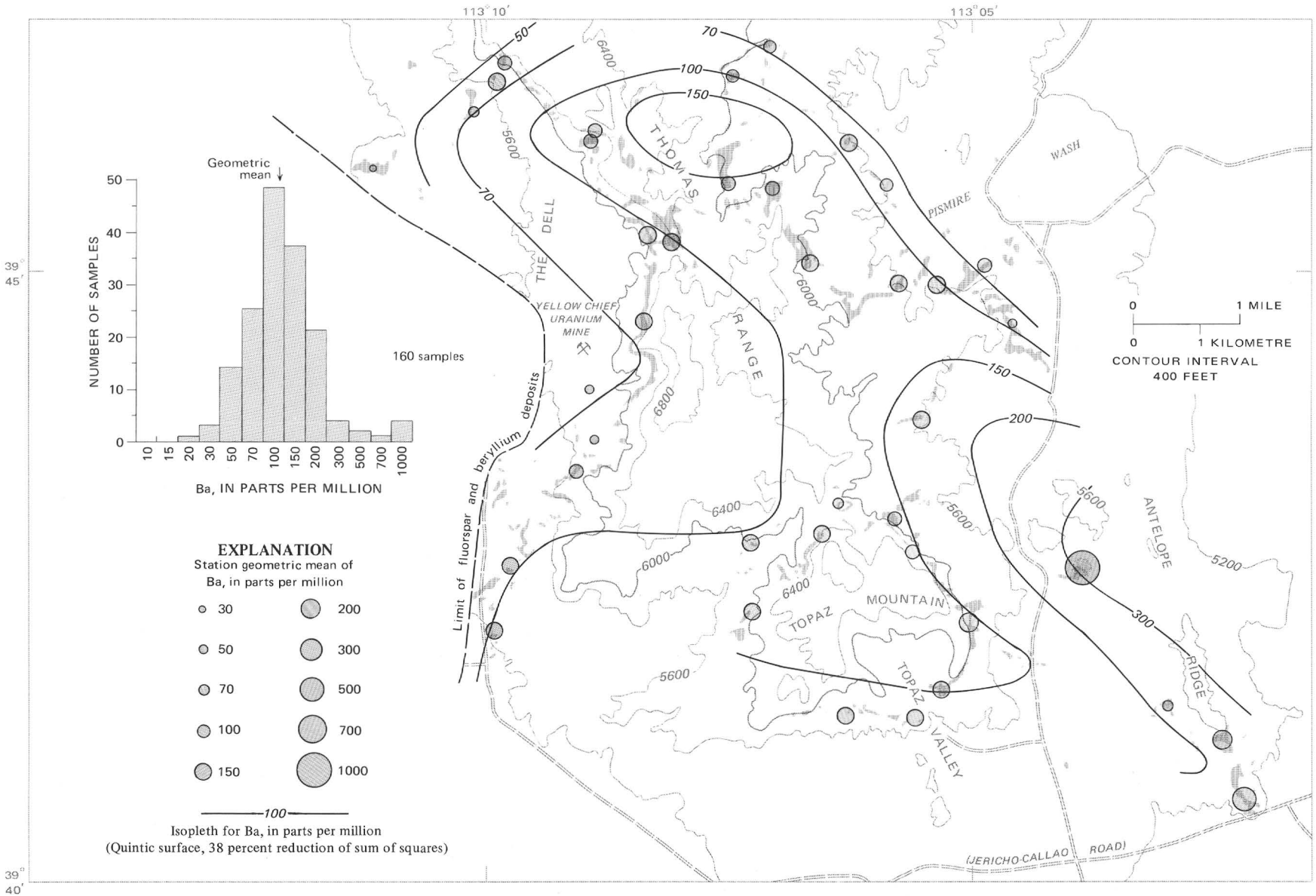

FIGURE 29. — Barium content of water-laid tuff in the Thomas Range.

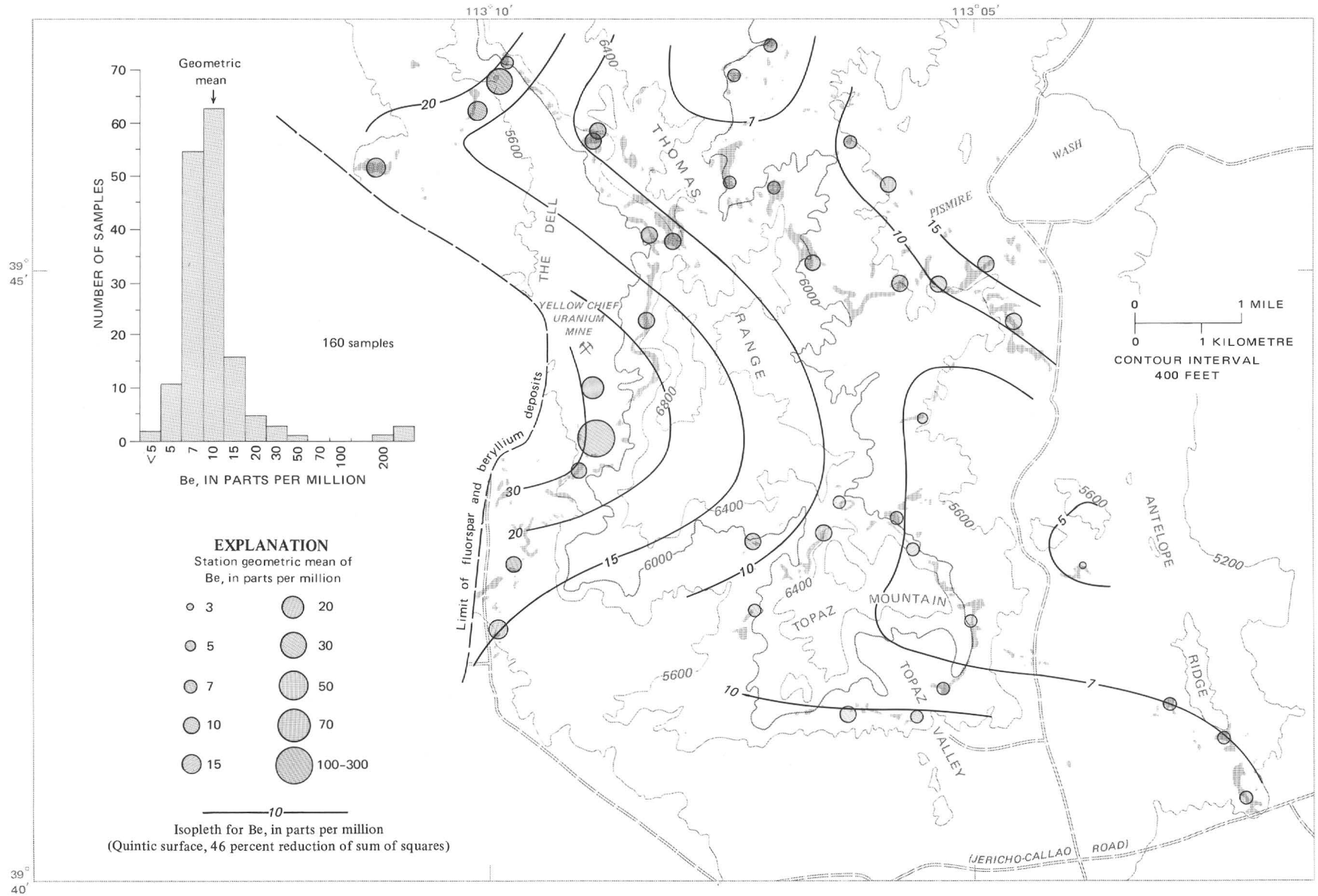

FIGURE 30. — Beryllium content of water-laid tuff in the Thomas Range.

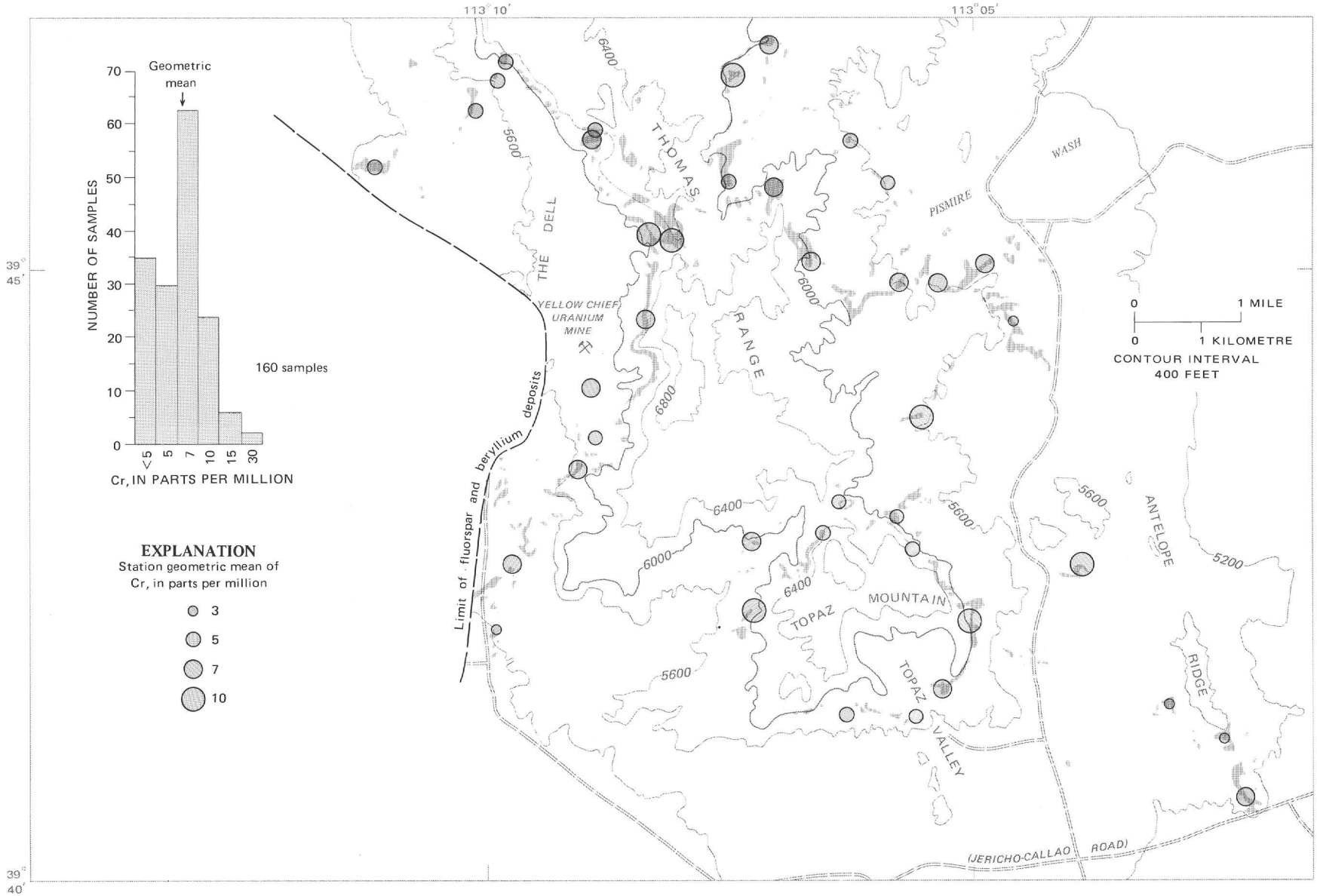

FIGURE 31. — Chromium content of water-laid tuff in the Thomas Range.

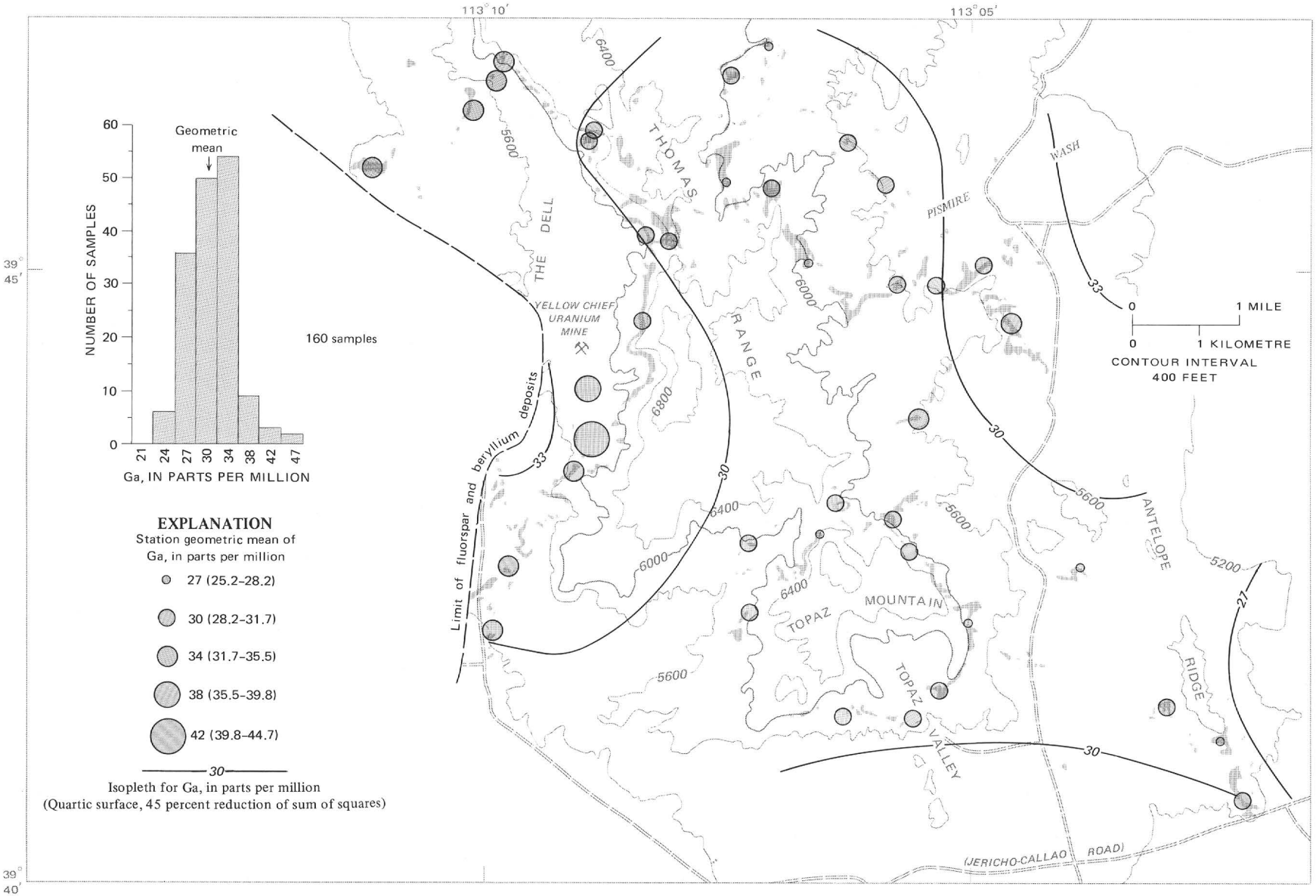

FIGURE 32. — Gallium content of water-laid tuff in the Thomas Range.

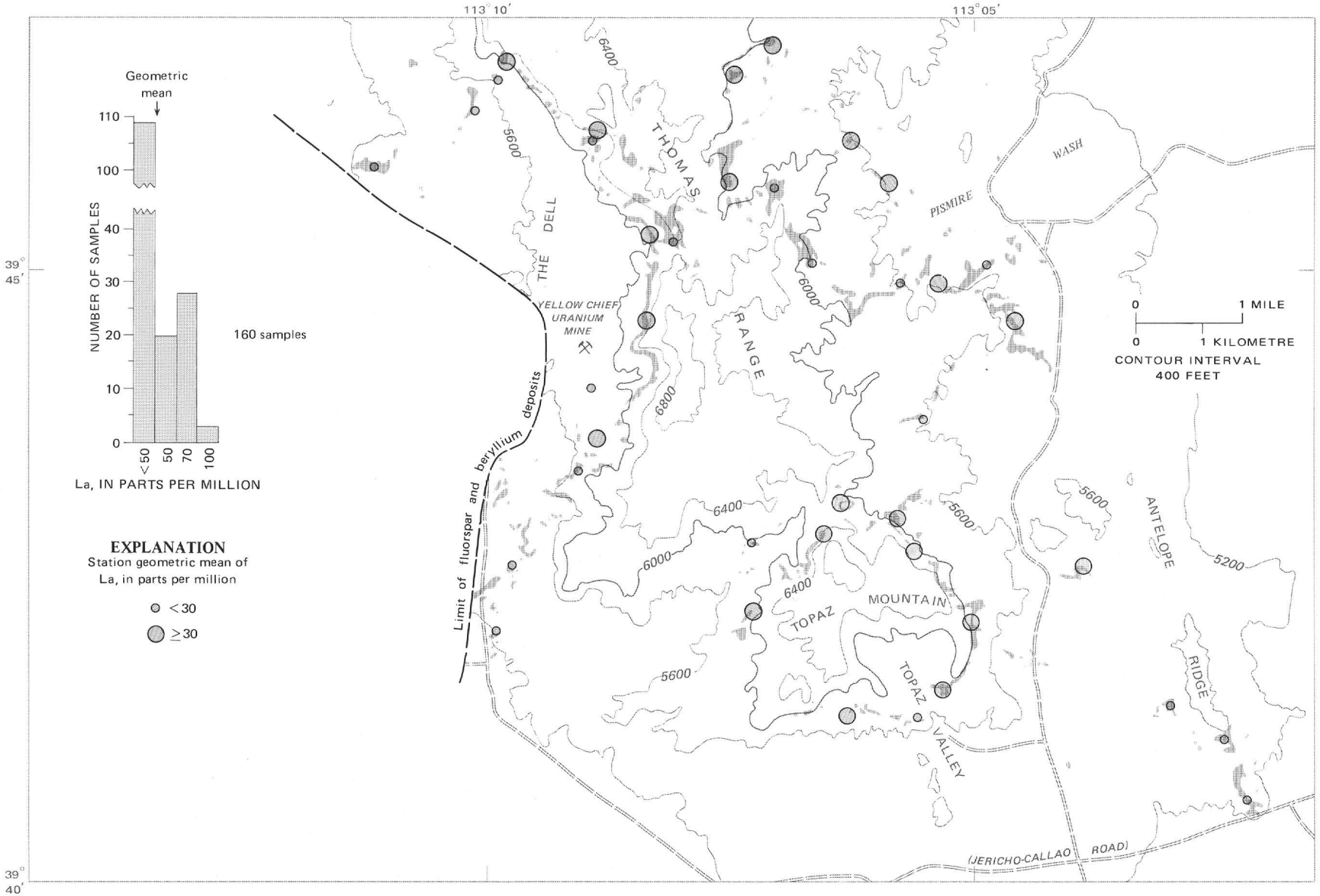

FIGURE 33. — Lanthanum content of water-laid tuff in the Thomas Range.

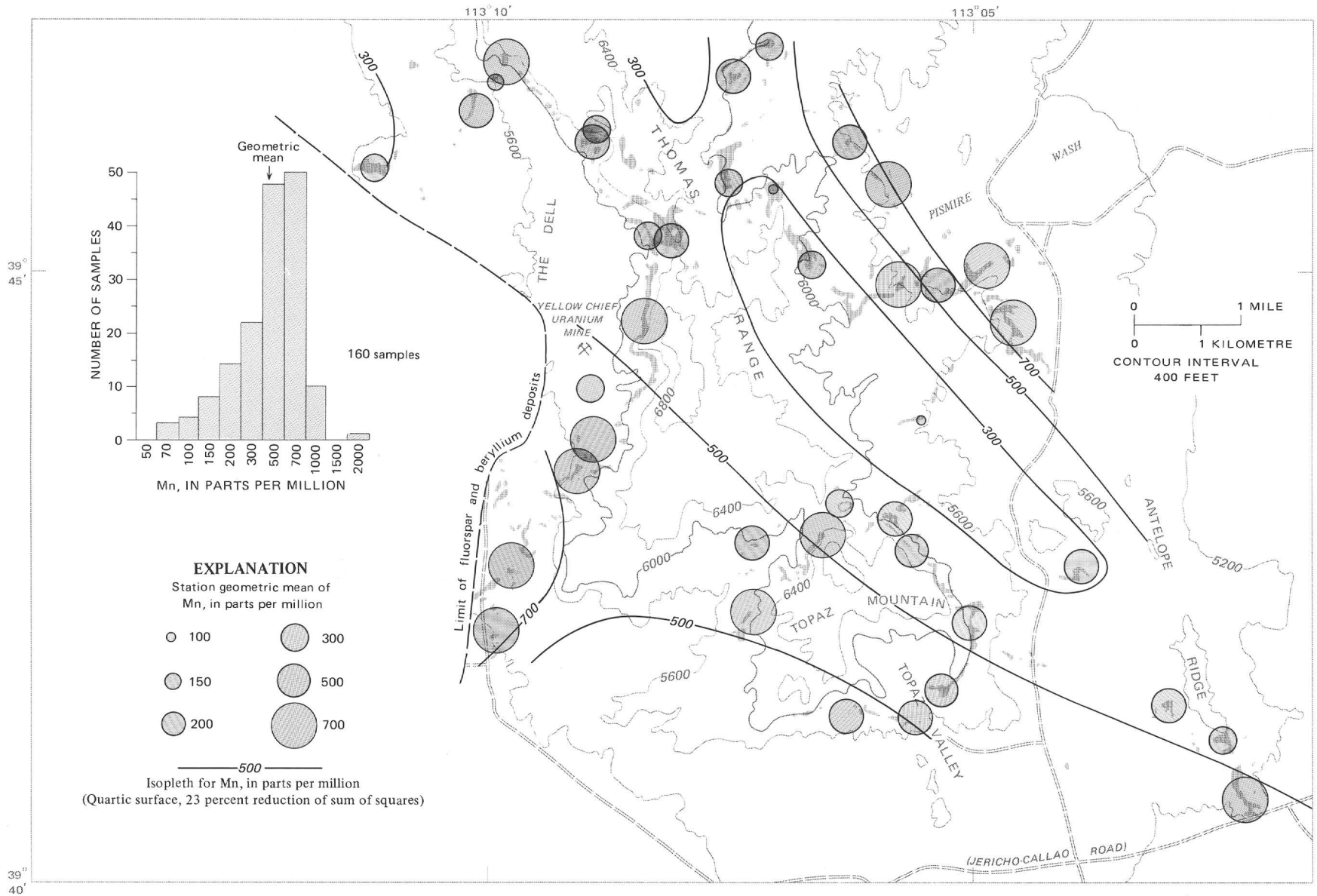

FIGURE 34. — Manganese content of water-laid tuff in the Thomas Range.

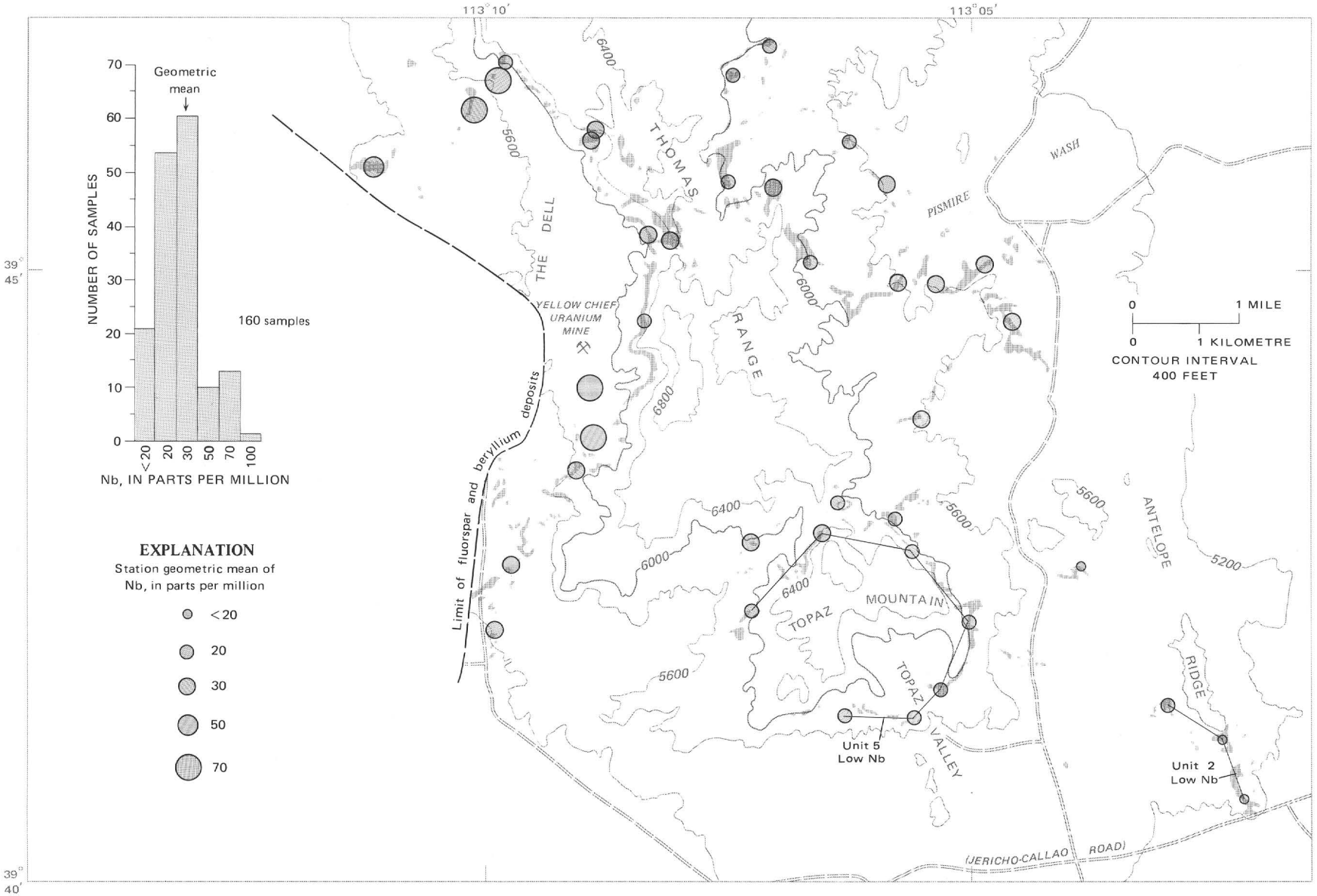

FIGURE 35. — Niobium content of water-laid tuff in the Thomas Range.

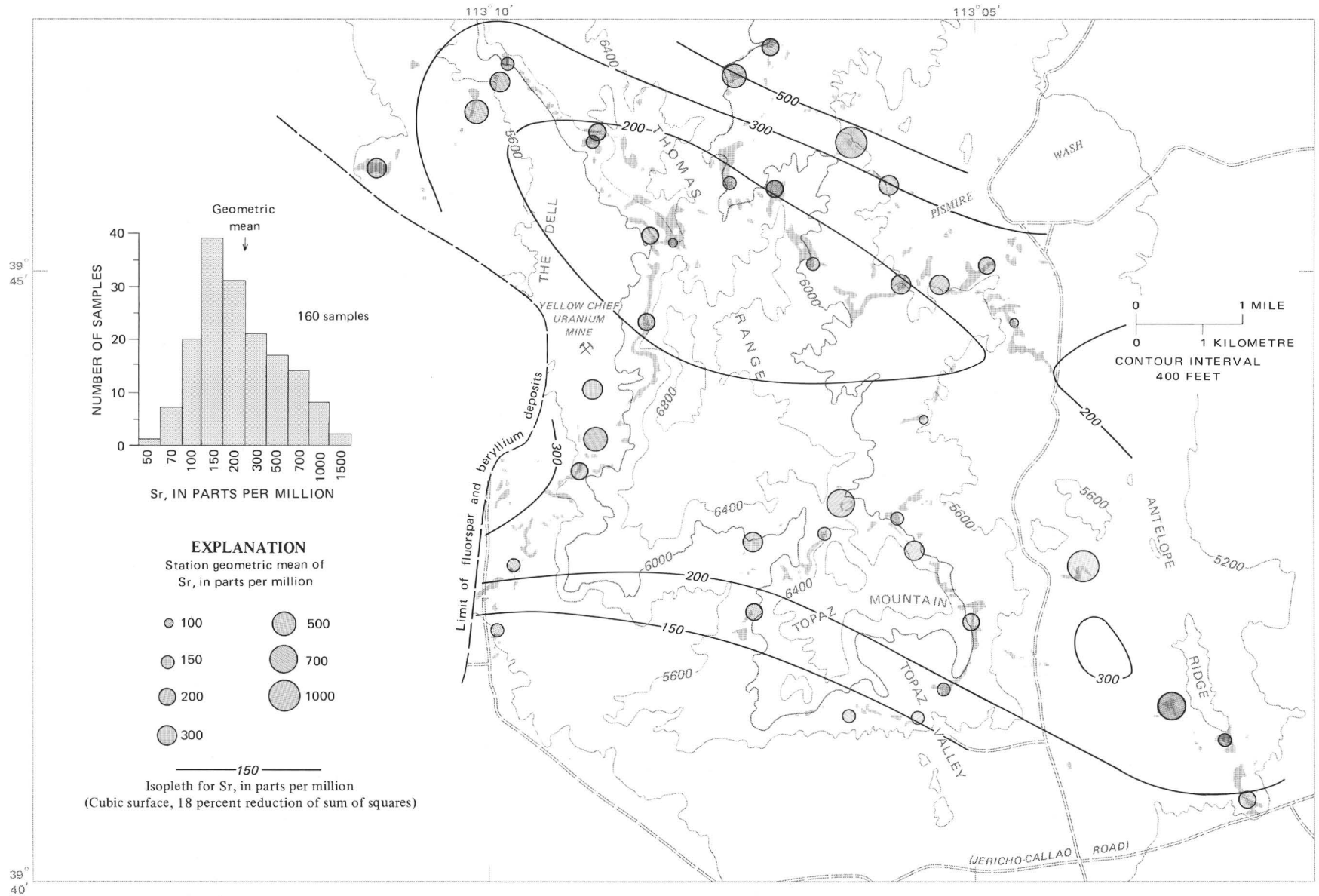

FIGURE 36. — Strontium content of water-laid tuff in the Thomas Range.

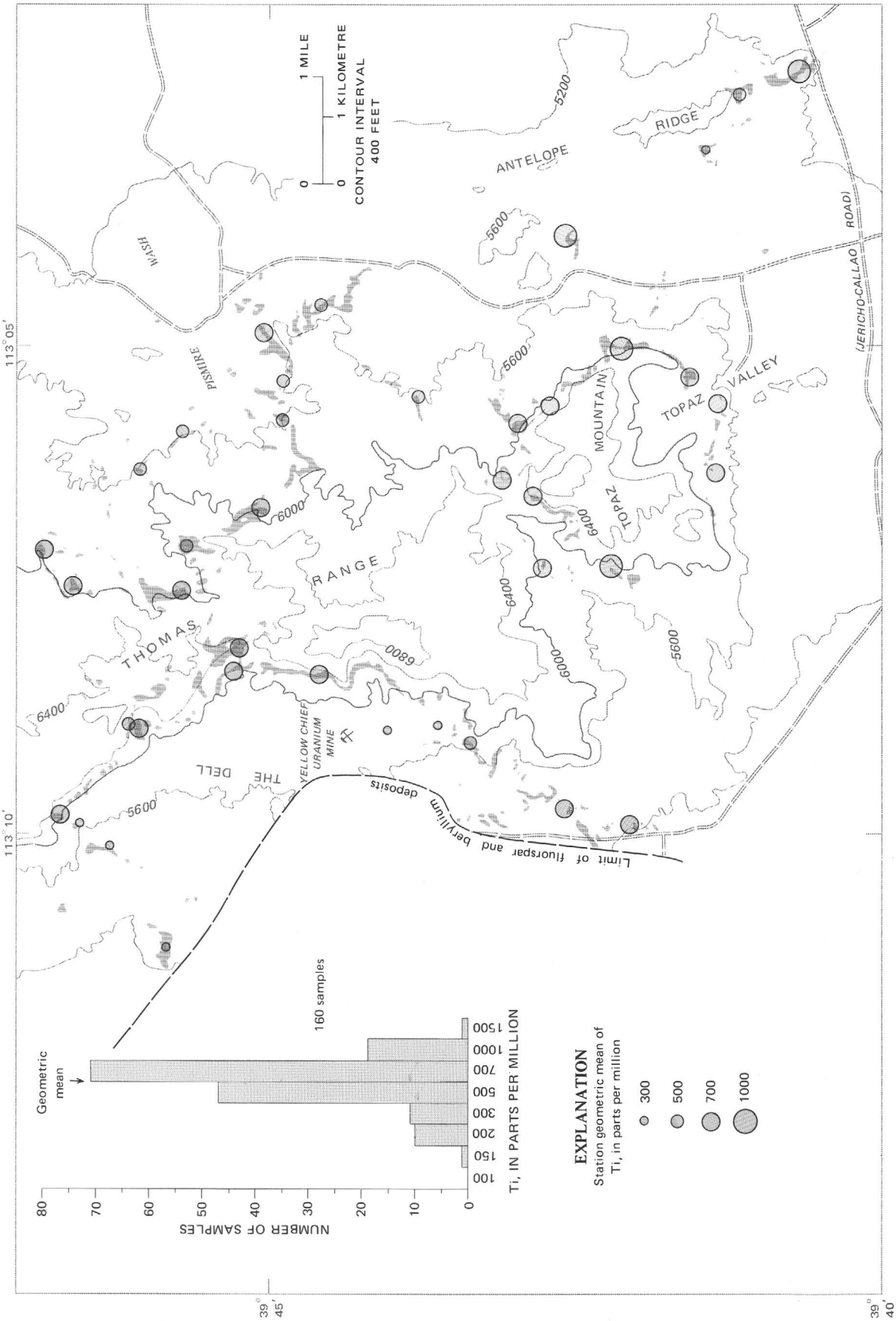

FIGURE 37. — Titanium content of water-laid tuff in the Thomas Range.

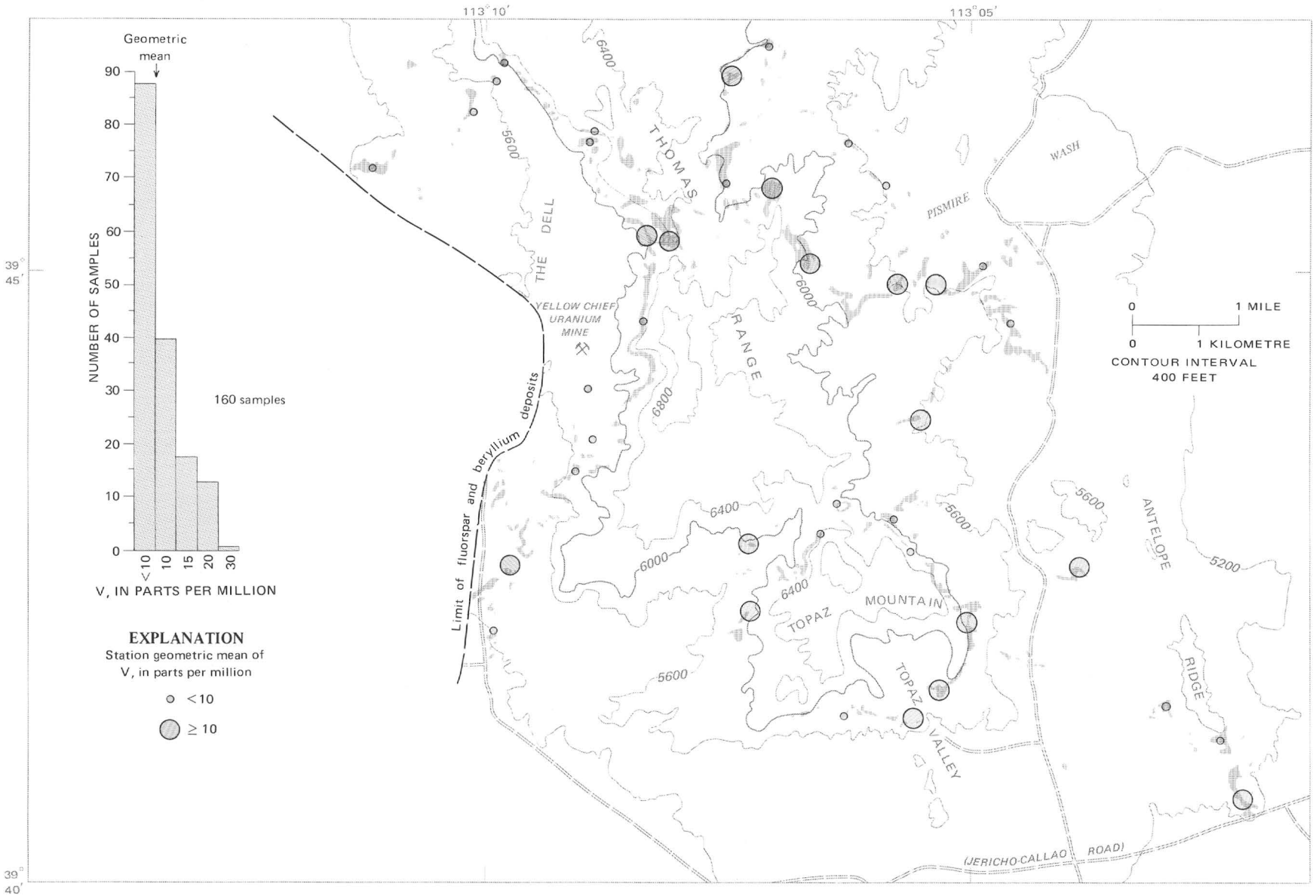

FIGURE 38. — Vanadium content of water-laid tuff in the Thomas Range.

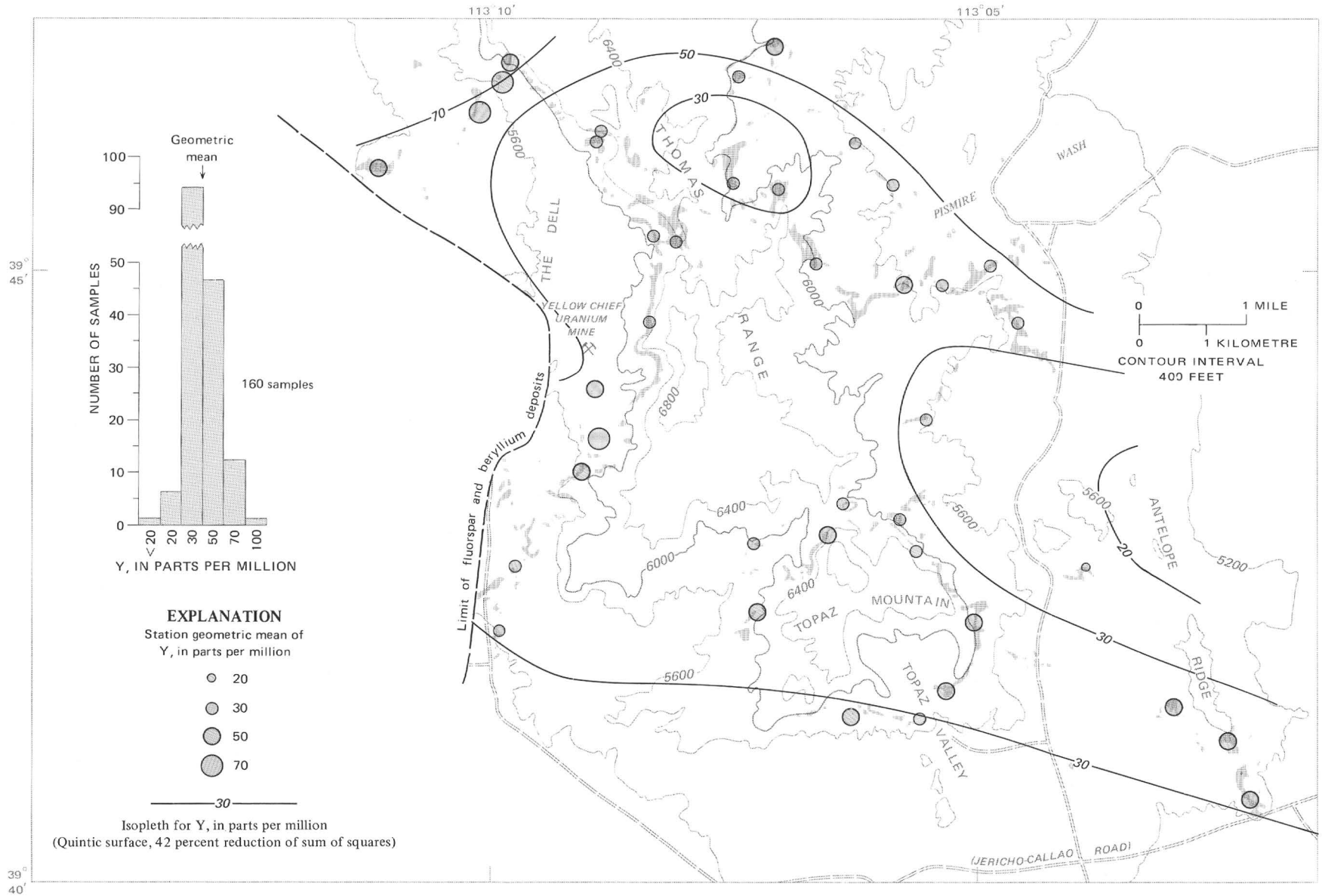

FIGURE 39. — Yttrium content of water-laid tuff in the Thomas Range.

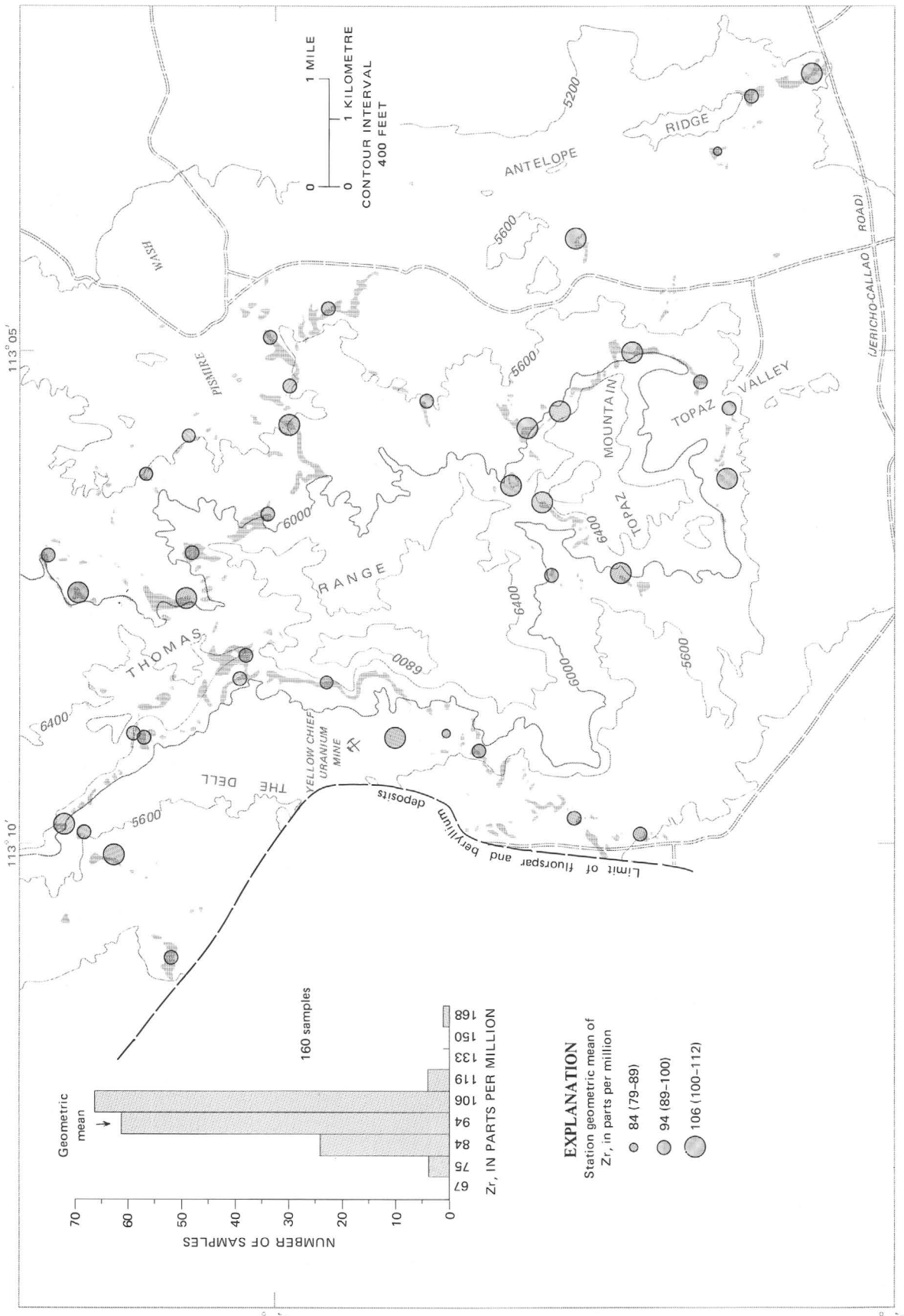

FIGURE 40. — Zirconium content of water-laid tuff in the Thomas Range.

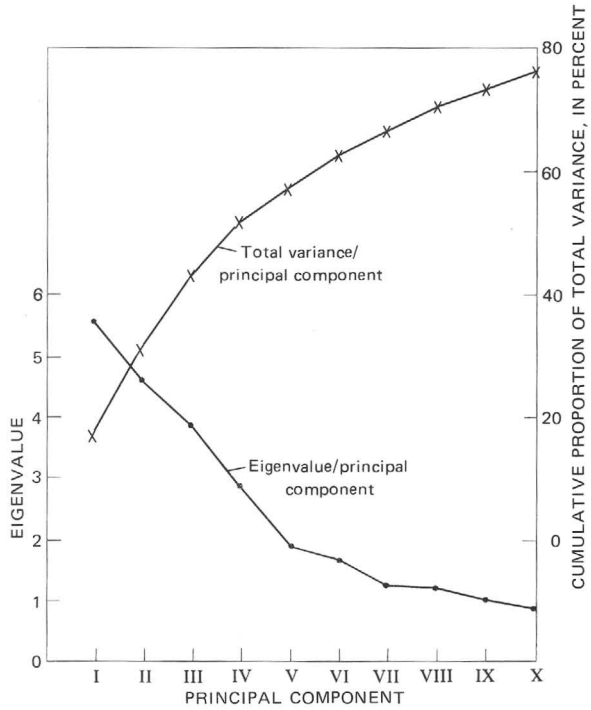

FIGURE 41. — Eigenvalues and cumulative proportion of total variance explained by the first 10 principal components. Note break in slope of eigenvalue curves between principal components IV and V and VI and VII.

Beryllium-Bearing Tuffs in Western Utah

GEOLOGICAL SURVEY PROFESSIONAL PAPER 818

This volume was published as separate chapters A-C

UNITED STATES DEPARTMENT OF THE INTERIOR

GEOLOGICAL SURVEY

V. E. McKelvey, *Director*

CONTENTS

[Letters designate the separately published chapters]

(A) Hydrothermal alteration associated with beryllium deposits at Spor Mountain, Utah, by David A. Lindsey, Harold Ganow, and Wayne Mountjoy.
(B) Mineralization halos and diagenesis in water-laid tuff of the Thomas Range, Utah, by David A. Lindsey.
(C) The effect of sedimentation and diagenesis on trace element composition of water-laid tuff in the Keg Mountain area, Utah, by David A. Lindsey.

☆U.S. GOVERNMENT PRINTING OFFICE: 1975—677-340/ 4